Ferroptosis pathway regulation by the Dynamin Superfamily of large GTPases

Inaugural-Dissertation

zur

Erlangung des Doktorgrades

Dr.rer.nat

der Mathematisch-Naturwissenschaftlichen Fakultät

der Universität zu Köln

vorgelegt von

Laura Prieto Clemente

aus Madrid, Spanien

Köln, 2021

Berichterstatter/in: Prof. Dr. Silvia von Karstedt
Prof. Dr. Thomas Langer
Prof. Dr. Jan Riemer

Tag der mündlichen Prüfung: 01/12/2021

TABLE OF CONTENT

LIST OF FIGURES

LIST OF TABLES

LIST OF ABBREVIATIONS

12/15-LOX	12/15 lipoxygenases
AA	Arachidonic acid
ACD	Accidental cell death
AdA	Adrenic acid
ADCD	Autophagy-dependent cell death
ADP	Adenosine diphosphate
AIF	Apoptosis-inducing factor
ALOX	Lipoxygenases
ALS	Amyotrophic lateral sclerosis
ASCL4	Acyl-CoA synthetase long-chain family member 4
ATM	Mutated in Ataxia-Telangiectasia
ATP	Adenosine 5'-triphosphate
BAK	Bcl-2 homologous antagonist/killer
BAX	Bcl-2 associated X protein
BCA	Bicinchoninic acid
Bcl-2	B-cell lymphoma 2
BH3	Bcl-2 Homology 3
BID	BH3-interacting domain death agonist
BSA	Bovine serum albumin
BSO	Buthionine sulfoximine
Ca2+	Calcium
CaMKI-α	$Ca^{2+/}$calmodulin-dependent protein kinase I α
CaMKII-α	$Ca^{2+/}$calmodulin-dependent protein kinase II α
CASP1	Caspase 1
CCVs	Clathrin-coated vesicles
CDI	Cysteine-deprivation-induced ferroptosis
Cdk1	Cyclin-dependent kinase 1
ChOOH	Cholesterol hydroperoxide
CISD1	CDGSH iron sulfur domain 1
CL	Cardiolipin
CME	Clathrin-mediated endocytosis
CO_2	Carbon dioxide

CoA	Coenzyme A
CRISPR	Clustered Regularly Interspaced Short Palindromic Repeats
CyDP	Cyclophilin D
DAMPs	Damage-associated molecular patterns
DFO	Deferoxamine
DLPs	Dynamin-related proteins
DMEM	Dulbecco´s modified Eagle´s medium
DMSO	Dimethyl sulfoxide
DMT1	Divalent metal transporter 1
DNA	Deoxyribonucleic acid
DNM1	Dynamin 1
DNM2	Dynamin 2
DPPH	2,2-diphenyl-1-picrylhydrazyl
Drp1	Dynamin-related protein 1
DSPs	Dynamin superfamily proteins
DTT	Dithiothreitol
EDTA	Ethylenediamine tetraacetic acid
ER	Endoplasmic Reticulum
Erastin	Eradicator of RAS and ST-expressing cells
ERK1/2	Extracellular signal-regulated kinase ½
ETC	Electron transport chain
FA	Formaldehyde
FACS	Fluorescence-Activated Cell Sorting
FCS	Fetal Calf Serum
FDA	Food and drugs administration
Fer-1	Ferrostatin-1
FH	Fumarate hydratase
Fis1	Mitochondrial fission 1 protein
FITC	Fluorescein isothiocyanate
FSP1	Ferroptosis supressor protein 1
GAPDH	Glyceraldehyde 3-phosphate dehydrogenase
GBPs	Guanylate-binding proteins
GCL	Glutamate cysteine ligase
GED	GTPase effector domain

GPX4	Glutathione peroxidase 4
GSH	Glutathione
GSR	Glutathione-disulfide reductase
GSS	Glutathione synthetase
GSSG	Glutathione disulfide
GTP	Guanosine triphosphate
H	Hours
H2DCFDF	2',7'-dichlorodihydrofluoresceindiacetate
H2O2	Hydroperoxide
HEKs	Human embryonic kidney 293 cells
HO·	Hydroxyl radicals
HRP	Horse radish peroxidase
I/R	Ischemia-reperfusion
ICD	Immunogenic cell death
IP_3R	Inositol 1,4,5-triphosphate calcium receptors
KD	Knockdown
KO	Knockout
KRAS	Kirsten Rat Sarcoma virus
LDCD	Lysosome-dependent cell death
LDS	Lithium dodecyl sulfate
LG-domain	Large GTPase domain
LOXs	Lipoxygenases
LPCAT3	Lysophosphatidylcholine acyltransferase 3
MAPK	Microtubule associated protein kinase
MCB	Monochloromobimane
MD	Middle domain
Mdivi	Mitochondrial division inhibitor 1
MEFs	Mouse embryonic fibroblasts
Mff	Mitochondrial fission factor
MFI	Mean fluorescence intensity
Mfn1/2	Mitofusins 1 and 2
MiD49	Mitochondrial dynamics of 49 kDa
MiD51	Mitochondrial dynamics of 51 kDa
MLKL	Mixed lineage kinase domain-like

MMP	Mitochondrial membrane potential
MOMP	Mitochondrial outer membrane permeabilization
MPT	Mitochondrial permeability transition
mPTP	Mitochondrial permeability transition pores
mtDNA	mitochondrial DNA
MTT	3-(4,5-dimethylthiazol-2-yl)-2,5-diphenyltetrazolium bromide
NAC	N-acetylcysteine
NADH	Nicotinamide adenine dinucleotide + hydrogen
Nec-1	Necrostatin-1
NO	Nitric oxide
NOX	NADPH oxidases
NSCLC	Non-small cell lung cancer cell
OE	Overexpression
OMM	Outer mitochondrial membrane
OPA-1	Optic-atrophy factor 1
OXPHOS	Oxidative phosphorylation
P/S	Penicilin/Streptomycin
PA	Phosphatidic acid
PBS	Phosphate-buffered salin
PBST	Phosphate-buffered salin-Tween 20
PE	Phosphatidylethanolamine
PG-SK	Phen Green SK diacetate
PGAM5	Phosphoglycerate Mutase Family Member 5
PH	Pleckstrin-homology
PHD	EGLN prolylhydroxylases
PI	Propidium iodide
PKA	Protein kinase A
PKCδ	Protein kinase C δ
PLOOH	Phospholipid hydroperoxide
POR	P450 oxidoreductase
PRD	Proline-rich domain
PTMs	Posttranslational modifications
PUFAs	Polyunsaturated fatty acids

RAS	Rat Sarcoma
RCD	Regulated cell death
RIPA	Radioimmunoprecipitation assay
RIPK1/3	Receptor-interacting serine/threonine-protein kinase 1/3
RNA	Ribonucleic acid
ROS	Reactive oxygen species
RPMI	Roswell Park Memorial Institute Medium
RSL3	Rat sarcoma viral oncogene homolog (RAS)-selective lethal 3
RTAs	Radical-trapping agents
RyR	Ryanodine calcium receptors
SCLC	Small cell lung cancer cell
SCLC	Small cell lung cancer cell
SCP-2	Sterol carrier protein 2
SDS	Sodium dodecyl sulfate
SEM	Standard error of the mean
Ser	Serine
SFA	Saturated fatty acids
siRNA	Small interfering RNA
Smac	Second mitochondria-derived activator of caspases
SR/ER	Sarcoplasmic/endoplasmic reticulum
ß-AR	ß-adrenergic stimulation
STEAP3	Six-transmembrane epithelial antigen of prostate 3
STING1	Stimulator of interferon genes 1
TA	Tail-anchored
tBID	Truncated BID
TCA	Tricarboxylic acid cycle
Tf-TfR1	Transferrin-transferrin receptor 1
TFR1 (CD71)	Transferrin receptor 1
Thr	Threonine
TLRs	Toll-like receptors
TRIS-HCL	Trizma hydrochloride
VDCC	Voltage-dependent Ca^{2+} channels
WB	Western Blot

WT	Wild-type
zVAD	Cell-Permeant Pan Caspase Inhibitor of Apoptosis
α-KG	α-ketoglutarate

ZUSAMMENFASSUNG

Ferroptose ist eine kürzlich beschriebene Form des regulierten Zelltods, der durch die eisenabhängige Entstehung von Lipid-reaktiver Sauerstoffspezies (ROS) gekennzeichnet ist, die zu einer Destabilisierung der Membran führen können. Daher ist der Eisenimport ein wesentlicher Bestandteil des Ferroptose-Signalwegs. Die Eisenaufnahme über die Endozytose des Transferrinrezeptors ist von den GTPasen Dynamin 1 und 2 abhängig. Tatsächlich kann der Dynamin 1 und 2-Inhibitor Dynasore vor Gewebsschäden durch Ischämie/Reperfusion schützen und der Gleiche Effekt kann durch den Ferroptose-Inhibitor Ferrostatin-1 erreicht werden. Es ist jedoch nicht bekannt, ob die Regulierung der Eisenaufnahme durch Dynamin 1 und 2 eine Voraussetzung für den durch Ferroptose ausgelösten Zelltod ist. Ein zweites charakteristisches Merkmal der Ferroptose ist die Akkumulation von ROS. Die Mitochondrien spielen eine zentrale Rolle bei der Erzeugung von ROS durch oxidative Phosphorylierung (OXPHOS). Es konnte gezeigt werden, dass die experimentelle Induktion der Ferroptose die mitochondriale Fragmentierung und die Entstehung von mitochondrialem ROS auslöst. Morphologische Veränderungen der Mitochondrien werden hauptsächlich durch ein anderes Mitglied der Dynamin-Familie von GTPasen, Dynamin-related Protein 1 (Drp1), reguliert. Interessanterweise zeigen heterozygote Drp1-Knockout-Mäuse eine defekte mitochondriale Fission und verminderte Lipid-ROS Mengen im Gewebe. Wie die mitochondrialen Prozesse während der Ferroptose reguliert werden, einschließlich einer möglichen Rolle von Drp1, ist jedoch noch nicht erforscht worden. Ziel dieser Studie war es, die mögliche Rolle der Dynamin-Familienmitglieder Dynamin 1, 2 und Drp1 bei der Regulierung des Ferroptose-Signalwegs zu untersuchen und die zugrunde liegenden molekularen Mechanismen aufzuklären. Überraschenderweise konnte der der Dynamin 1 und 2-Inhibitor Dynasore zwar effizient die Ferroptose-Induktion blockieren, aber der Knockdown seiner wichtigsten molekularen Ziele Dynamin 1 und 2 war nicht ausreichend, um Zelltod durch Ferroptose zu blockieren. Stattdessen konnte in zellfreien Systemen gezeigt werden, dass dynasore Eigenschaften eines Radikalfängers besitzt und als breit wirksames Antioxidans fungiert. Darüber hinaus fanden wir heraus, dass Drp1 in die Mitochondrien transloziert und die

durch Cystin-Entzug induzierte Ferroptose (CDI) fördert. Bemerkenswert ist, dass wir beobachtet haben, dass die Phosphorylierung von Drp1 bei der Induktion der Ferroptose von CamKIIalpha abhängig ist. Insgesamt deuten diese Daten darauf hin, dass Dynasore über eine kombinierte Modulation des Eisenpools und die Hemmung allgemeiner ROS Spezies als hochaktiver Inhibitor von ROS-getriebenen Arten des Zelltods fungieren kann. Andererseits zeigen unsere Daten, dass der Knockdown von Dynamin 1 und 2 nicht ausreicht, um Ferroptose zu regulieren. Darüber hinaus haben wir eine Schlüsselrolle von Drp1 bei der Regulierung der mitochondrialen Fragmentierung in der CDI-Ferroptose entdeckt. Diese Ergebnisse tragen zu unserem Verständnis des Ferroptose-Signalwegs bei sowie seiner Bedeutung für die Physiopathologie von Krankheiten bei, die mit dieser Art von Zelltod einhergehen.

SUMMARY

Ferroptosis is a recently described form of regulated cell death characterised by the iron-dependent generation of lethal amounts of lipid reactive oxygen species (ROS). Therefore, iron import is an essential process for the execution of ferroptosis. Iron uptake via transferrin receptor endocytosis is dependent on the GTPases dynamin 1 and 2. Indeed, the dynamin 1 and 2 inhibitor dynasore, can protect from ischemia/reperfusion injury, a type of tissue damage that has been shown to be also blocked by the ferroptosis inhibitor ferrostatin-1. Yet, it is unknown whether the regulation of iron uptake by dynamin 1 and 2 is essential for the execution of ferroptosis. A second characteristic hallmark of ferroptosis is the accumulation of ROS. Mitochondria play a central role in the generation of ROS through oxidative phosphorylation (OXPHOS). Importantly, experimental induction of ferroptosis was shown to induce mitochondrial fragmentation and mitochondrial ROS. Morphological changes of mitochondria are mainly regulated by another member of the dynamin family of GTPases, dynamin-related protein 1 (Drp1). Interestingly, heterozygous *drp1* knockout mice show defective mitochondrial fission and low levels of lipid ROS in tissues. Yet, how mitochondrial events are regulated during ferroptosis, including a potential role of Drp1, have remained unexplored. The aim of this study was to investigate potential roles for the dynamin family members dynamin 1, 2 and Drp1 in the regulation of the ferroptosis pathway and to elucidate underlying molecular mechanisms. Surprisingly, while the dynamin 1 and 2 inhibitor dynasore efficiently blocked ferroptosis induction, silencing of its main molecular targets dynamin 1 and 2 was not sufficient to block ferroptosis. Instead, in cell free systems, dynasore showed radical scavenger properties and acted as a broadly active antioxidant. Moreover, we found that Drp1 translocates to mitochondria and promotes cysteine-deprivation induced (CDI) ferroptosis. Of note, we observed Drp1 to be phosphorylated upon induction of ferroptosis in a manner dependent on CaMKIIα. Collectively, these data propose that dynasore can function as a highly active inhibitor of ROS-driven types of cell death via combined modulation of the iron pool and inhibition of general ROS. On the other hand, our data reveal that dynamin 1 and 2 silencing is insufficient to regulate ferroptosis execution. Furthermore, we have reported a key role of Drp1 in the

regulation of mitochondrial fragmentation in CDI ferroptosis. These findings contribute towards our understanding of the ferroptosis pathway, as well as its implication in the physiopathology of diseases associated with this type of cell death.

1. INTRODUCTION

1.1. Cell death

It is not a surprise that cells in a complex organism die. Although necrotic cell death was described for the first time in the 19th century, cell death is not only related to pathological circumstances or aging. During embryogenesis, in response to stress or during tissue homeostasis, cells also die in a ´´programmed´´ manner (Ellis and Horvitz 1986; Kerr et al., 1972).

Mammalian cells can undergo two different types of cell death; accidental cell death (ACD), an uncontrolled process that occurs upon instantaneous damage of cells expose to physical, chemical or mechanical factors (Galluzzi et al., 2016; Galuzzi et al., 2015), or regulated cell death (RCD), a process which is highly regulated by a molecular machinery that can be altered by pharmacological or genetic interventions (Galluzzi et al., 2018). Regulated cell death can be induced in the absence of environmental signals, operating as a physiological mechanism for development or tissue replacement (Jorgensen et al., 2017; Nagata et al., 2017; Green et al., 2016; Fuchs et al., 2011). However, RCD can also occur from intracellular or extracellular alterations that are either too prolonged or intense. These changes, can interfere with the adaptive immune response that results unable to deal with stress and to restore cellular homeostasis (Galluzzi et al., 2016).

1.1.1. Types of cell death

Cell death has historically been classified into three different modalities based on macroscopic morphological alterations: (1) **apoptosis**, manifesting with reduction of cytoplasm size, chromatin condensation, DNA fragmentation and the formation of small vesicles (apoptotic bodies); (2) **autophagy**, which exhibits cytoplasmic vacuolization and lysosomal degradation; and (3) **necrosis**, a type of cell death that do not share features of apoptosis or autophagy, but is characterised by cell lysis and the release of the cytosol content into the extracellular space (Galluzzi et al., 2018).

Since the cell death field continues to progress and novel signalling pathways are described and still being defined, the Nomenclature Committee on Cell

Death has provided an updated classification of cell death modalities focused on molecular and essential aspects of the pathways (represented in **table 1**).

Type of cell death	Hallmarks
Intrinsic apoptosis	Initiated by intracellular perturbations (DNA damage, ROS, endoplasmic reticulum (ER) stress), maintenance of plasma membrane integrity (apoptotic bodies), mitochondrial outer membrane permeabilization (MOMP), activation of initiator and executioner caspases, formation of the apoptosome and DNA fragmentation
Extrinsic apoptosis	Initiated by ligand/receptor binding, caspase 8 activation, MOMP, DNA fragmentation and formation of apoptotic bodies
MPT-driven necrosis	Triggered by perturbations of the intracellular milieu (oxidative stress or Ca^{2+} overload), mitochondrial inner membrane permeabilization, relies on Cyclophilin D (CyPD)
Necroptosis	Initiated by ligand/receptor binding or disruption of intracellular homeostasis (oxidative stress, calcium overload etc), depends on MLKL, RIPK3 and RIPK1 (in some settings) activity, cellular swelling, plasma membrane permeabilization and rupture, release of damage-associated molecular patterns (DAMPs)
Ferroptosis	Initiated by intra or extracellular perturbations, iron-dependent lipid peroxidation, high ROS levels, cell membrane rupture, independent of caspases or necroptosis components, necrotic morphology, release of DAMPs
Pyroptosis	Formation of plasma membrane pores by the gasdermin protein family, chromatin condensation, plasma membrane permeabilization, resembles apoptosis but depends on inflammatory caspase 1 (CASP1)

Parthanatos	Triggered by hyperactivation of a component of the DNA damage response machinery, oxidative stress or hypoxia. Contributes to various pathological conditions (cardiovascular or renal disorders)
Entotic cell death	Originates from entosis (form of cell cannibalism in healthy or malignant tissues), executed by lysosomes
NETotic cell death	Characterised in neutrophils, triggered by activation of Toll-like receptors (TLRs), ROS-dependent
LDCD	Activation of cathepsins and caspases, MOMP and permeabilization of lysosomal membranes. Relevant for inflammation, tissue remodelling or intracellular pathogen response
ADCD	Depends on the autophagy machinery. Important for adaptation to stress, is cytoprotective
ICD	Activates the adaptive immune response. It can be initiated by viral infections, some FDA (Food and drugs administration) drugs or radiation

Table 1. Classification of cell death modalities. Mammalian cells exposed to perturbations are able to activate a variety of signaling pathways that lead to their elimination. Each of these regulated cell death pathways is initiated by molecular mechanisms that might be shared by some of the signaling pathways. Moreover, each type of RCD is characterised by its own morphological features and immunomodulatory profile. *ADCD*: autophagy-dependent cell death, *ICD*: immunogenic cell death, *LDCD*: lysosome-dependent cell death, *MPT*: mitochondrial permeability transition. Table adapted from Galluzzi et al., 2018.

1.1.2. Ferroptosis (Adapted from Bebber, ...Prieto-Clemente et al., 2020)

Over the last years, ferroptosis was described as a new type of iron-dependent form of regulated cell death which is triggered upon collapse of a lipid-radical-specific antioxidant defence (Dixon et al., 2012). Whereas the RCD types previously explained are mainly dependent on or inhibited by caspases, ferroptosis seems to have evolved separately and very little is known about

direct molecular cross-talk to other cell death pathways (Galluzzi et al., 2018). However, most researchers agree that cells undergoing ferroptosis display a necrosis-like phenotype (Vanden Berghe et al., 2014). These characteristics include a loss of plasma membrane integrity, cytoplasmic swelling and chromatin condensation. Occasionally, when cells undergo ferroptosis, they round up and detach (Dixon et al., 2012, Dolma et al., 2003, Yagoda et al., 2007, Friedmann Angeli et al., 2014), and ferroptosis occurring in one cell can be propagated to adjacent cells (Riegman et al., 2020, Katikaneni et al., 2020).

1.1.2.1. Ferroptosis Pathway Regulation

Ferroptosis is characterised by presenting two main hallmarks, iron accumulation and increased lipid peroxidation. The requirement for intracellular divalent iron pools was demonstrated by the fact that chelation of iron by deferoxamine (DFO) impairs experimental induction of ferroptosis (Dixon et al., 2012). Iron is an essential nutrient for life that has two oxidation states: ferrous (Fe^{2+}) and ferric (Fe^{3+}). Non-heme iron is mainly Fe^{3+} which binds to transferrin (Tf) in the serum. The major Fe^{3+} delivery system into cells is the transferrin-transferrin receptor 1 (Tf-TfR1) complex. This complex forms a recycling endosome that is internalized into cells through receptor-mediated endocytosis in clathrin-coated pits. Once Fe^{3+} is imported, endosomal six-transmembrane epithelial antigen of prostate 3 (STEAP3) mediates the conversion to the reduced form (Fe^{2+}). Following its reduction, the divalent iron form is released into the cellular labile iron pool through the divalent metal transporter 1 (DMT1) (Hardin et al., 1993; Yanatori et al., 2015; Gao et al.,2015). Importantly, clathrin-mediated endocytosis (CME) is regulated by the Dynamin Superfamily classical members dynamin-1 and 2, which control earlier rate-limiting steps of clathrin-coated vesicle formation (Hinshaw and Schmid, 1995). However, their role in ferroptosis has not been elucidated yet. Supporting the importance of this import route, both transferrin and TFR1 were shown to promote ferroptosis (Yang et al., 2008; Gao et al., 2008). Moreover, *DMT1* was shown to be up-regulated during ferroptosis induction (Yu et al., 2019). Iron can directly induce the generation of aberrant amounts of ROS through the Fenton reaction, where active divalent iron and hydroperoxide (H_2O_2) react, generating hydroxyl radicals ($HO\cdot$) (Dixon et al., 2012). Moreover, iron may indirectly increase the

activity of lipoxygenases (ALOX) or EGLN prolylhydroxylases (or PHD), enzymes responsible for lipid peroxidation and oxygen homeostasis, respectively (Chen et al., 2020). It has not been elucidated why only iron, but not other metals which promote Fenton reaction, is able to induce ferroptosis (Ayala et al., 2014, Dixon et al., 2012). One explanation could be that increased iron levels activate other specific downstream executers of ferroptosis (**Figure 1**).

The second most important hallmark of ferroptosis is the accumulation of peroxidised membrane lipids, which are thought to destabilized the plasma membrane bilayer (Dixon et al, 2012; Agmon et al., 2018). Lipid peroxidation is a free radical-driven reaction, that primarily affect polyunsaturated fatty acids (PUFAs). Through the use of lipidomics, arachidonic acid (AA)- and adrenic acid (AdA)- containing phosphatidylethanolamine (PE) species were identified as peroxidised lipid products of ferroptosis (Kagan et al., 2017). The analysis of ferroptosis-resistant cells found two genes significantly enriched for gene trap insertions, acyl-CoA synthetase long-chain family member 4 (ASCL4) and lysophosphatidylcholine acyltransferase 3 (LPCAT3) (Kagan et al., 2017, Yuan et al., 2016, Doll et al., 2017). ASCL4 catalyse the esterification of AA and AdA with coenzyme A (CoA) forming Acyl-CoA, which can then undergo either ß-oxidation or PUFA biosynthesis (Doll et al., 2017; Tang et al., 2018; Yuan et al., 2016). Indeed, ACSL4 has been shown to contribute to ferroptosis induction by generating the target lipid pool which is peroxidised during ferroptosis (Angeli et al., 2019; Doll et al., 2017). In addition, *acsl4* is overexpressed during ferroptosis, thereby it has been considered as a specific biomarker of ferroptosis (Kagan et al., 2017, Yuan et al., 2016, Doll et al., 2017). Nevertheless, ACSL4 is not essential for ferroptosis in specific circumstances due to ACSL4-depleted cells can undergo ferroptosis (Chu et al., 2019). LPCAT3 catalyses the biosynthesis of AA/AdA-CoA and membrane PE to form AA/AdA-PE. These lipids can undergo spontaneous peroxidation through Fenton reaction in different cellular membranes. The oxidized PUFAs can initiate a chain reaction of lipid ROS attacking other proximal PUFAs (Conrad and Pratt, 2019). Alternatively, lipid peroxidation can be catalysed by ALOXs, which mediate the peroxidation of PUFAs into AA/AdA-PE-OOHs, thereby inducing ferroptosis

(Reviewed in Tang et al., 2021) (**Figure 1**). ALOXs are not the only mediators of lipid peroxidation. Of note, cytochrome P450 oxidoreductase (POR) provides electrons to the P450 enzyme promoting PUFA peroxidation in cancer cells (Zou et al., 2020).

Intracellular lipids are stored in lipid droplets that derive from the endoplasmic reticulum. In response to oxidative stress, lipid droplets are formed to prevent cell death by isolating PUFAs from membrane phospholipids (Reviewed in Tang et al., 2021). The degradation of lipid droplets by lipophagy allows the production of free fatty acids and boosts lipid peroxidation and consequently, ferroptosis (Bai et al., 2019). In contrast, lipid storage inhibits ferroptosis (Bai et al., 2019). Hence, increased lipid storage may impair ferroptosis, whereas increased lipid droplet degradation promotes it.

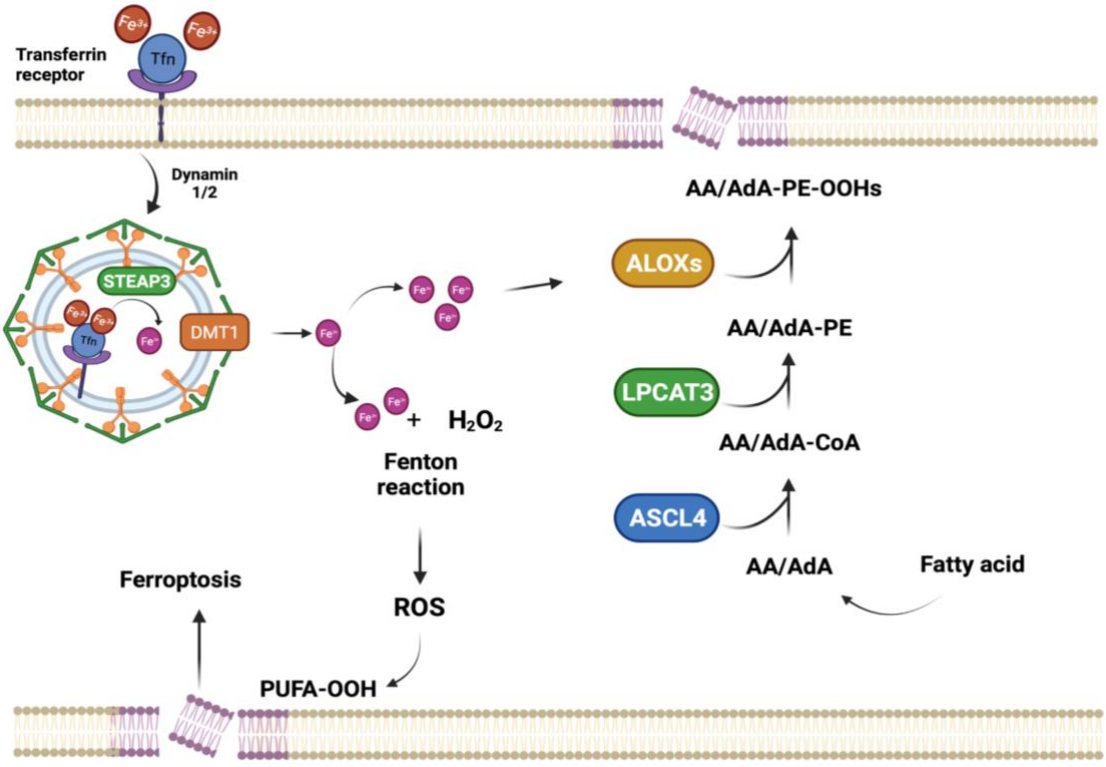

Figure 1. Iron uptake and lipid peroxidation. Ferroptosis is characterised by an aberrant accumulation of lipid reactive oxygen species (ROS) which leads to peroxidation (-OOH) of polyunsaturated fatty acids (PUFAs) and glutathione (GSH) depletion. The main targets of this peroxidation are arachidonic acid (AA) phosphatidylethanolamine (PE) lipid species. Lipid peroxidation can be induced by cytosolic active iron (Fe^{2+}) imported into cells bound to transferrin via transferrin receptor (TFR1) endocytosis and released to the labile cytosolic iron pool through the divalent metal transporter 1 (DMT1). STEAP3 mediates the conversion of Fe^{3+} to the reduced form (Fe^{2+}) in the recycling endosome. In the presence

of H_2O_2, Fe^{2+} triggers the generation of hydroxyl radicals (HO·) in a Fenton reaction. Moreover, lipoxygenases (ALOXs) can catalyse lipid peroxidation using Fe^{2+} as a cofactor. ACSL4 and LPCAT3 generate the pool of AA-containing target lipids. This figure was created using a licensed version of Biorender.com.

Importantly, to prevent constitutive membrane peroxidation, glutathione peroxidase 4 (GPX4) was shown to reduce lipid hydroperoxides (AA/AdA-PE-OOH) to the corresponding alcohols (PLOH), and thereby provides cellular protection from ferroptosis (Angeli et al., 2014; Yang et al., 2014). Antagonising GPX4 activity with the small molecule inhibitor rat sarcoma viral oncogene homolog (RAS)-selective lethal 3 (RSL3) leads to potent induction of ferroptosis (Angeli et al.,2014). GPX4 in turn requires glutathione (GSH) as an electron donor to reduce lipid hydroperoxides, which is thereby oxidised to GSH disulphide (GSSG). The recovery of GSH from GSSG is regulated by the NADH-consuming enzyme glutathione-disulfide reductase (GSR) (Reviewed in Tang et al., 2021). GSH is an abundant cellular tripeptide consisting of glycine, glutamate and cysteine that is considered as one of the main cellular non-protein antioxidants within cells (Meister et al., 1983). GSH synthesis depends on intracellular cysteine availability, which can be provided by the sodium-independent cystine/glutamate antiporter System xc-. Of note, this antiporter protein protects cells from ferroptosis by sustaining the production of GSH (Dixon et al., 2012). System xc- is a heterodimer consisting of two core components: the heavy-chain subunit (4F2, gene name *SLC3A2)* and the light-chain (xCT, gene name *SLC7A11*) (Proneth et al., 2019). Interestingly, xCT, the subunit responsible for specific amino acid antiport, was shown to be a molecular target of the small molecule eradicator of RAS and ST-expressing cells (Erastin). The resulting cystine pharmacological depletion induces ferroptosis efficiently (Burdo et al., 2006; Dixon et al., 2014). Moreover, depletion of cystine from cell culture media can also induce ferroptosis, avoiding the use of pharmacological inhibitors and mimicking a more physiological scenario of cell death induction (Gao et al., 2015). The synthesis of GSH not only depends on the availability of cysteine (derived from its precursor cystine) but also on the levels of sulfur amino acid precursors and the enzymes glutamate-cysteine ligase (GCL) and glutathione synthetase (GSS). The pharmacological inhibition of GCL by buthionine sulfoximine (BSO) also induces ferroptosis (Dixon et al., 2012, Sun et al., 2016, Xie et al., 2017) (**Figure 2**).

Lipophilic antioxidants, including vitamin E derivates (Yagoda et al., 2007) and the small molecules ferrostatin-1, liproxstatin-1(Angeli et al., 2014) and dynasore (Prieto Clemente et al., 2020) block ferroptosis by acting as radical trapping agents (RTAs) within membranes (Zilka et al., 2017). Moreover, the activation of antioxidant genes such us the glutathione system (Dixon et al., 2012) or the endogenous ubiquinol generated from ubiquinone through ferroptosis suppressor protein 1 (Fsp1) activity (Doll et al., 2019; Bersuker et al., 2019) counteract the membrane damage during ferroptosis. Fsp1 is a classic apoptosis inducer in mitochondria. Regardless of its role in these organelles, Fsp1 was recently described as an antioxidant regulator in ferroptosis (Bersuker et al., 2019, Doll et al., 2019). Fsp1 translocates from mitochondria to the cell membrane where it catalyses the formation of ubiquinone (CoQ10), thereby trapping lipid peroxides independently of GPX4 activity (Bersuker et al., 2019, Doll et al., 2019). Moreover, Fsp1 contributes to ferroptosis inhibition by activating ESCRT-III-dependent membrane repair regardless of its oxidoreductase function (Dai et al., 2020). One of the consequences of ferroptosis is the membrane damage, which can be repaired by two distinct mechanisms. The first one is to counteract lipid peroxidation by activating specific enzyme systems such as GPX4 or Fsp1. When this first barriers fails, cells undergo exocytosis and endocytosis to repair the membrane damage. The ESCRT-III machinery emerges to be a membrane repair protein that prevent different types of cell death including ferroptosis (Gong et al., 2017, Rühl et al., 2018, Dai et al., 2020) (**Figure 2**).

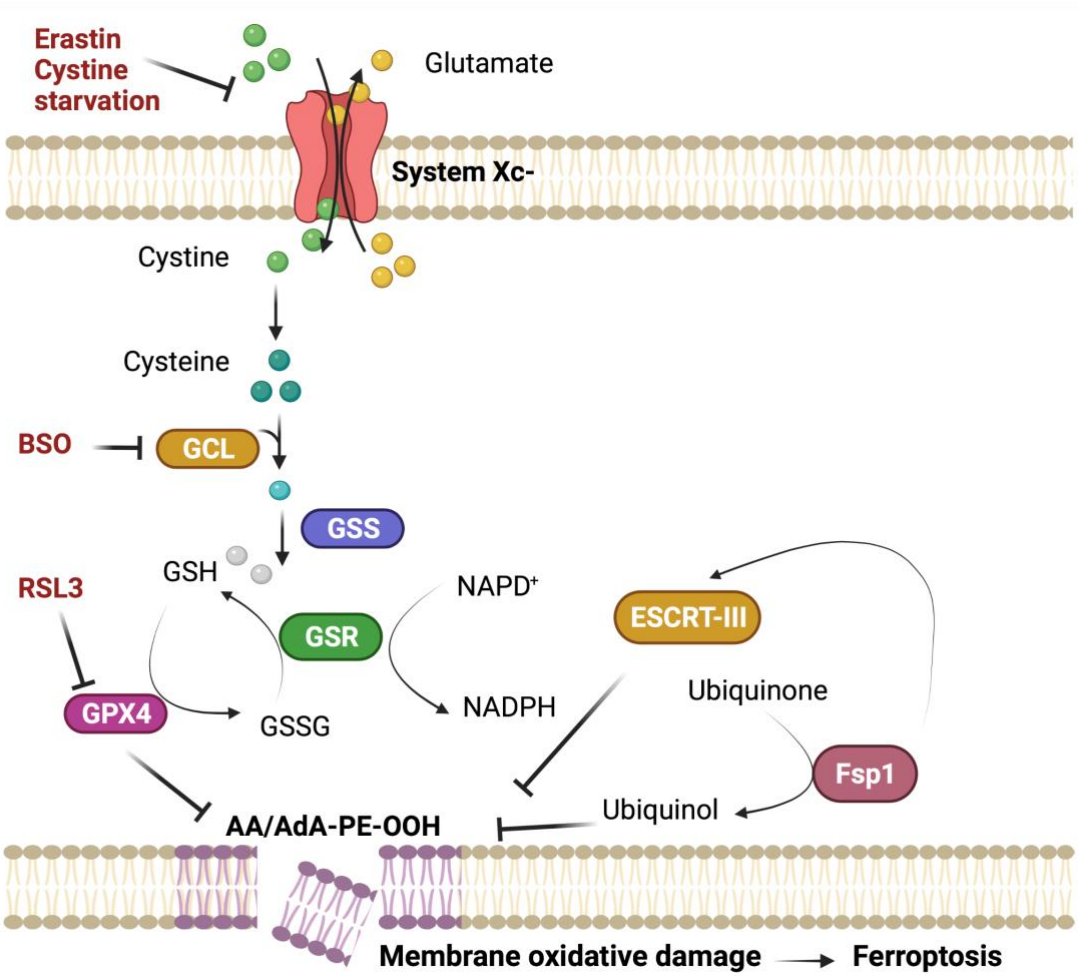

Figure 2. Ferroptosis pathway. Ferroptosis is characterised by the iron-dependent accumulation of lethal amounts of lipid ROS. To prevent constitutive membrane peroxidation. GPX4 counteracts lipid ROS accumulation by hydrolysing lipid peroxides converting them into their respective reduced forms (-OH). GPX4 requires glutathione as an electron donor, which upon oxidation (GSSG), is reduced to GSH by glutathione reductase (GR). GSH synthesis depends on the enzymes glutamate cysteine ligase (GCL) and glutathione synthetase (GSS) as well as on available intracellular cysteine pool. System xc- (SLC3A2 and SCL7A11/xCT) is an antiporter transmembrane protein that shuttles cystine into the cell in exchange for glutamate to feed the intracellular cystine pool. Fsp1 generates ubiquinol from ubiquinone (Coenzyme 10) which is a lipophilic radical trapping agent within membranes that protect cells from ferroptosis. Regardless of its oxidoreductase function, Fsp1 contributes to ferroptosis inhibition by activating the ESCRT-III-dependent membrane repair machinery. This figure was created using a licensed version of Biorender.com.

1.1.2.2. Relevance of ferroptosis *in vivo*

One of the key requirements for cell protection from ferroptosis is the availability of GSH, which serves as a cofactor for GPXs. As previously mentioned, for GSH synthesis is important to preserve a source of intracellular cystine, which is imported via xCT. This antiporter subunit is highly expressed in neurons, border

membranes of the kidney and duodenum and thyroid gland (Burdo et al., 2006; Sato et al., 2005). Its expression can be induced by oxidative stress stimuli such as hydrogen peroxide or oxygen, which leads to an increase in GSH synthesis (Sato et al., 2005; Sato et al., 2004). In agreement with its role in cystine import, xCT-deficient mice show increased cystine levels in blood plasma and decreased intracellular GSH levels in comparison to wild-type (WT) mice. However, *in vitro*, cellular cysteine levels are similar between knockout (KO) and WT cells generated from xCT-deficient mice, suggesting an activation of the compensatory cysteine synthesis through the transsulfuration pathway (Sato et al., 2005).

Downstream of GSH synthesis, GPX4 is a key regulator of ferroptosis. GPX4 has been reported to be essential for embryogenesis as *Gpx4* KO mice die before being born at gastrulation stage (Imai et al., 2003; Yant et al., 2003). Whole-body inducible *gpx4* knockout mice experience increased oxidative stress and mitochondrial dysfunction in *gpx4*-depleted organs, which leads to a decreased activity of the electron transport chain members complex I and IV. Interestingly, these evidences suggest that GPX4 is an important protector of mitochondrial integrity (Yoo et al., 2012). Adult mice die within two weeks by acute renal failure after systemic induction of *gpx4* KO, demonstrating the indispensable role of GPX4 also for adult tissue homeostasis (Angeli et al., 2014).

Ferroptosis is also linked to mediating tissue injury in various human pathologies. For example, it has been suggested to be responsible for neurodegeneration of motor neurons, which occurs in a range of neurodegenerative diseases such as amyotrophic lateral sclerosis (ALS) (Devos et al., 2019; Chen et al., 2015) and Huntington´s disease (Paul et al., 2014). Moreover, ferroptosis was demonstrated to be implicated in post-ischemic renal necrosis (Angeli et al., 2014, Linkermann et al., 2014) and to participate in several other malignancies, including carcinogenesis, stroke, intracerebral haemorrhage and traumatic brain injury, and ischemia-reperfusion injury (Stockwell et al., 2017; Halestrap et al., 2004).

Thereby, cellular protection from ferroptosis plays a crucial role for tissue homeostasis and embryogenesis and it is also important to prevent the development of different pathological conditions.

1.1.2.3. Ferroptosis and Mitochondria

Mitochondria are indispensable for most normal cell types due to their role in generating ATP through oxidative phosphorylation (OXPHOS) (Gao et al., 2015; Gao et al., 2019). However, this process comes at a cost of ROS production as a byproduct of OXPHOS (Are-Gomez et al., 2019). Moreover, mitochondria play an essential role in the regulation of several types of RCD, including ferroptosis, and consequently, in tissue homeostasis (Mattson et al., 2008; Xie et al., 2018). Indeed, mitochondria seem to be required for cystine deprivation-induced ferroptosis (CDI) (Gao et al., 2019). Interestingly, experimental inhibition of xCT was shown to induce mitochondrial fragmentation, mitochondrial ROS production, loss of the mitochondrial membrane potential (MMP) and ATP depletion (Zhou et al., 2019; Gao et al., 2019; Neitemeier et al., 2017; Xie et al., 2016; Yagoda et al., 2007; Yuan et al., 2016). Nevertheless, the regulation of some of these events remain unknown. It is still controversial whether the dysregulation of the mitochondrial homeostasis is able, per se, to induce ferroptosis or if is just a consequence of the activation of the cell death pathway. Supporting a requirement for mitochondrial metabolism in the execution of ferroptosis (Xie et al., 2016), the depletion of mitochondria via Parkin-mediated mitophagy *in vitro* or the inhibition of OXPHOS, rescued cells from ferroptosis induced by cystine deprivation or erastin treatment (Gao et al., 2019). Yet, in the initial characterisation of ferroptosis, mitochondrial DNA (mtDNA)-depleted $\rho 0$ cells remained sensitive to oxidative stress and ferroptosis induction (Dixon et al., 2012).

There seems to be a marked difference in the requirement for mitochondrial metabolism in the execution of ferroptosis depending on the strategy by which ferroptosis is triggered. When triggered by cystine starvation or by erastin, resulting in GSH depletion, activity of the mitochondrial tricarboxylic acid cycle (TCA) was shown to be necessary for ferroptosis induction (Gao et al., 2015). In fact, cancer cells deficient for the mitochondrial tumour suppressor fumarate

hydratase (FH), a metabolic enzyme of the TCA cycle, were unable to undergo ferroptosis upon cystine deprivation (Gao et al., 2019). Yet, when GPX4 was pharmacologically inhibited or deleted, cells underwent ferroptosis regardless of the TCA cycle, functional OXPHOS or mitochondria, suggesting GPX4 activity required for ferroptosis prevention to lie downstream of mitochondria (Gao et al., 2019) (**Figure 3**).

GPX4 is one of the major intracellular enzymes involved in hydrolysing lipid peroxides, thereby ensuring repair of lipid peroxide-perturbed cellular membranes. Although the current view of ferroptosis favours the idea of lipid peroxide accumulation in the plasma membrane leading to cellular rupture (Agmon et al., 2018), lipid peroxides have also been shown to accumulate in the mitochondrial membrane during ferroptosis (Yuan et al., 2016). In addition to 12/15-ALOX regulating this process, CDGSH iron sulfur domain 1 (CISD1) is an iron-containing protein whose N-terminus is inserted into the outer mitochondrial membrane (OMM) where it regulates mitochondrial iron uptake. Upon CISD1 deletion, iron accumulation inside the mitochondria facilitates the generation of mitochondrial lipid peroxides contributing to ferroptosis (Yuan et al., 2016). On the other hand, cholesterol hydroperoxide (ChOOH) species (5alpha-OOH, 6alpha/6beta-OOH, 7alpha/7beta-OOH) and phospholipid hydroperoxide (PLOOH) families (PCOOH, PEOOH, PSOOH) which are peroxidised in the cytosol can be transported to mitochondria via the sterol carrier protein 2 (SCP-2) upon cystine deprivation (Vila et al., 2004). This suggests a potential role for these lipid peroxides in mitochondria during ferroptosis triggered via this route (**Figure 3**).

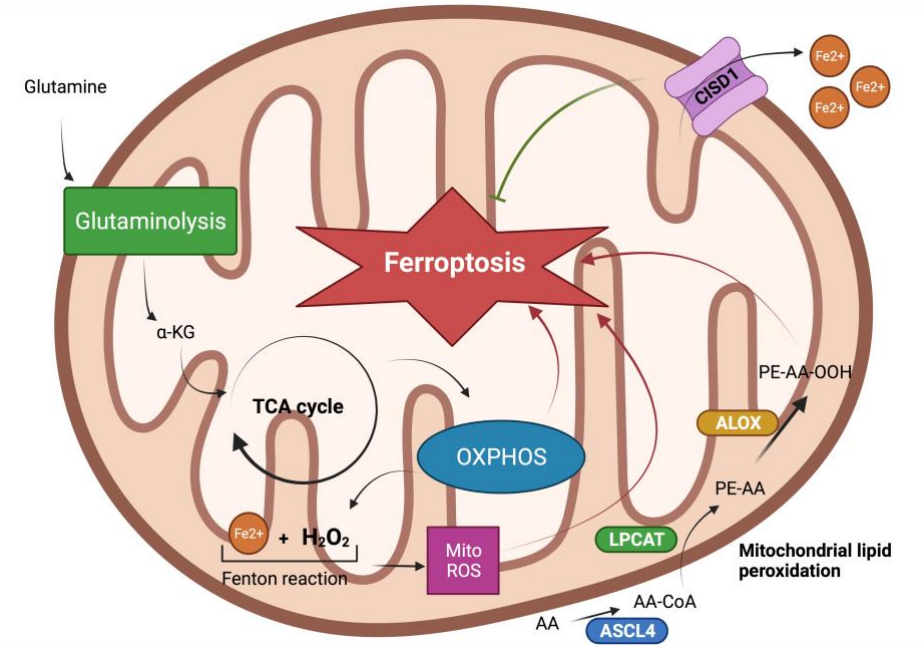

Figure 3. Mitochondria regulation in ferroptosis. Mitochondria play a pivotal role in cystine deprivation induced-ferroptosis (CDI), which, indeed, is associated with mitochondrial fragmentation and lipid peroxide accumulation (Gao et al., 2019). Mitochondrial iron storage contributes to the generation of mitochondrial ROS through Fenton Reaction, thereby promoting ferroptosis. OXPHOS, glutaminolysis and the tricarboxylic acid cycle (TCA) have been described to be essential for cysteine-deprivation-induced (CDI) ferroptosis but are not required for ferroptosis triggered by GPX4 inhibition. Glutamine is imported to mitochondria where through glutaminolysis is converted in CLopa (α-KG), providing fuel for the TCA cycle. Superoxide anion from the electron transport chain (ETC) is converted to H_2O_2 which takes part into Fenton Reaction. CISD1 regulates mitochondrial iron export, thus suppressing ferroptosis. ASCL4, LPCAT and ALOXs promotes lipid peroxidation, inducing ferroptosis. This figure was created using a licensed version of Biorender.com.

Importantly, the ultrastructural changes of mitochondria are considered one of the main morphological hallmarks of ferroptosis that is used to differentiate this cell death from apoptosis, necroptosis or autophagy (Wang et al., 2018). As previously mentioned, cells undergoing ferroptosis following erastin treatment report shrinkage of mitochondria, increased mitochondrial membrane density, reduction of their volume and mitochondrial cristae (Xie et al., 2016). In contrast, following erastin treatment no morphological features associated to necrosis, apoptosis or autophagy are observed (Dixon et al., 2012, Yu et al., 2017). The mitochondrial morphological changes in ferroptosis can be grouped based on the grade of mitochondrial fragmentation and their dissemination: (**i**) elongated mitochondria consistently distributed, (**ii**) fragmented mitochondria consistently distributed, (**iii**) fragmented mitochondria around the nucleus, (**iv**) small rounded

mitochondria around the nucleus (Neitemeier et al., 2017, Grohm et al., 2010, Jelinek et al., 2018). Mitochondrial fragmentation results from a misbalance between fusion and fission events. Of note, these events are regulated by different proteins of the Dynamin Superfamily members. Mitochondrial fusion is mediated by Mitofusin-1 (Mfn1) and 2 (Mfn2) and Optic-atrophy factor 1 (OPA-1) (Zuchner et al., 2004; Santel and Fuller, 2001; Alexander et al., 2000; Delettre et al., 2000; Cipolat et al., 2004), whereas mitochondrial fission, and along with that, fragmentation, are primarily regulated by dynamin-related protein 1 (Drp1) (Xie et al., 2018). Interestingly, homozygous *drp1* knockout mice are characterised by presenting developmental abnormalities related to defective mitochondrial fission and metabolism (Ishihara et al., 2009; Wakabayashi et al., 2009).

Taken together, mitochondrial metabolism is a main source of cellular ROS and contributes to ferroptosis in many cellular systems. However, mechanisms of how ferroptosis and mitochondria cross signal and whether xCT and GPX4 always signal in a single hierarchical pathway is poorly understood. Therefore, additional studies on the mechanistic contribution of mitochondria (including a potential role of Drp1 in regulating mitochondrial fragmentation) in ferroptosis are warranted.

1.2. Dynamin Superfamily Proteins

Dynamin superfamily proteins (DSPs) are large (~100 kDa) multidomain mechano-chemical GTPases that are mainly implicated in membrane remodelling events and can associate with microtubules *in vitro* (Shpetner et al., 1989; Obar et al., 1990). Dynamins are also known as `large GTPases´ to distinguish them from other families of G-proteins such us the small Ras superfamily, which are small monomeric GTPases (20-25kDa). Dynamins use the energy from the GTP hydrolysis to participate in fission and fusion events of cellular membranes, intracellular trafficking of vesicles and organelles and cell division (Praefcke et al., 2004; Faelber et al., 2013). Among the wide variety of biological processes regulated by dynamin proteins, it is important to highlight the endocytosis of the Tf-TFR1 complex, and the regulation of mitochondrial fission and fragmentation. Both processes are essential for ferroptosis, however, it has not been elucidated yet whether dynamin proteins participate in the ferroptosis pathway.

1.2.1. Structural features of dynamin superfamily proteins:

The members of this family of proteins are charaterised by sharing three conserved domains: N-terminal GTPase domain, middle domain (MD), and GTPase effector domain (GED) (**Figure 4**).

- **Amino-terminal or large GTPase domain (LG-domain):** this domain represents the most highly conserved domain (Niemann et al., 2001). The typical size of the GTPase domain is about 300 amino acid residues and contains five motifs (G1-G5) that are involved in nucleotide-binding (Saraste et al., 1990). Dynamin members are characterized by a high GTPase activity and simultaneous low affinity for GTP. Thereby, they have an overall low basal GTPase activity which is regulated by self-assembly or lipid binding. Mutations in the GTPase domain can lead to defective GTP binding rendering these mutants inactive (Anggono and Robinson, 2009).
- **Middle domain (MD) and GTPase effector domain (GED):** the LG-domain is followed by a middle domain and the GTPase effector domain. The MD domain is mainly involved in oligomerization into tetramers and/or

into higher-order-self-assembly such as rings or helices (Anggono and Robinson, 2009). The GED binds to the GTPase domain, to the MD, and to itself to form homodimers. These interactions mainly regulate the GTPase catalytic activity (Cao et al., 1998; Anggono and Robinson, 2009).

- **Pleckstrin-homology domain (PH):** it is only present in classical dynamins. The PH domain is implicated in the mediation of protein-protein and protein-phospholipid interactions, targeting their host proteins to phosphoinositide-containing membranes (Archiriloaie et al., 1999; Lemmon and Ferguson, 2000).
- **C-terminal proline-rich domain (PRD):** as well as the PH domain, the PRD is a component of the molecular structure of classical dynamins. It consists of a protein-protein interaction domain for signalling or cytoskeletal proteins.
- **Other effector and Regulatory regions: The A and B-inserts of dynamin-related proteins:** mammalian dynamin-related protein 1 and its orthologues contain various important inserts for regulating their function. For example, the short region in the Drp1 GTPase domain called A-insert, regulates G domain dimerization for mediating GTPase activity. Drp1 also presents a variable B-insert, which connects the MD and GED. This domain selectively binds the mitochondrion-specific phospholipid cardiolipin in the absence of target membrane interactions, and auto-inhibits Drp1 higher-order self-assembly (Ramachandran and Schmid, 2018).

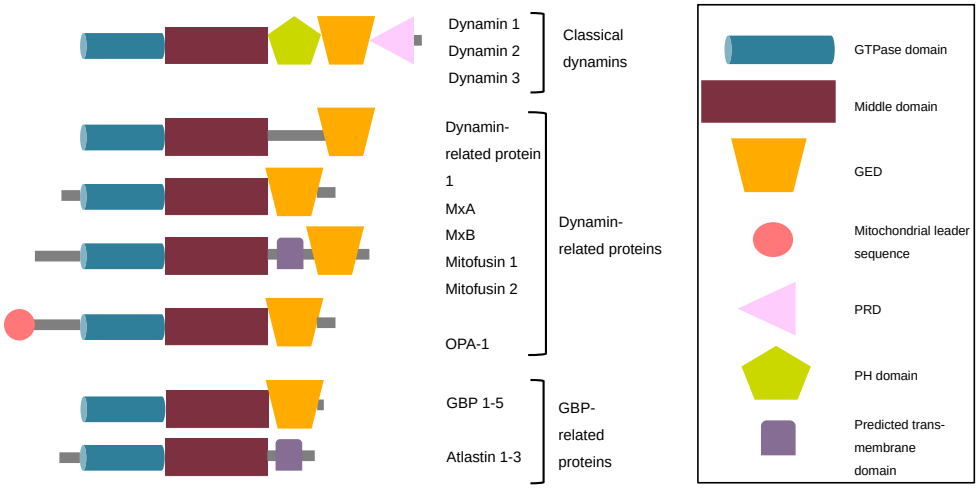

Figure 4. Domain structure of dynamin superfamily proteins. All dynamin superfamily members share three main domains; the GTPase domain, the middle domain (MD) and the GTPase effector domain (GED). Classical dynamins also contain a pleckstrin-homology (PH) domain and a C-terminal proline-rich domain (PRD). Other family members might have divergent and specific domains which provides them with different cellular functions or allow for concrete subcellular locations.

1.2.2. Biochemical and biophysical features of dynamin superfamily proteins

- **Oligomeric state, basal and assembly-stimulated GTPase activities:** in addition to having a larger GTPase domain, dynamin superfamily proteins are distinguished from other GTPases by their capability to self-assemble into oligomers that can form rings or helices. Indeed, their GTPase activation depends on their oligomerization state (Takei et al., 1995). Some DSPs present a basal GTP hydrolysis rate that is stimulated upon self-assembly. For example, the basal GTPase activity of Drp1 undergoes additional stimulation upon helical assembly on cardiolipin-containing liposomes or mitochondrial membranes (Ramachandran and Schmid, 2018). Besides that, dynamin superfamily proteins are characterised by their low nucleotide binding affinities, so they do not require guanine nucleotide exchange factors for catalysing nucleotide exchange (Krishnan et al., 2001).

- **Mechanism of GTP hydrolysis:** the GTPase domain comprises 4 motifs (G1-G4) that participate in specific interactions with the nucleotide base, sugar and phosphate moieties. There is a fifth motif, which is only conserved in a subset of DSPs, including Drp1, that can also interact with the base and/or sugar regulating the nucleotide-binding affinity. Homo-dimerization across the G domain nucleotide-binding pocket leads to GTP hydrolysis; however, the catalytic mechanisms vary among DSPs (Ramachandran and Schmid, 2018).

1.2.3. Overview of dynamin superfamily members

Based on DSPs structural similarity, these proteins can be classified into three groups; (**1**) Classical dynamins, (**2**) Dynamin-related proteins (Dlps) and (**3**) Guanylate-binding proteins (GBPs). All dynamin superfamily members share

two unique properties: self-assembly and the ability to bind and tubulate lipids, which allows them to be anchored in lipid membranes (Anggono and Robinson, 2009).

- **Classical dynamins:** mammalian dynamins are encoded by three different genes, *dynamin 1*, *2* and *3*, and constitute the main members of the dynamin superfamily. These large GTPases are approximately 100 kDa in size and are characterised by presenting five different domains: GTPase domain, middle domain, PH domain, GED and PRD domains. Dynamin 1 is the most studied isoform and is mainly expressed in the brain. Dynamin 2 is ubiquitously expressed and therefore, is present in all tissues, and dynamin 3 is predominantly expressed in testis and some regions of the brain (Nakata et al., 1993; Sontag et al., 1994; Gray et al., 2003). Mammalian dynamins 1 and 2 fulfil essential functions in cellular membrane shape regulation, including endocytosis of surface receptors via clathrin-coated vesicles (CCVs) and their membrane scission. Importantly, the best described clahtrin-dependent endocytosis process regulated by dynamin 1 and 2 is transferrin-transferrin receptor endocytosis, which represents the main iron uptake rout in cells (Shpetner and Vallee., 1992). Therefore, small molecules targeting dynamin 1 and 2 have been frequently used for the investigation of these processes worldwide. For example, dynasore, a classical dynamin inhibitor, was described to successfully block transferrin endocytosis and iron uptake (Macia et al., 2006; Prieto-Clemente et al., 2020).
- **Dynamin-related proteins:** as well as the classical dynamins, dynamin-related proteins are large in size (70-100 kDa) and are characterised by their low affinity for GTP and their high GTPase activity (Anggono and Robinson, 2009). However, in comparison to the five-domain definition for classical dynamins, dynamin-related proteins miss both, the PH and the PRD domain. They share the common feature to self-assemble into rings and an elevated GTPase activity afforded by assembly. Most of the dynamin-related proteins are implicated in the morphogenesis and maintenance of intracellular organelles such as mitochondria, the endoplasmic reticulum or peroxisomes (Gammie et al., 1995; Shin et al.,

1997; Kamimoto et al., 1998; Hong et al., 1998; Smirnova et al., 1998; Imoto et al., 1998; Labrousse et al., 1999; Wienke et al., 1999). So far, the most studied and well described dynamin related-protein is dynamin-related protein-1, mitofusins 1 and 2, optic-atrophy factor 1, Mx proteins and atlastins. Drp1 and Mx proteins are involved in organelle fission events, whereas Mfn1 and 2 and OPA-1 are proteins responsible for the fusion of mitochondrial inner and outer membranes, respectively (Anggono and Robinson, 2009; Merkwirth et al., 2008).

- **Guanylate-binding proteins:** the crystal structure of human GBPs places these proteins into the dynamin superfamily group. They are characterised by their low GTP-binding affinity and fast GTP hydrolysis. Moreover, the expression of GBPs is mainly induced by type II interferons (Staeheli et al., 1984; Anderson et al., 1999; Anggono and Robinson, 2009). As members of the dynamin superfamily of GTPases, GBPs exhibit such features as nucleotide-dependent oligomerization and concentration-dependent GTP activity (Vestal and Jeyaratnam, 2011). The main function of GBPs is involved in protection against intracellular pathogens. However, they are also implicated in the regulation of membrane, cytoskeleton and cell cycle progression dynamics (Honkala et al., 2020).

1.3. Dynamin related protein-1

In mammalian cells, Drp1 is the major protein that regulates mitochondrial fission. Under non-stimulated cellular conditions, and unlike other dynamin-related GTPases involved in mitochondrial dynamics, Drp1 is mainly located at the cytosol, with only approximately 3% of total protein associated with the outer mitochondrial membrane (Smirnova et al., 2001). Upon activation, Drp1 is recruited to the OMM, where it oligomerises into a spiral around GTP-dependent mitochondrial scission sites (Smirnova et al., 2001; Bui and Shaw, 2013).

Unlike other dynamin superfamily members, Drp1 does not comprise a lipid-binding domain, therefore, to oligomerising around the fission sites, it requires protein adaptors. In mammals, four protein adaptors/receptors of Drp1 have been described: mitochondrial fission factor (Mff), mitochondrial fission 1 protein (Fis1), mitochondrial dynamics of 49 kDa (MiD49) and mitochondrial dynamics of 51 kDa (MiD51) (Osellame et al., 2016). Mff and Fis1 are tail-anchored (TA) proteins that are also found in the ER and peroxisomes, where Drp1 also mediates fission events, whereas MiD49 and MiD51, are only present in mitochondria (Koch and Brocard, 2012; Schrader et al., 2016; Ji et al., 2017). Despite the absence of a lipid-binding domain, Drp1 can directly bind to cardiolipin (CL) and phosphatidic acid (PA) in the mitochondrial outer membrane through its B-insert (Bustillo-Zabalbeitia et al., 2014; Stepanyants et al.,2015). CL stimulates Drp1 oligomerisation, thereby its GTP hydrolysis activity, promoting the constriction of the lipid tubules formed by Drp1 oligomerisation (Stepanyants et al.,2015; Francy et al., 2017; Macdonald et al., 2014). Even though Drp1 can induce the tubulation and the constriction of liposomes it cannot complete their scission or induce small vesicle formation. Therefore, classical dynamin-2, is recruited to the mitochondrial division sites completing the mitochondrial scission (Lee et al., 2016).

PA also regulates mitochondrial fission through interactions with Drp1 (Adachi et al., 2016). Drp1 binds to liposomes that contains both unsaturated PA and saturated PA, but not to liposomes that consist of only one or the other. In contrast to CL, saturated PA inhibits Drp1 GTPase activity after its oligomerisation in the

OMM, making the mitochondria resistant to the fission induced by mitochondrial stress (Adachi et al., 2016).

1.3.1. Posttranslational modifications of Drp1

Dynamin-related protein 1 undergoes a wide variety of posttranslational modifications (PTMs) by different enzymes. These PTMs are essential for regulating its self-assembly order and the GTPase activity, and are implicated in both, physiological and pathological processes (Lackner and Nunnari, 2009; Santel et al., 2008; Chang et al., 2007). Among these covalent modifications are included protein phosphorylation, sumoylation, ubiquitination and *S*-nitrosylation (represented in **table 2**).

1.3.1.1. Protein phospho- and dephosphorylation

Protein phospho- and dephosphorylation are PTMs mediated by protein kinases and phosphatases, respectively. Among the PTMs on Drp1, phospho- and dephosphorylation are the most studied so far. As mentioned in previous sections, Drp1 is a cytosolic protein that must translocate to mitochondria to induce mitochondrial fission. This translocation mainly depends on its phopho/dephosphorylation state (Review. Giacomello et al., 2020).

The first reported Drp1 phosphorylation site was at Serine 616 by CDK1/Cyclin B. This mitotic phosphorylation promotes Drp1-dependent activation and mitochondrial fission, which leads to mitochondrial fragmentation in cells undergoing cell cycle division. Besides CDK1/cyclin B, other kinases involved in Drp1 phosphorylation at Ser616 have been identified: MAP kinase ERK1/2, protein kinase C δ (PKCδ), and calmodulin-dependent protein kinase II (CaMKII) (Qi et al., 2011; Yu et al., 2011; Xu et al., 2016; Bo et al., 2018). Interestingly, phosphorylation of Drp1 at Ser616 by CaMKII induces mitochondrial fission and the opening of mitochondrial permeability transition pores (mPTP) during chronic ß-adrenergic stimulation (ß-AR) (Xu et al., 2016). Massive or prolonged mPTP opening induced by mitochondrial fission leads to mitochondrial swelling, the releasing of cytochrome c and eventually to cell death. All these events are reported to be implicated in different pathological conditions such as heart disease or ischemia reperfusion injury (Halestrap et al., 2004; Ong et al., 2010).

Another Drp1 phosphorylation site that has been widely studied is Serine 637. This site was shown to be phosphorylated by protein kinase A (PKA) (Cribbs et al., 2007; Chang and Blackstone, 2007) and Ca2+/calmodulin-dependent protein kinase I α (CaMKIα) (Han et al., 2008). Phosphorylation at this position inhibits mitochondrial fission through a decrease in GTPase activity and/or inhibition of Drp1 translocation to mitochondria (Chang et al., 2007; Cribbs et al., 2007; Cereghetti et al., 2008). The same site can be dephosphorylated by the Ca^{2+} dependent phosphatase calcineurin and the mitochondrial phosphoglycerate mutase/protein phosphatase 5 (PGAM5), which participates as a convergent point for multiple necrotic cell death pathways (Chang et al., 2007; Cribbs et al., 2007; Cereghetti et al., 2008; Wang et al., 2012). Dephosphorylation of Drp1 at Ser637 has the same effect on Drp1 activity as its phosphorylation at Ser616 (Cereghetti et al., 2008; Wang et al., 2012).

1.3.1.2. Protein sumoylation

The small ubiquitin-like modifier (sumo) protein is also involved in Drp1 PTMs (Harder et al., 2004). Sumo attachment often influences subcellular localization of proteins or protects them from ubiquitin-mediated destruction. Interestingly, there is a BAX/BAK-dependent association of Drp1 at the mitochondrial membrane, with associated conjugation of Sumo to Drp1 (Wasiak et al., 2007). This modification occurs at the mitochondrial outer membrane (Braschi et al., 2009; Zunino et al., 2007). During regulated cell death, a mutated form of Drp1 protein that cannot be sumoylated did not exhibit differences in mitochondrial recruitment of Drp1, suggesting that sumoylation itself is not required for mitochondrial fission and fragmentation during programmed cell death (Figueroa-Romero et al., 2009). Sumoylation seems to occur within the B insert of Drp1, meaning that it may exert an effect on Drp1 interactions with the outer mitochondrial membrane lipids or others proteins.

1.3.1.3. Protein ubiquitination

The ubiquitination of Drp1 is mediated by an ubiquitinase ligase located at the mitochondrial outer membrane (Nakamura et al., 2006; Yonashiro et al., 2006; Karbowski et al., 2007). Some studies have proposed that Drp1 ubiquitination

enhances fission, possibly by facilitating trafficking of the protein to mitochondrial scission sites (Karbowski et al., 2007).

1.3.1.4. Protein *S*-Nytrosilation

Protein *S*-Nytrosilation is a redox-related modification of thiol groups by nitric oxide (NO) (Foster et al., 2009). The NO produced in response to ß-amyloid protein, a mediator in Alzheimer disease, induces mitochondrial fission and neuronal damage via *S*-Nitrosylation of Drp1 at cysteine 644 (Cho et al., 2009).

Protein	PTM	Biological effect
Dynamin-related protein 1	Phosphorylation (Ser616) by CDK1-cyclin B	Mitochondrial fission in mitotic cells
	Phosphorylation (Ser637) by PKA and CaMKIIα	Inhibits fission by reducing Drp1 GTPase activity
	Phosphorylation (Ser616) by CaMKII, MAP kinase ERK1/2 and PKCδ)	Activates fission by increasing Drp1 GTPase activity
	Dephosphorylation (Ser637) by calcineurin and PGAM5 (Phosphoglycerate mutase family member 5)	Activates fission
	Sumoylation	Regulates positively mitochondrial fission
	S-Nitrosylation (Cys644)	Increases Drp1 dimerization and mitochondrial fission
	Ubiquitylation	Targets Drp1 for proteasomal degradation

Table 2. Post-translational modifications of dynamin-related protein 1. This table summaries the main PTM of Drp1 and their most relevant biological effect (Giacomello et al., 2020).

1.3.2. Drp1 and mitochondrial membrane dynamics

The maintenance of a functional mitochondrial network is particularly important for highly metabolically active tissues such as neurons or cardiac muscles. These tissues consist of post-mitotic cells, which use the fusion and fission machinery to preserve mitochondrial function. Mitochondrial morphology and function depend on the balance between fusion and fission events. Whereas fusion induces the formation of a large and interconnected mitochondrial network that prevents the accumulation of defective mitochondria, mitochondrial fission segregates components of the mitochondrial network that are damaged or dysfunctional (Romanello and Sandri., 2016).

In mammalian cells, mitochondrial fission and fusion processes are regulated by members of the dynamin superfamily. Mitochondrial fusion is controlled by Mitofusins 1 and 2 and OPA-1 (Zuchner et al., 2004; Santel and Fuller, 2001; Alexander et al., 2000; Delettre et al., 2000; Cipolat et al., 2004), while mitochondrial fission is primarily mediated by the cytosolic GTPase dynamin-related protein 1 (Chen and Chan, 2009).

As already described, upon phosphorylation at Ser616 or dephosphorylation at Ser637(Yu et al., 2019), Drp1 translocates from the cytosol to the outer mitochondrial membrane, binding to its OMM receptors: Mff, MiD49, MiD51 and Fis1 (Otera et al., 2010; James et al., 2003; Palmer et al., 2011; Losón et al., 2013). Following this binding, Drp1 oligomerises forming linear polymers around the outer mitochondrial membrane. Subsequent GTP-hydrolysis induces polymers to short and curl into closed rings completing the mitochondrial constriction (Kalia et al., 2018). Importantly, the process of mitochondrial fission is much more complex than Drp1-mediated membrane scission. It is important to consider that OMM is engaged in an extended network of interactions with membranes of other organelles such as the endoplasmic reticulum (de Brito and Scorrano., 2008). In fact, in mammals, Fis1 was reported to regulate contacts with the ER and lysosomes (Smirnova et al., 2001; Wong et al., 2018). Indeed,

interactions with the ER are essential for Drp1-mediated mitochondrial fission. Moreover, the actin filaments along the ER-mitochondria contact site support the initial constriction of the mitochondrial membrane and the formation of Drp1 polymers (Cho et al., 2017; Pernas and Scorrano.,2016) (**Figure 5**).

A failure of OMM constriction in a Drp1-depdent manner can lead to organ dysfunction and degeneration (Vainshtein et al., 2014; Otera and Mihara et al., 2011; Romanello and Sandri., 2013). Strikingly, Drp1 was reported to play an essential role in diseases such as ischemia-reperfusion (I/R), Alzheimer´s disease, pulmonary arterial hypertension, and other lung diseases (Archer., 2013; Chen and Chan., 2009; Knott and Bossy-Wetzel., 2008; Liesa et al., 2009). Indeed, defects in Drp1-mediated mitochondrial fission events have been related to cell death processes. Of note, over the past decade, several studies have demonstrated the significance of Drp1 in regulating the initial stages of apoptosis. The pre-apoptotic pore-forming proteins BAX and BAK translocate to mitochondria and colocalize with Drp1 forming the mitochondrial fission sites (Maes et al., 2019). These foci act as fusion blockers, perturbing the balance between fusion and fission events and resulting in apoptotic mitochondrial fragmentation (Karbowski et al., 2004).

Hence, Drp1-mediated mitochondrial fragmentation is observed in various types of programmed cells death including necroptosis (She et al., 2019; Wang et al., 2012) or autophagy (Martinez et al., 2018; Breitzig et al., 2018). Interestingly, mitochondrial fragmentation can also be observed during ferroptosis (Dixon et al., 2012; Doll et al., 2017). However, the underlying regulatory mechanism of mitochondrial fragmentation during ferroptosis has not been elucidated yet.

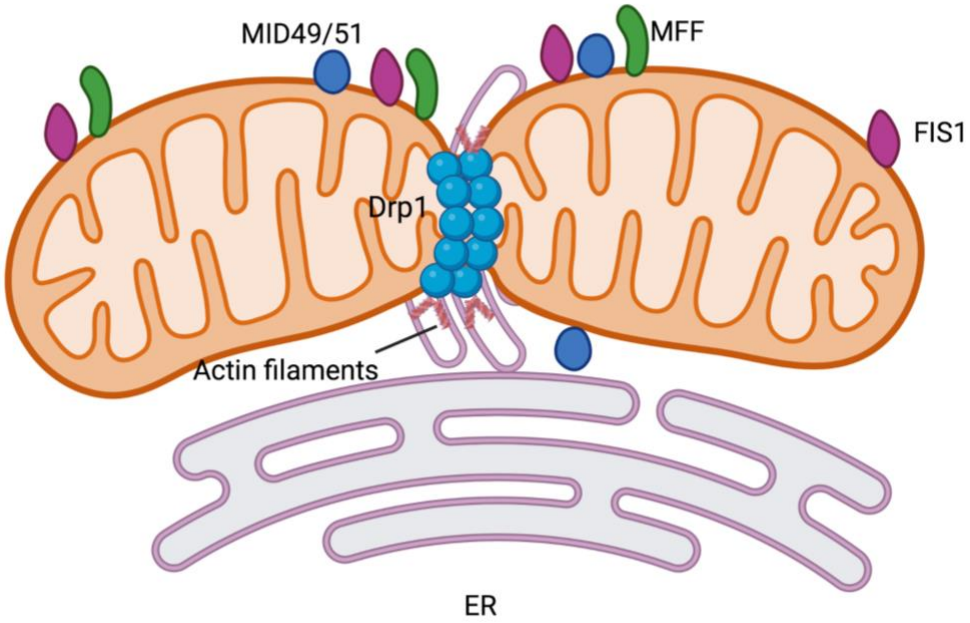

Figure 5. Dynamin related protein 1 and mitochondrial fission. Drp1 translocates to mitochondria by phosphorylation at Ser616 or dephosphorylation at Ser637. Following recruitment, Fis1, Mff and MiD49/51 are crucial for directing Drp1 to the fission site to form a multimer around the scission sites, which are in close contact with the ER. Actin filaments along ER-mitochondrial contact sites polimeryze between Drp1 and a membrane-bond protein on the ER, guiding and facilitating the initial constriction events. Subsequently, Drp1 hydrolyses GTP and mediates complete fission of the OMM. This figure was created using a licensed version of Biorender.com.

2. AIMS OF THE STUDY

Ferroptosis was first described as an iron-dependent form of regulated necrosis (Dixon et al., 2012). One characteristic hallmark of ferroptosis is the iron-dependent accumulation of peroxidised lipids (Agmon et al., 2018). The main cellular iron uptake route is via transferrin-transferrin receptor binding followed by endocytosis (Harding et al., 1983). Supporting the importance of this import route, both transferrin and transferrin receptor were shown to promote ferroptosis (Yang et al., 2008). Interestingly, transferrin receptor endocytosis is dependent on the GTPase dynamin 1 and 2 under steady-state turnover (Van and Stoorvogel, 2002). The small molecule dynasore, an inhibitor developed against dynamin 1 and 2 (Macia et al., 2006), was described to successfully block transferrin endocytosis and uptake. Intriguingly, dynasore has been shown to protect neurons from cell death after spinal cord injury (Li et al., 2017) and ischemia/reperfusion injury in mouse hearts, a type of tissue injury that is blocked by the ferroptosis inhibitor ferrostatin-1 (Li et al., 2019; Linkermann et al., 2014). However, iron uptake regulation by the large GTPases dynamin 1 and 2 and the implication of both proteins in ferroptosis until now has remained elusive.

A second characteristic hallmark of ferroptosis is the accumulation of cellular lipid reactive oxygen species (ROS) that overcome glutathione-aided anti-oxidant defense. Lipid ROS species are generated from different steps of cellular metabolism, nevertheless, mitochondrial oxidative metabolism turns to be essential for cysteine-deprivation-induced ferroptosis. Moreover, mitochondrial fragmentation and morphological changes of mitochondria are known to occur in different programmed cell death pathways, including ferroptosis (Cereghetti et al., 2010; Xie et al., 2018). Mitochondrial fission and, along with that, fragmentation is mainly regulated by the large GTPase dynamin-related protein 1 (Xie et al., 2018). Interestingly, homozygous knockout mice are embryonically lethal due to severe developmental abnormalities related to defective mitochondrial fission and metabolism (Ishihara et al., 2009; Wakabayashi et al., 2009). However, heterozygous *Drp1* knockout mice, survive and show lower levels of H_2O_2 and lipid peroxides in tissues in comparison to the wild type (Manczak et al., 2012). Collectively, these findings suggest a functionality of Drp1 in fragmenting

mitochondria, promoting ROS generation and interestingly also lipid peroxidation *in vivo*. Although accumulating evidence supports an important role for mitochondria in CDI-ferroptosis, several important aspects of mitochondrial involvement in ferroptosis (including a potential role of Drp1 in regulating ferroptosis) are only poorly understood.

Therefore, this work aims to:

I. Investigate the impact of iron uptake regulation by the classical dynamins 1 and 2 on ferroptosis
II. Study the implication of Drp1 in ferroptosis
III. Mechanistically define and characterise the early crucial steps involved in Drp1 activation during ferroptosis
IV. Elucidate the functional consequence of Drp1 activation in its ferroptosis-induced activation

3. RESULTS

3.1. Dynasore is a new highly effective inhibitor of ferroptosis that blocks cell death through modulation of iron uptake and ROS scavenging (Prieto-Clemente et al., 2020)

To achieve our aims, we first needed to set up a cellular system that was sensitive to ferroptosis. Therefore, we tested a panel of KRAS-mutant lung cancer cell lines for their response to erastin, which has been shown to inhibit system xCT, thereby inducing ferroptosis (Dixon et al., 2014). Most cell lines tested showed a concentration-dependent decline in cell viability after exposure to erastin **(Figure 6.a)**. Loss of viability could partially be rescued by the lipophilic antioxidant ferrostatin-1 (Fer-1), suggesting that these cells may be sensitive to ferroptotic cell death **(Figure 6.b).** Thus, the non-small cell lung cancer cell lines A549 and H441 were chosen for further analysis, as they demonstrated to be the most erastin-sensitive cell lines **(Figure 6.b).** We next wanted to elucidate whether erastin could induce other types of regulated cell death. Importantly, erastin-induced cell death, as quantified by propidium iodide (PI) uptake, was entirely rescued by Fer-1 but not by the pan-caspase inhibitor zVAD or the RIPK1 inhibitor necrostatin-1 (Nec-1s). Thus, as apoptotic cell death is dependent on caspase activity and necroptosis on RIPK1 activity, we could exclude apoptotic and necroptotic cell death, further proposing ferroptotic cell death to be induced by erastin treatment in these cells **(Figure 6.c.)**. One of the main hallmarks of ferroptosis is the aberrant accumulation of Lipid ROS species (Dixon et al., 2012). To further confirm that erastin induces ferroptosis in our cells, we studied the accumulation of Lipid ROS levels upon erastin treatment. Indeed, after 16 h treatment, we could observe an increase in lipid ROS levels which were efficiently counteracted by ferrostatin-1 (**Figure 6.d**).

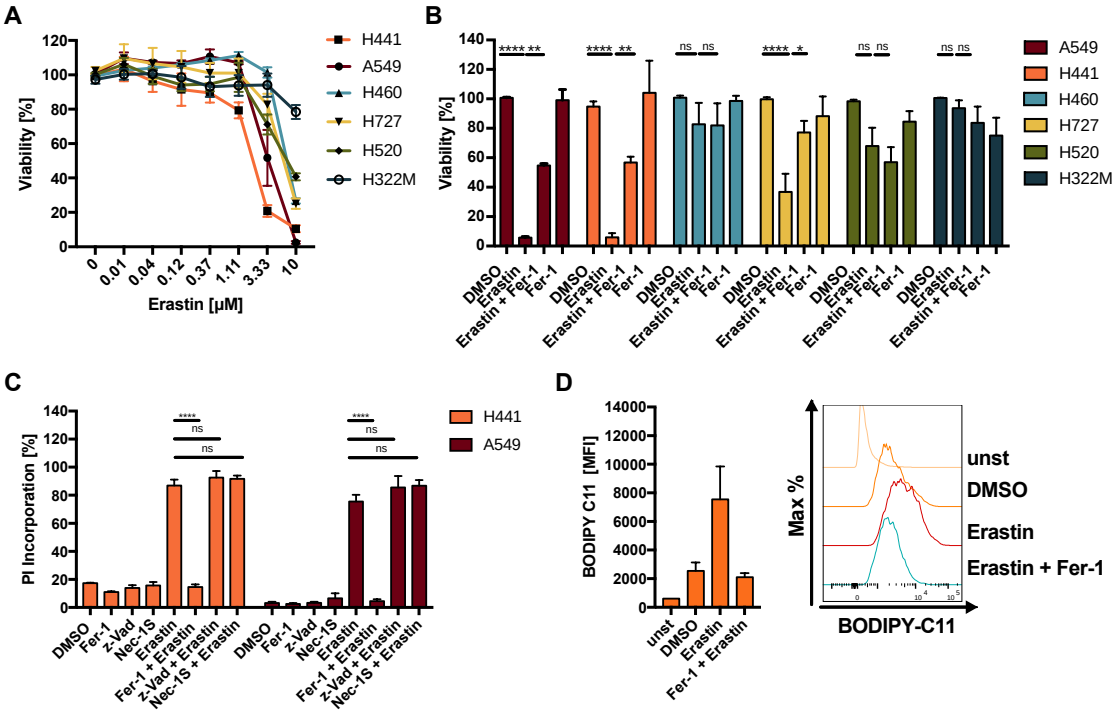

Figure 6. Erastin induced cell death is reverted by Ferrostatin-1 in the non-small cell lung cancer cell lines H441 and A549 (**a**). The indicated panel of non-small cell lung cancer cell lines was treated with different concentrations of erastin. The drug was titrated starting from a concentration of 10 µM. Cell viability was measured by Cell Titer Blue (**b**). Indicated cells were treated with erastin (10 µM) alone or in combination with ferrostatin-1 (5 µM) for 48 h. Cell viability was quantified as in ***a*** (**c**). H441 and A549 cells were treated with DMSO, ferrostatin-1 (5 µM), erastin (10 µM), zVAD (20 µM), Nec-1 (20 µM) or the indicated combinations for 48 h. Cell death was quantified by propidium iodide (PI) uptake and flow cytometry (**d**). Indicated cells were treated with erastin (10 µM) for 16 h to induce lipid ROS accumulation. During the last 30 min, BODIPY-C11 was added at 5 µM to each well. Mean fluorescence intensity (MFI) was quantified by flow cytometry. All data are means +/− standard error mean (SEM) of at least three independent experiments. * indicates p<0.05; ** indicates p<0.01; *** indicates p<0.001; **** indicates p<0.0001; ns indicates non-significant differences. Figure adapted from Prieto Clemente et al. 2020 Cells.

3.1.1. Dynasore blocks transferrin receptor uptake and ferroptosis

Upregulation of transferrin and transferrin receptor 1 (TFR1) have been shown to promote ferroptosis (Yang et al., 2008; Gao et al., 2015). TFR1 (CD71) has long been used as bona-fide surface receptor in mechanistic studies on endocytosis. Dynamin 1 and 2 are known to mediate terminal membrane fission during clathrin-mediated endocytosis (CME) of transferrin receptor (Cocucci et al., 2014). Therefore, we tested whether short-term dynamin-regulated TFR1 endocytosis would affect ferroptosis signaling. First, we studied how the inhibition of dynamin 1 and 2-either by siRNA-mediated suppression or by using

the well-established classical dynamin 1 and 2 inhibitor dynasore- could influence TRF1 turnover in our cellular system. To test that, we measured CD71 levels on the cell surface and we quantified its expression by flow cytometry. Indeed, the erastin-sensitive cell line H441 expressed TFR1 (CD71) on the surface and siRNA-mediated suppression of dynamin 1 and 2 elevated this expression (**Figure 7.a**), confirming a role for dynamin 1 and 2 in steady-state turnover of CD71 surface levels in these cells. In line with this data, the inhibitor dynasore also increased surface levels of CD71, supporting a functionality of dynamins in the endocytosis of CD71 (**Figure 7.b**). Next, we analysed whether the pharmacological inhibition of either dynamin 1 or dynamin 2 by dynasore treatment could affect ferroptosis induction. Strikingly, co-treatment with dynasore entirely blocked ferroptosis induced by erastin or by the GPX4 inhibitor RSL3 in a range of different lung cancer cell lines (**Figure 7.c**). Importantly, despite the fact that dynasore is commonly used at 80 µM to efficiently block dynamin 1 and 2, dynasore also potently inhibited ferroptosis at a range of lower concentrations (**Figure 7.d**). Lastly, in time-lapse imaging experiments, dynasore efficiently blocked RSL3 and erastin-induced ferroptosis, comparable to ferroptosis blockade by Fer-1, whereas zVAD did not affect cell death induction (**Figure 7.e**). Taken together, these data identify dynasore as a highly effective inhibitor of ferroptosis in various cellular systems.

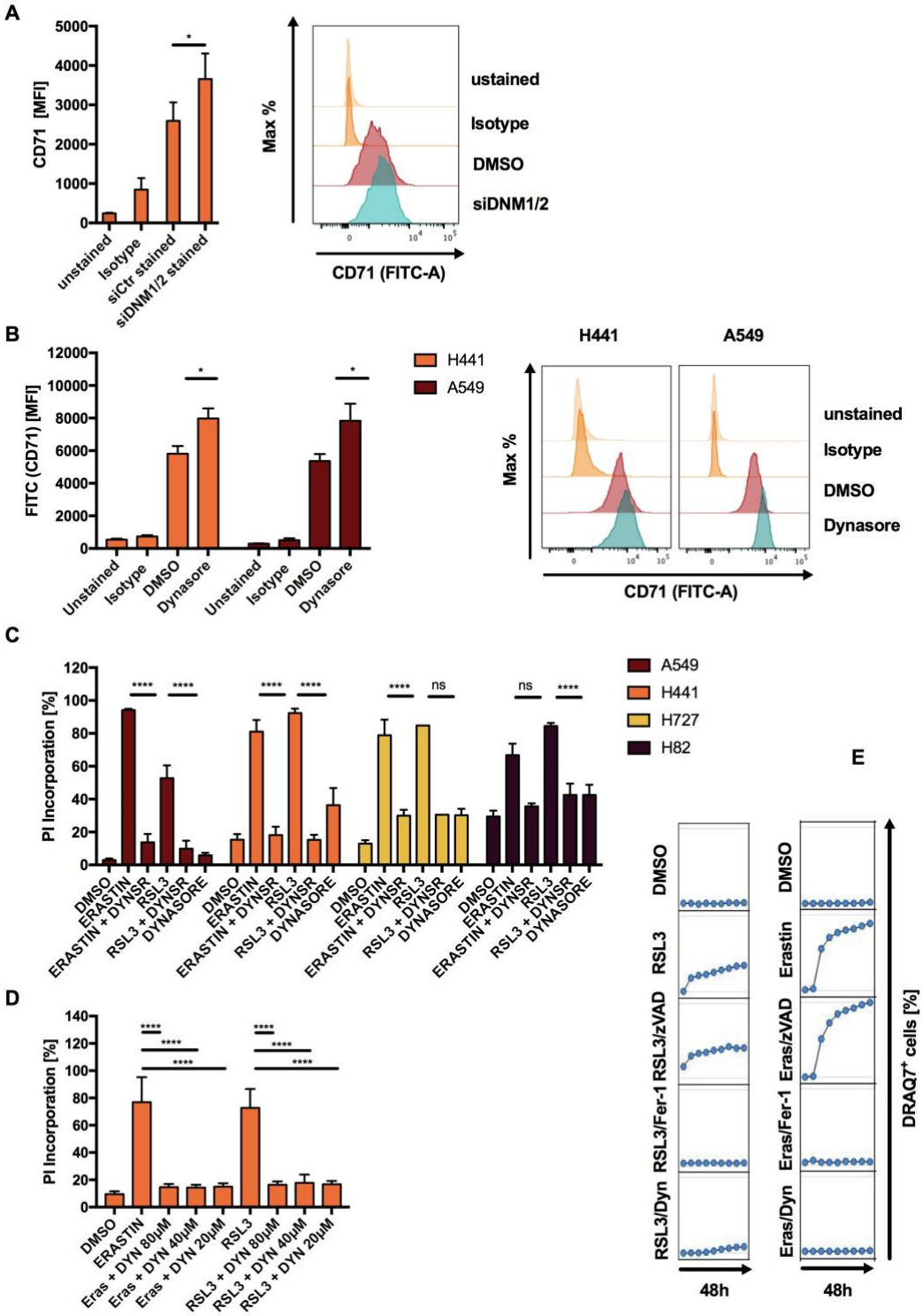

Figure 7. Dynasore blocks transferrin receptor uptake and ferroptosis (**a**). H441 cells were transfected with control or dynamin 1 and 2 (DNM1-2)-targeting small interfering RNA (siRNA) for 72 h. Surface expression of CD71 was determined by CD71 specific antibody staining and flow cytometry (**b**). Indicated cells were treated with dynasore for 48 h. Surface expression of CD71 was quantified as in ***a*** (**c**). Cells were treated as indicated but replacing ferrostatin-1 by dynasore (80 µM) and cell death was quantified by propidium iodide (PI) uptake and flow cytometry (**d**). H441 cells were treated with DMSO, erastin (10 µM), RSL3 (1 µM) +/- the indicated concentrations of dynasore for 48 h. Cell

death was quantified as in ***c***. (**e**) A549 cells were treated with DMSO, ferrostatin-1 (5 μM), erastin (10 μM), zVAD (20 μM), dynasore (80 μM) or the indicated combinations. Images were acquired every 8 h for 48 h. Dead cells were quantified as % DRAQ7 + cells using the IncuCyte image analysis software. All data are means +/− standard error of the mean (SEM) of at least three independent experiments, or representative images where applicable. MFI—mean fluorescence intensity. * indicates p<0.05; ** indicates p<0.01; *** indicates p<0.001; **** indicates p<0.0001; ns indicates non-significant differences. Figure adapted from Prieto-Clemente et al., 2020 Cells.

3.1.2. Direct inhibition of Clathrin-Mediated Endocytosis does not block transferrin receptor uptake and ferroptosis

Since dynamin 1 and 2 can regulate the early steps in the scission of the clathrin coated pits containing CD71, we next studied whether general inhibitors of endocytosis could also block ferroptosis as efficiently as dynasore did. To test that, we made use of the small molecule Pitstop-2, a novel and selective cell-permeable clathrin mediated endocytosis inhibitor. Pitstop-2 competitively inhibits clathrin terminal domains to selectively inhibit clathrin-mediated endocytosis (CME) (Dutta et al., 2012). Interestingly, Pitstop-2 could not block RSL3 or erastin-induced ferroptosis **(Figure 8.a)**. Moreover, we quantified CD71 levels on the surface of the cells upon Pitstop-2 treatment, but, as expected, we did not observe an increase in CD71 levels **(Figure 8.b)**. Together these data suggest that, whereas the general inhibition of CME does not influence ferroptosis induction nor significantly influences CD71 surface levels in these cells, the specific blockade of CD71 turnover might be required for the pathway. To support our hypothesis, we next used a second dynamin 1 and 2 inhibitor. We chose the small molecule Dynole 34-2, a potent cell-permeable dynamin 1 and 2 inhibitor that targets the GTPase domain at the allosteric site (Robertson et al., 2014). It potently inhibits receptor-mediated and vesicle endocytosis and is 15-fold more active than dynasore against dynamin 1. As expected, similar to dynasore, dynole 34-2 inhibited both, erastin and RSL3-induced ferroptosis (**Figure 8.c**). Thus, two distinct inhibitors of dynamin 1 and 2 but not the broad inhibition of CME were capable of blocking ferroptosis.

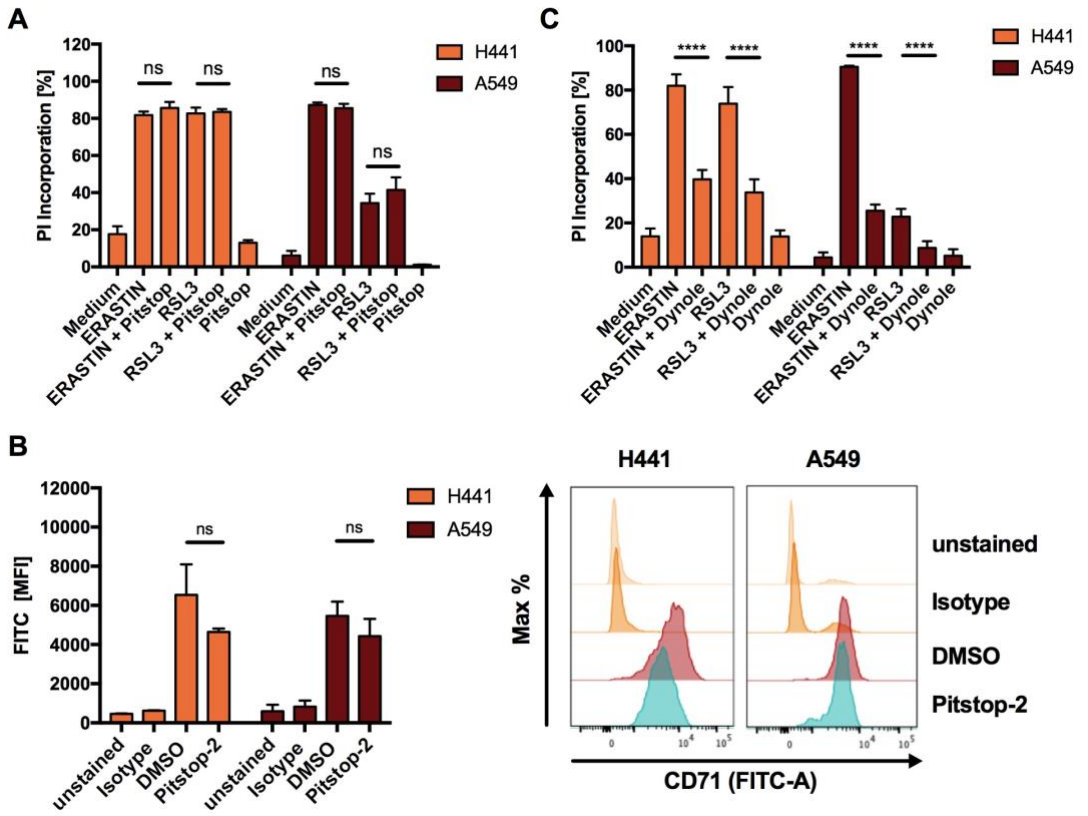

Figure 8. Inhibition of Clathrin-mediated endocytosis does not block transferrin receptor uptake and ferroptosis (**a**). H441 and A549 were treated as indicated with DMSO, erastin (10 µM), RSL3 (1µM) and Pitstop-2 (10 µM) for 48 h. Cell death was quantified by propidium iodide (PI) uptake and flow cytometry (**b**). Indicated cells were treated with Pitstop-2 (10 µM) for 48 h. Surface expression of CD71 was determined by CD71 staining and flow cytometry (**c**). H441 and A549 were treated as indicated in ***a*** but replacing Pitstop-2 by Dynole 34-2 (5 µM). Cell death was quantified as in ***a***. All data are means +/− standard error of the mean (SEM) of at least three independent experiments. MFI—mean fluorescence intensity. * indicates p<0.05; ** indicates p<0.01; *** indicates p<0.001; **** indicates p<0.0001; ns indicates non-significant differences.

3.1.3. Inhibition of Dynamin 1- and 2 impairs iron uptake but is insufficient to block ferroptosis

To validate whether dynasore-mediated inhibition of ferroptosis was mediated by its on-target activity against dynamin 1 and 2, we next performed siRNA-mediated silencing of dynamin 1 and 2 (**Figure 9.a)**. First, we validated whether iron import was compromised by suppression of dynamin 1 and 2. In order to do that, we made use of the heavy metal indicator dye Phen Green SK diacetate (PG-SK), of which the fluorescence has been shown to be quenched by intracellular labile iron pools (Yang et al., 2008; Du et al., 2015). As expected, since CD71 turnover was regulated by dynamin 1 and 2 in our cells (**Figure**

7.a,b), suppression of dynamin 1 and 2 resulted in a loss of fluorescence quenching and thereby increased fluorescent signal, suggesting a decrease in intracellular labile iron pools (**Figure 9.b)**. Similarly, dynasore treatment also induced a comparable loss of fluorescent quenching, yet neither dynamin silencing nor dynasore treatment were as efficient as the iron-selective chelating agent DFO in decreasing intracellular iron pools (**Figure 9.c).**

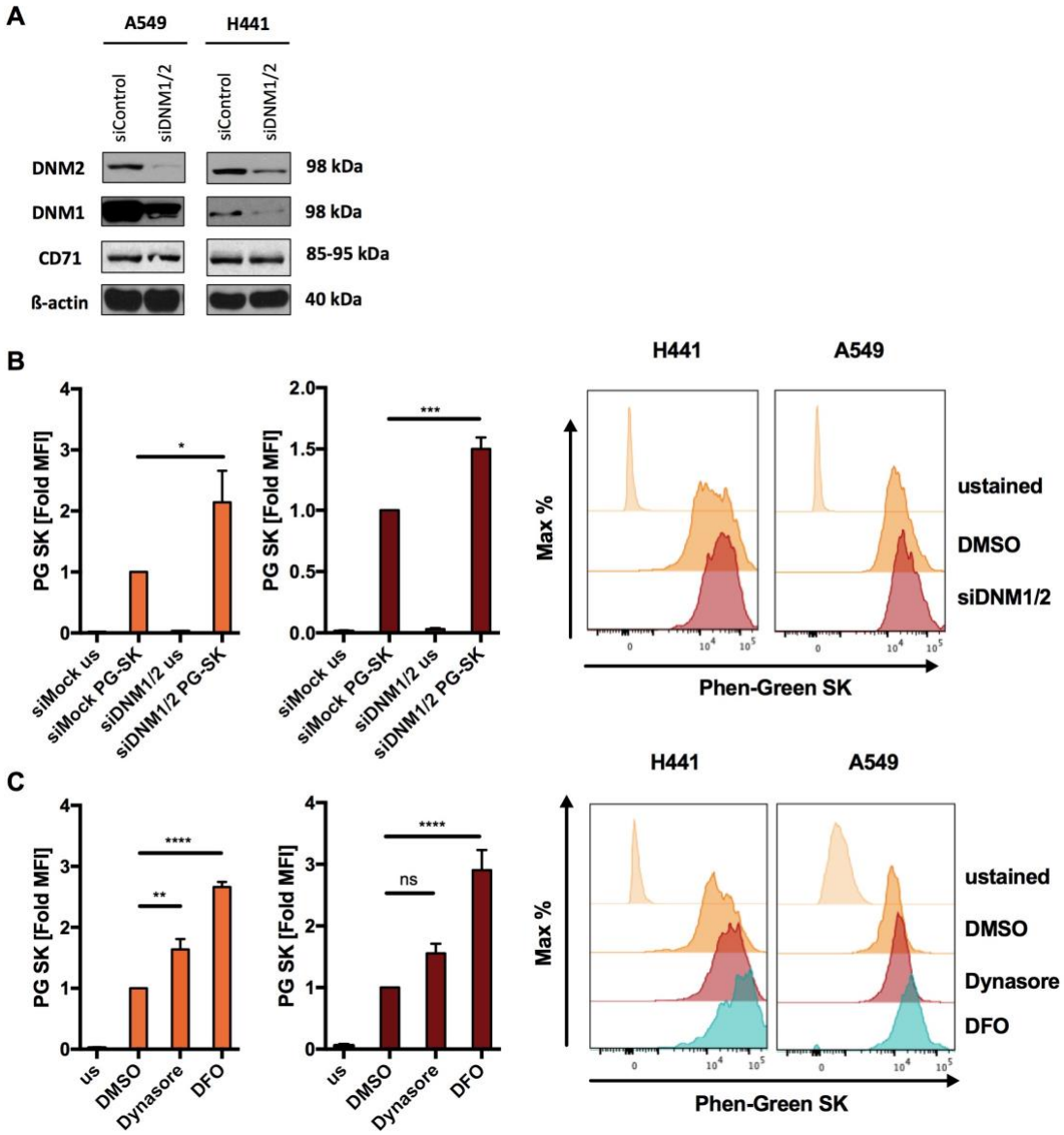

Figure 9. Suppression of Dynamin 1- and 2 expression impairs iron uptake (**a**). Indicated cells were subjected to control or dynamin 1 and 2 (DNM1-2)-targeting siRNA for 72 h, a representative blot is shown (**b**). Cells as in ***a*** were stained by Phen Green SK (PG SK). Fold mean fluorescence intensity (MFI) was determined by flow cytometry (**c**). H441 and A549 cells were treated with dynasore (80µM) or DFO (100 µM) for 48 h. MFI was determined as in ***b***. All data are means +/− standard error of the mean (SEM) of at least three independent experiments. MFI—mean fluorescence intensity. * indicates p<0.05; **

indicates p<0.01; *** indicates p<0.001; **** indicates p<0.0001; ns indicates non-significant differences. Figure adapted from Prieto-Clemente et al., 2020 Cells.

Since siRNA-mediated suppression of dynamin 1 and 2 as well as dynasore treatment reduced cellular iron pools (**Figure 9**), we hypothesised that both, dynamin 1 and 2 might promote ferroptotic cell death. Therefore, we next analysed whether silencing of dynamin 1 or 2 by siRNA could affect ferroptosis induction using flow cytometry. Strikingly, despite decreasing intracellular iron pools, neither RSL3- nor erastin-induced cell death were rescued by dynamin 1 and 2 silencing (**Figure 10.a,b)**. Moreover, RSL3-induced lipid ROS accumulation was also not rescued by dynamin 1 and 2 silencing, suggesting that in our cellular system, dynamin-mediated short-term extracellular iron uptake is dispensable for ferroptosis execution (**Figure 10.c)**.

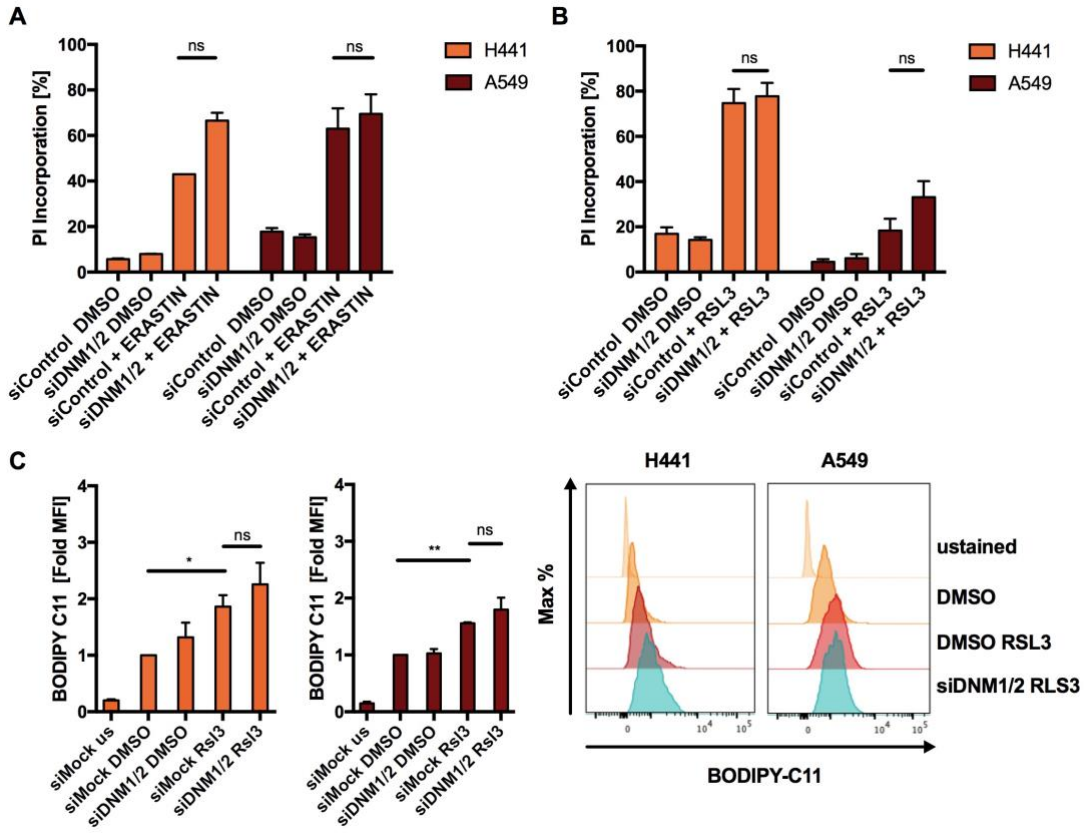

Figure 10. Suppression of Dynamin 1-and 2 expression is insufficient to block ferroptosis (**a,b**). H441 and A549 cells were subjected to control or dynamin 1 and 2 (DNM1-2)-targeting siRNA for 72 h and were treated with DMSO, erastin (10 µM) or RSL3 (1 µM) for 48 h. Cell death was determined by propidium iodide (PI) uptake and flow cytometry (**c**). Indicated cells were treated with RSL3 (1µM) for 5 h to induce lipid ROS accumulation. During the last 30 min, BODIPY-C11 was added at 5 µM to each well. Mean fluorescence intensity (MFI) was quantified by flow cytometry. All data are means +/− SEM of at least three independent experiments. * indicates p<0.05; ** indicates p<0.01; ***

indicates p<0.001; **** indicates p<0.0001; ns indicates non-significant differences. Figure adapted from Prieto Clemente et al. 2020 Cells.

These data strongly suggested that the on-target activity of dynasore against dynamin 1 and 2, the resulting increase in CD71 levels on the cell surface and the consequent decrease in intracellular iron levels, are not sufficient to explain the strong ferroptosis inhibitory effect observed with dynasore. Collectively, we hypothesised that the inhibition of ferroptosis by dynasore must additionally depend on off-target effects and/or side effects that have not been elucidated yet.

3.1.4. Dynasore functions as a broadly effective radical-trapping agent in cell-free assays

During ferroptosis, lipid ROS accumulation has been proposed to result in plasma membrane rupture and cell death (Dixon et al., 2012). Dynasore can efficiently block both, erastin and RSL3-induced-ferroptosis (**Figure 7**), but its on target activity against dynamin 1 and 2 is insufficient to block ferroptosis (**Figure 10**). Based on our data, we next investigated whether dynasore´s inhibitory effect could be linked to ROS and Lipid ROS production. To achieve that, we first measured the accumulation of Lipid ROS levels upon ferroptosis induction by BODIPY-C11 staining. Indeed, RSL3- and erastin-induced accumulation of lipid ROS was entirely rescued by dynasore co-treatment (**Figure 11.a,b**). Moreover, we made use of the cell permeable and fluorescent ROS indicator H2DCFDF, which becomes fluorescent when oxidised. Strikingly, we found that dynasore not only strongly inhibited overall cellular ROS induced by RSL3 or erastin treatment, but also significantly lowered the amount of basal ROS present in cells without RSL3 or erastin treatment (**Figure 11.c,d**). The chemical structure of dynasore suggested the possibility that it may function as a direct ROS scavenger via its phenol or amine moiety (Kareem et al., 2015). Therefore, our collaborators from the laboratory of Prf. Dr. Carsten Culmsee performed an assay to test whether dynasore can directly scavenge ROS in cell-free systems. Interestingly, dynasore reduced the stable radical 2,2-diphenyl-1-picrylhydrazyl (DPPH) almost as efficiently as Trolox, a well-established antioxidant vitamin E derivative and blocker of ferroptosis (**Figure 11.e)**.

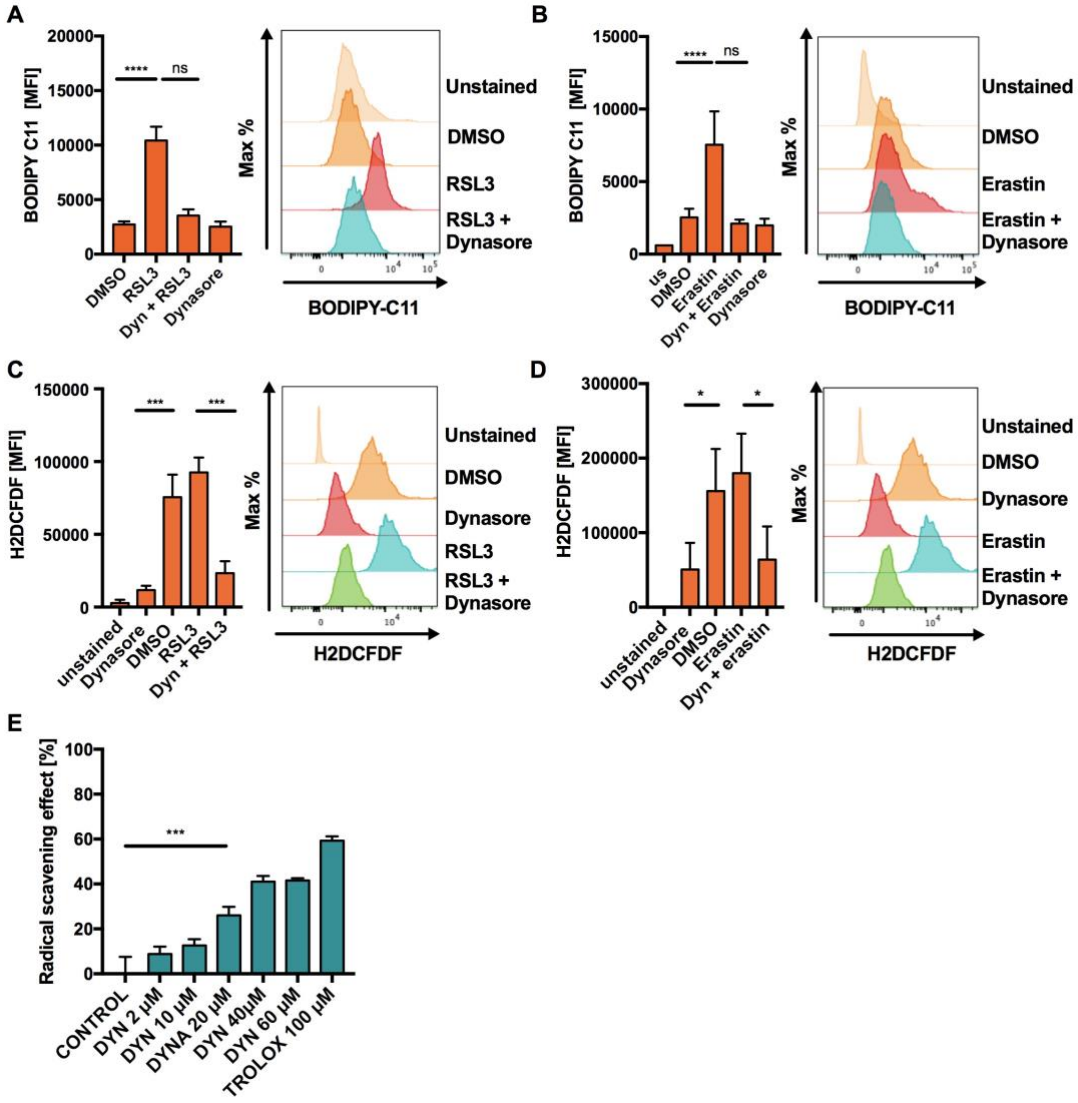

Figure 11. Dynasore functions as a broadly active radical scavenger (**a,b**). H441 cells were treated with RSL3 (1µM) for 5 h or erastin (10 µM) for 16 h. During the last 30 min BODIPY-C11 was added at 5 µM to each well. Mean fluorescence intensity (MFI) was quantified by flow cytometry (**c**). Indicated cell lines were treated with DMSO, RSL3 (1 µM), dynasore (80 µM) or both for 5 h and 48 h, respectively. During the last 30 min H2DCFDF was added at 20 µM to each well (**d**). Indicated cell lines were treated with DMSO, erastin (10 µM), dynasore (80 µM) or both for 16 h and 48 h, respectively. During the last 30 min H2DCFDF was added at 20 µM to each well. Mean fluorescence intensity (MFI) was quantified by flow cytometry (**e**). Dynasore (2–60 µM) and Trolox (100 µM) were incubated with DPPH (100 µM) for 30 min in the dark, then absorbance was measured at 517 nm to determine radical scavenging activity. All data are means +/− SEM of at least three independent experiments. * indicates p<0.05; ** indicates p<0.01; *** indicates p<0.001; **** indicates p<0.0001; ns indicates non-significant differences. Figure adapted from Prieto Clemente et al. 2020 Cells.

3.1.5. Dynasore is a highly active pan-ROS cell death blocker

Given that dynasore demonstrated to be a strong general ROS scavenging agent in cells and cell-free systems (**Figure 11**), we next tested whether dynasore may protect cells also from non-ferroptotic oxidative cell death induced by hydrogen peroxide (H_2O_2), which unlike ferroptosis does not rely on lipid ROS formation or iron (Dixon et al., 2012). Interestingly, dynasore also potently blocked H_2O_2-induced cell death (**Figure 12.a,b)**. Lastly, we performed a time-lapse imaging experiment where we induced either ferroptosis or H_2O_2-induced cell death with or without the general antioxidant N-acetylcysteine (NAC), the pan-caspase inhibitor z-Vad or dynasore as cell death inhibitors. Indeed, while NAC—known to block H_2O_2-induced cell death—was very ineffective in blocking RSL3-induced ferroptosis and Fer-1 was ineffective at blocking H_2O_2-induced cell death, dynasore was highly effective in blocking both types of cell death (**Figure 12.c,d).** Together, these data identify dynasore as a highly active pan-ROS cell death blocker which is equally potent in inhibiting cell death executed by lipid ROS as well as general ROS.

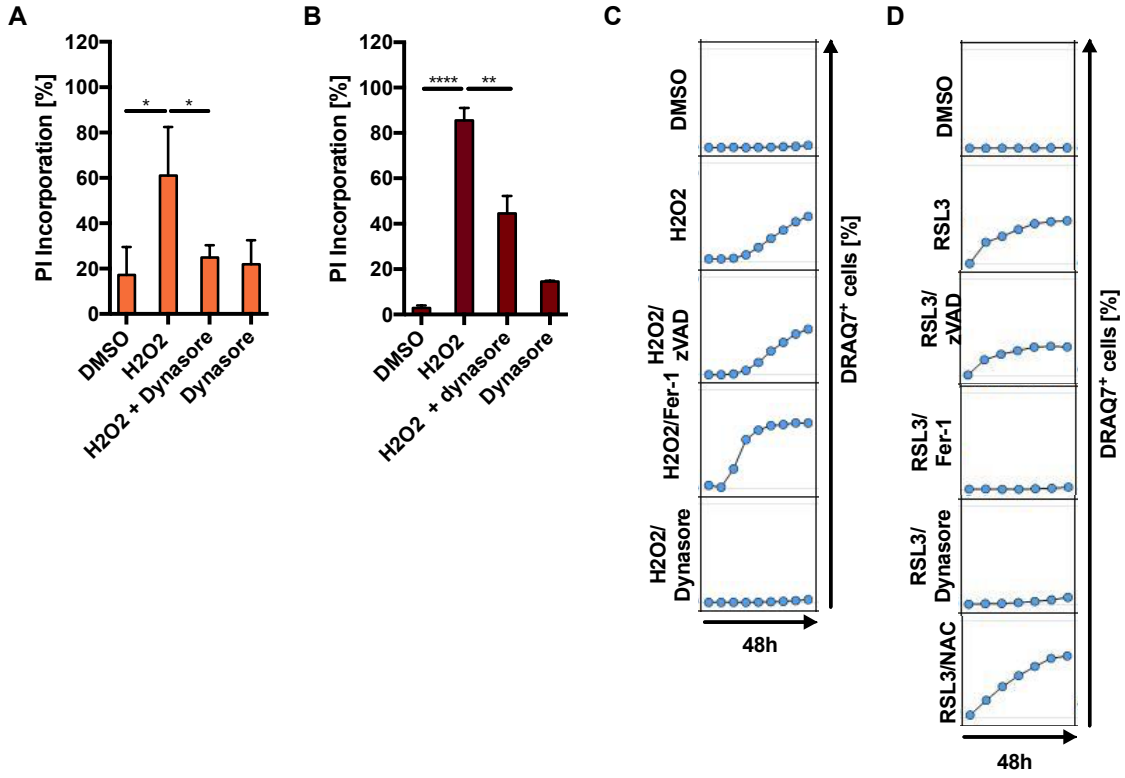

Figure 12. Dynasore is a highly active pan-ROS cell death blocker (**a,b**). H441 and A549 cells were treated with DMSO, H_2O_2 (100 nM), Dynasore (80 µM) or both for 48 h. Cell death was determined by propidium iodide (PI) uptake and flow cytometry (**c,d**). A549

cells were treated with DMSO, H_2O_2 (100 nM) or RSL3 (1 µM) alone or in combination with zVAD (20 µM), Fer-1 (5 µM), dynasore (80 µM) or NAC (1.5 mM). Images were acquired every 8 h for 48 h. Dead cells were quantified as % DRAQ7 + cells using the IncuCyte image analysis software. All data are means +/− SEM of three independent experiments or representative images where applicable. * indicates $p<0.05$; ** indicates $p<0.01$; *** indicates $p<0.001$; **** indicates $p<0.0001$; ns indicates non-significant differences. Figure adapted from Prieto Clemente et al. 2020 Cells.

Taken together, our findings identify an unexpected and novel activity of dynasore while suggesting that intracellular iron may be mobilised from alternative intracellular pools during ferroptosis. On the one hand, even though classical dynamin 1 and 2 regulate CD71 turnover and iron uptake, we find that they are dispensable for ferroptosis induction. We propose that dynasore blocks ferroptosis by combining the inhibition of dynamin 1 and 2 activity and thereby, inhibition of CD71-iron import, and direct radical-trapping activity that blocks both, general ROS and Lipid-ROS-induced cell death (**Figure 13**).

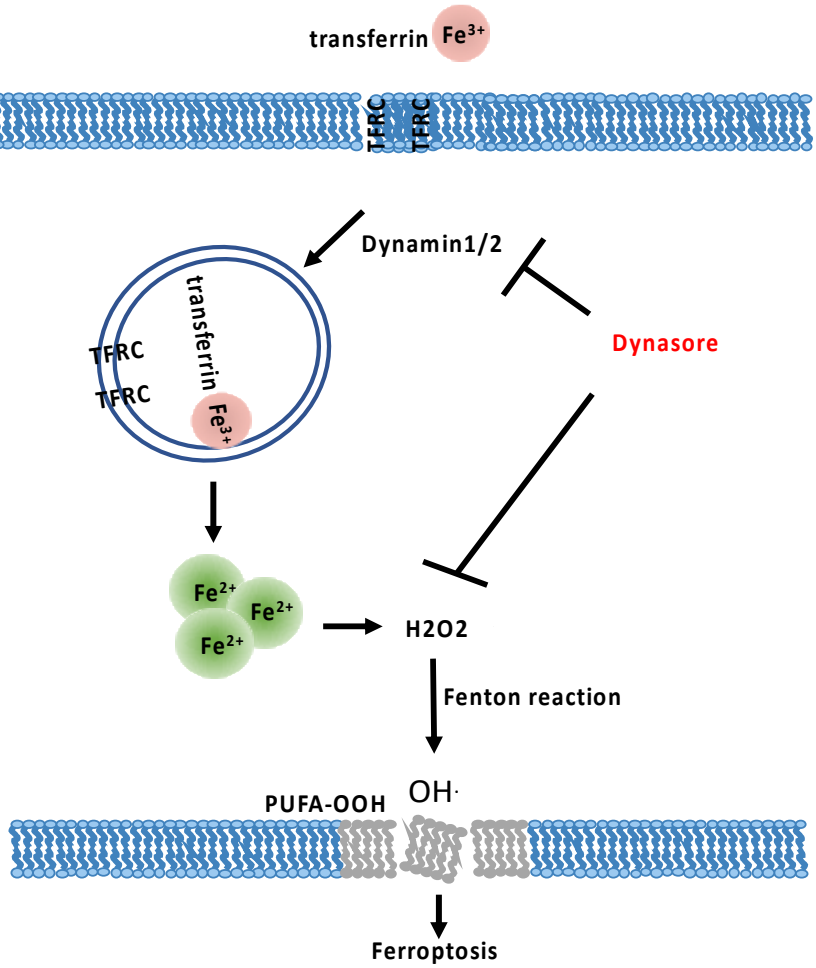

Figure 13. Dynasore blocks ferroptosis through combined modulation of iron uptake and ROS scavenging. Schematic overview of proposed mechanism of dynasore-mediated inhibition of ferroptosis. The figure was adapted from Prieto-Clemente et al. 2020.

3.2. Dynamin-Related Protein 1 promotes ferroptosis

Ferroptosis is not only characterized by its iron-dependency but also by the aberrant accumulation of cellular lipid reactive oxygen species (Dixon et al., 2012). Even though Lipid ROS species are generated at different steps of cellular metabolism, mitochondrial oxidative metabolism is essential for cysteine-deprivation-induced ferroptosis (Gao et al., 2019). To maintain mitochondrial homeostasis, it is highly important to keep a balance between mitochondrial fission and fusion events (Praefcke et al., 2004). In fact, mitochondrial fragmentation and morphological changes of mitochondria have been observed for a wide variety of programmed cell death pathways, including ferroptosis (Cereghetti et al., 2010; Xie et al., 2018). In mammals, mitochondrial fission and fragmentation, is regulated by the large GTPase Drp1 (Xie et al., 2018). To further understand the implication of dynamin superfamily proteins in ferroptosis and given its central role in mitochondrial fission/fragmentation observed during this type of regulated cell death, we sought to investigate the implication of Drp1 in the execution of ferroptotic cell death.

3.2.1. Inhibition and silencing of Dynamin-related protein 1 partially blocks erastin-induced ferroptosis

Drp1-mediated mitochondrial fragmentation has been described in various types of programmed cells death pathways such us necroptosis (She et al., 2019; Wang et al., 2012) or autophagy (Martinez et al., 2018; Breitzig et al., 2018). Interestingly, mitochondrial fragmentation can also be observed during ferroptosis (Dixon et al., 2012; Doll et al., 2017). However, whether this process is equally mediated by Drp1 activity has remained unknown.

To investigate a potential implication of Drp1 in ferroptosis, we first validated whether upon erastin treatment we could induce mitochondrial fragmentation in our cellular system. To do that, A549 cells were treated with erastin for 24 h.

After treatment mitochondria were stained with MitoTracker deep red and mitochondrial shape was studied by confocal microscopy. In agreement with literature, microscopy pictures showed that after 24 h erastin treatment mitochondria were indeed fragmented (**Figure 14**).

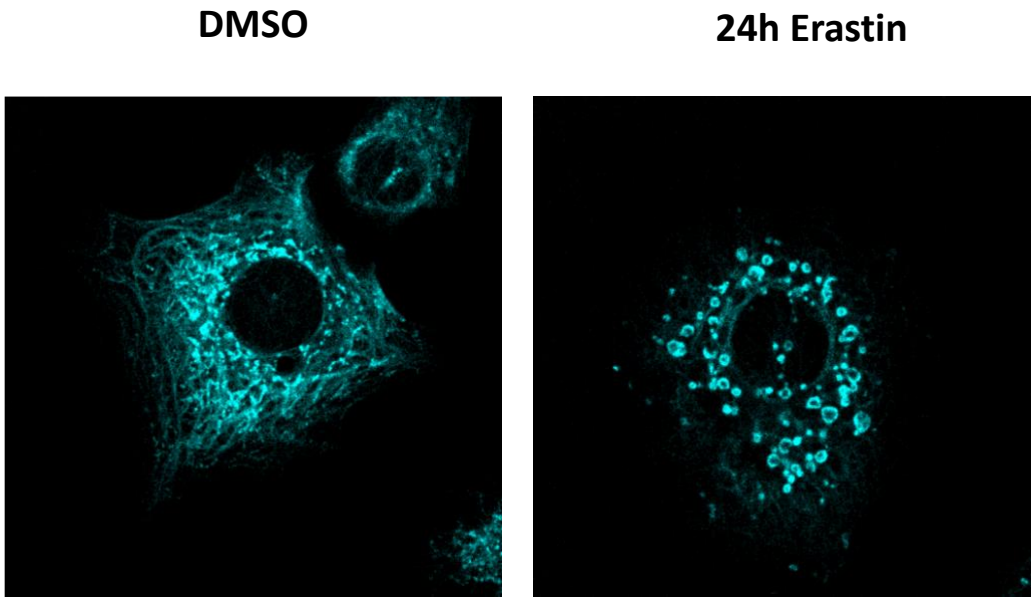

Figure 14. Erastin induces mitochondrial fragmentation. Mitochondrial fragmentation was studied by confocal microscopy. A549 cells were treated with DMSO and erastin (10 µM) for 24 h. Mitochondria were stained with MitoTracker deep Red (150 nM) which was added to the cells during the las 30 min of the treatment. Scale bar: 15 µM. 50 cells from three independent experiments were analysed.

Based on these data, we hypothesised that Drp1 activity could be the regulator of this event, so we next aimed to elucidate whether Drp1 might be required for ferroptotic cell death. To this end, we performed siRNA-mediated silencing of Drp1 (**Figure 15.a**) and we induced ferroptosis by erastin treatment in control and Drp1-silenced cells. Interestingly, Drp1 knockdown partially rescued ferroptosis induced by erastin treatment in both, H441 and A549 cells **(Figure 15.b).** In support of these data, Drp1 activity also promoted ferroptotic cell death as its inhibition using the well-establish Drp1 inhibitor Mdivi obtained similar results **(Figure 15.c).** Collectively, our data suggest that Drp1 might promote erastin-induced ferroptosis.

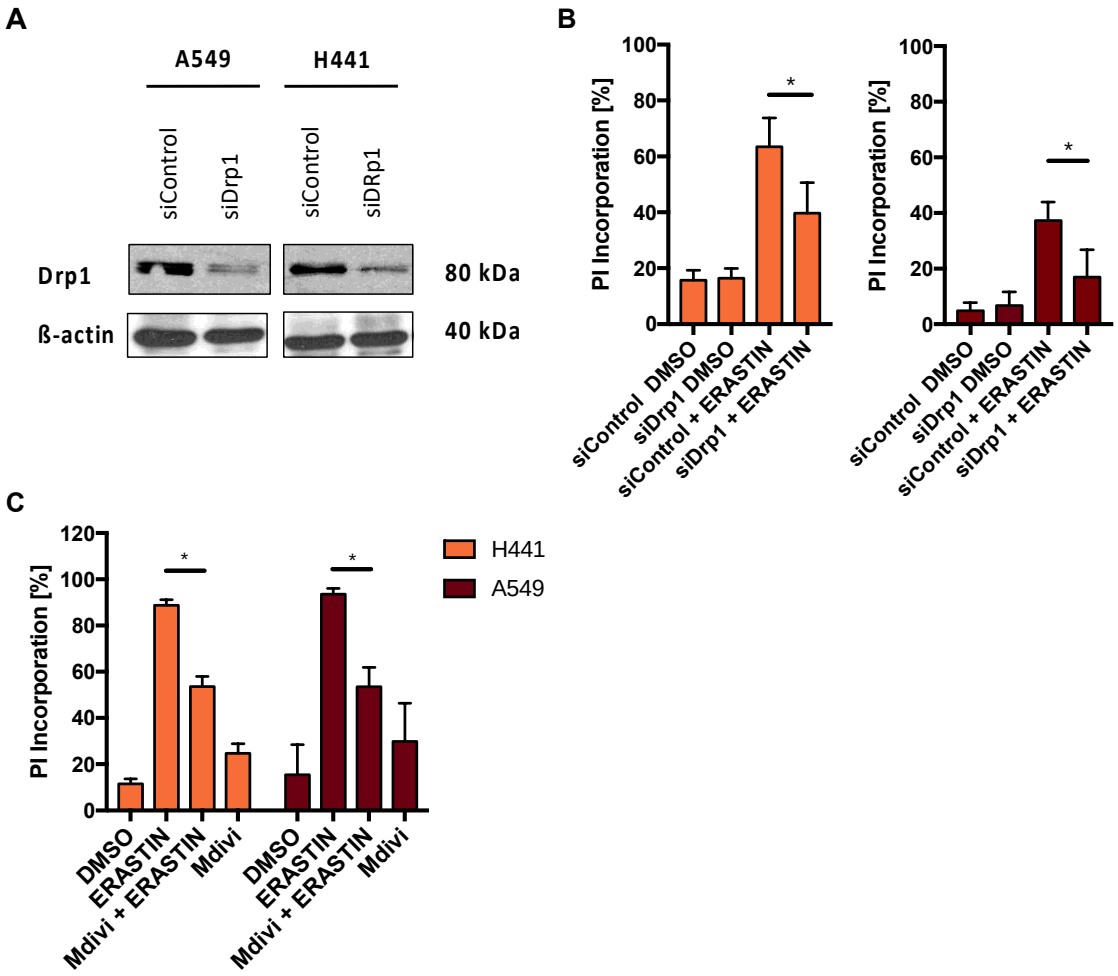

Figure 15. Inhibition of Dynamin-related protein 1 partially blocks erastin-induced ferroptosis (**a**). H441 and A549 cells were subjected to control or dynamin-related protein 1 (Drp1)-targeting siRNA for 72 h, a representative blot is shown (**b**). Indicated cells were treated with DMSO and erastin (10 µM) for 48 h. Cell death was determined by propidium iodide (PI) uptake and flow cytometry (**c**). H441 and A549 cells were treated with DMSO, erastin (10µM) and Mdivi (75 µM) or both for 48 h. Cell death was determined as in ***b***. All data are means +/− SEM of three independent experiments. * indicates p<0.05; ** indicates p<0.01; *** indicates p<0.001; **** indicates p<0.0001.

3.2.2. Inducible *drp1* KO cells are resistant to erastin-induced ferroptosis

To further characterize the requirement of Drp1 during erastin-induced ferroptosis, we generated *drp1*-knockout (KO) cells by CRISPR/Cas9 technology. To this end, human embryonic kidney (HEK) cells were transfected with 4 different RNA guides, and *drp1* KO clones were selected by single-cell cloning and knockouts were validated by western blot (**Figure 16.a)**. First, *drp1* KOs and *drp1* wild-type (WT) expressing cells were treated with erastin to compare their sensitivity to ferroptosis. Yet, *drp1* knockout cells generated in

this manner were as sensitive as the WT control to erastin treatment (**Figure 16.a**). Next, we sought to elucidate whether the lack of resistance in the KO cell line was caused by adaption of these cells to the *drp1* knockout status. For that, we induced a transient knockout in conditional *drp1* floxed mouse embryonic fibroblasts (MEFs) (A gift from. Prof. L. Scorrano). The indicated cells were infected with an Adenovirus Cre for 24 h that generated a transient KO of *Drp1*. Interestingly, the transient genetic depletion of *drp1* efficiently reduced erastin-induced ferroptosis (**Figure 16.b**). Taken together, our data suggest that HEK cells might adapt to a permanent *drp1* KO rendering cells as sensitive as the control to erastin treatment, whereas a transient genetic depletion of *drp1* impairs erastin-induced ferroptosis. These findings, together with our data obtained in siRNA experiments and using an inhibitor support a requirement for Drp1 in erastin-induced ferroptosis.

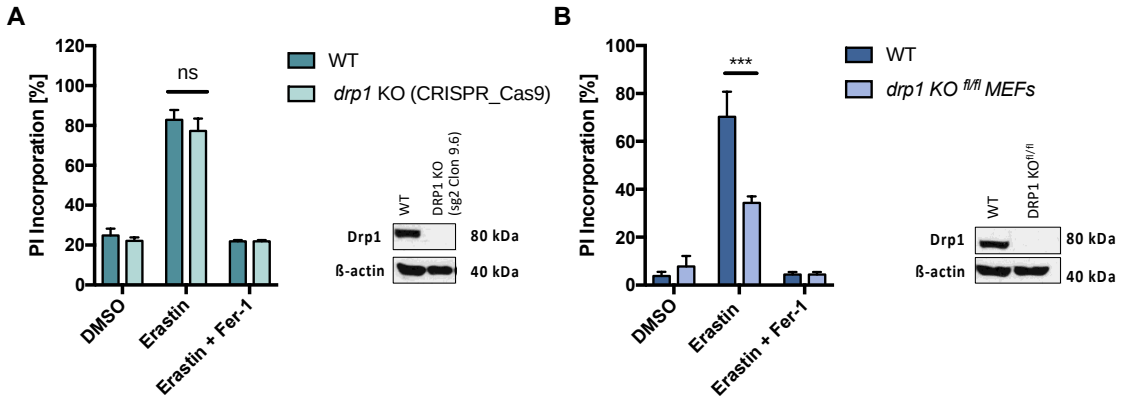

Figure 16. Transient *drp1* knockout cells are more resistant to erastin-induced ferroptosis (**a**). HEK cells were subjected to CRISPR_Cas9 technology with 4 different RNA guides. Single clones were selected and tested for protein expression, a representative blot from the clone 9.6 RNA guide 2 (sg2) is shown. Indicated cells were treated with DMSO and erastin (2,5 µM) for 16 h. Cell death was determined by propidium iodide (PI) uptake and flow cytometry (**b**). Inducible *drp1* floxed MEFs were subjected to transduction with AdenoCre Virus for 24 h, a representative blot is shown. Indicated cells were treated with DMSO and erastin (1 µM) for 16h. Cell death was determined as in ***a***. * indicates p<0.05; ** indicates p<0.01; *** indicates p<0.001; **** indicates p<0.0001; ns indicates non-significant differences.

3.2.3. Dynamin-related protein 1 is dispensable for GPX4-inhibition-induced ferroptosis

Importantly, although genetic deletion of *drp1* impaired erastin-induced ferroptosis, it can still be triggered by the pharmacological inhibition or genetic depletion of *gpx4*. Thus, we next studied the implication of Drp1 when ferroptosis was induced by the GPX4 inhibitor RSL3. Surprisingly, silencing of Drp1 by siRNA did not rescue RSL3-induced ferroptosis (**Figure 17.a,b**). Moreover, the Drp1 inhibitor Mdivi also failed to inhibit ferroptosis upon RSL3 treatment (**Figure 17.c**). Indeed, *drp1* floxed MEFs did not show significant resistance when ferroptosis was triggered by RSL3 (**Figure 17.d**). These data were further confirmed in a cellular system in which ferroptosis is triggered by the tamoxifen-inducible induction of *gpx4* knockout (**Figure 17.e**). In agreement with our previous data, silencing of Drp1 could not block ferroptosis triggered by induction of *gpx4* knockout (**Figure 17.e**). Lastly, in time-lapse imaging experiments we could confirm that silencing of Drp1 did not rescue cells from *gpx4*-depletion-induced ferroptosis (**Figure 17.f,g**). Collectively, these data indicate that Drp1 is dispensable for GPX4-inhibition-induced ferroptosis and its implication in the ferroptosis pathway discovered above likely relates to ferroptosis induced by GSH depletion.

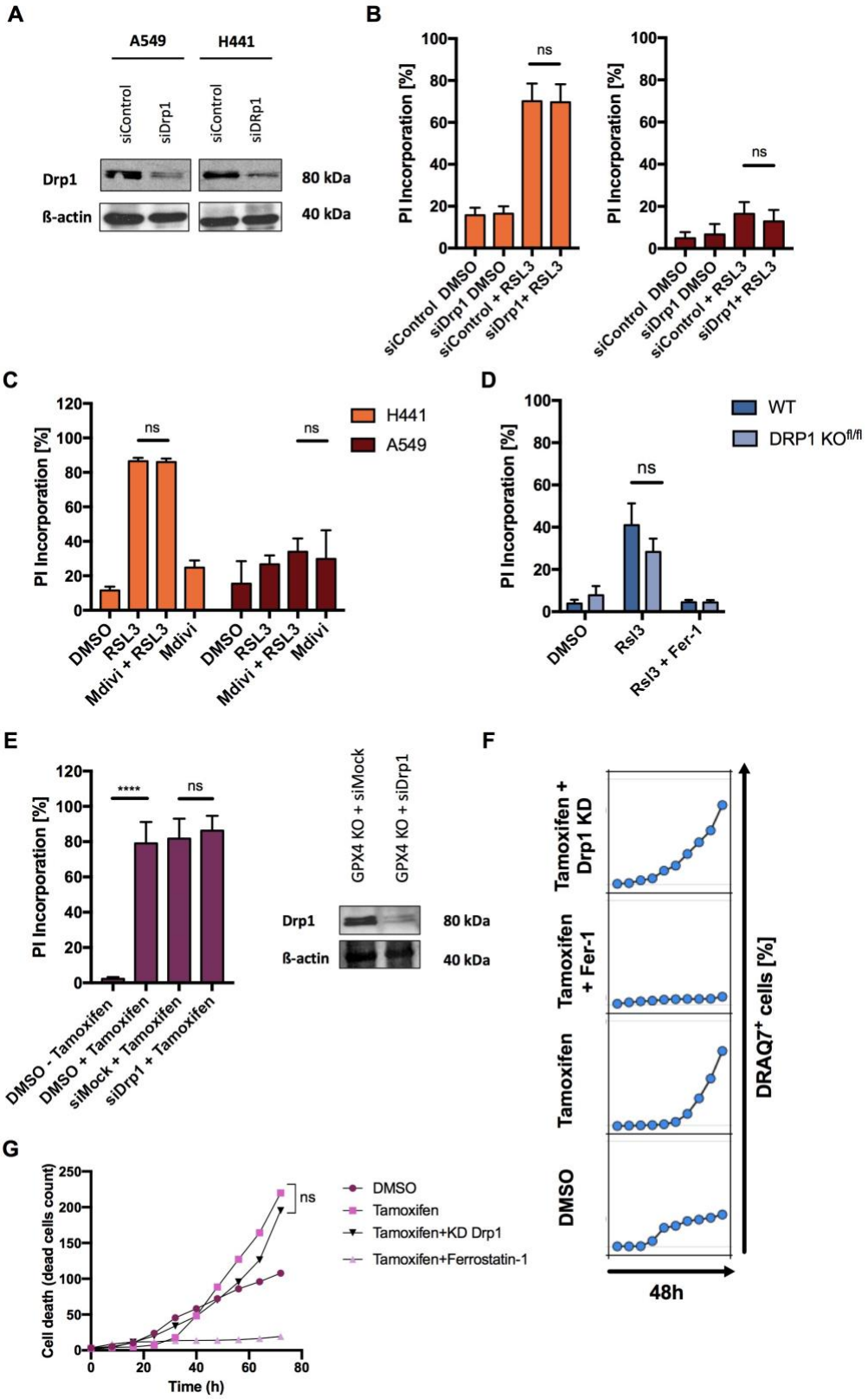

Figure 17. Dynamin-related protein 1 is dispensable for GPX4-inhibition-induced ferroptosis (**a**). H441 and A549 cells were subjected to control or Drp1-targeting siRNA for 72 h, a representative blot is shown (**b**). Indicated cells were treated with DMSO and RSL3 (1 µM) for 48 h. Cell death was determined by propidium iodide (PI) uptake and flow cytometry (**c**). H441 and A549 cells were treated with DMSO, RSL3 (1 µM) and Mdivi (75

µM) or both for 48 h. Cell death was determined as in ***b***. (**d**) Inducible *drp1* KO floxed MEFs were subjected to transduction with AdenoCre Virus for 24 h. The indicated cells were treated with DMSO and RSL3 (0,5 µM) for 16 h. Cell death was determined by propidium iodide (PI) uptake and flow cytometry (**e**). Inducible *gpx4* KO MEFs were treated with tamoxifen (1 µM) for 72 h. At the same time, cells were subjected to control or Drp1-targeting siRNA for 72 h. Cell death was determined by propidium iodide (PI) uptake and flow cytometry. A representative blot for the indicated cells is shown (**f,g**). Time-lapse experiment using the same cells as in ***e*** was performed. Images were acquired every 8 h for 48 h. Dead cells were quantified as % DRAQ7 + cells using the IncuCyte image analysis software. All data are means +/− SEM of three independent experiments or representative images where applicable. * indicates p<0.05; ** indicates p<0.01; *** indicates p<0.001; **** indicates p<0.0001; ns indicates non-significant differences.

3.2.4. Drp1 promotes ferroptosis induced by GSH depletion

Mitochondrial metabolism has been shown to promote cysteine-deprivation-induced ferroptosis, but not ferroptosis induced by GPX4 inhibition (Gao et al., 2019). One of the main differences between these two forms of inducing ferroptosis is the regulation of cellular GSH content. Whereas CDI ferroptosis causes a rapid exhaustion of glutathione levels, upon GPX4 inhibition glutathione contents remain unchanged (Friedmann Angeli et al., 2014; Ingold et al., 2018; Yang et al., 2014). Since the lack of Drp1 in our cellular system does not influence GPX4-inhibition-induced ferroptosis (**Figure 17**), we hypothesised that the implication of Drp1 in the ferroptosis pathway might occur in a GSH depleted scenario. CDI ferroptosis can be induced either by inhibiting system Xc- by erastin treatment or by depleting cystine from the culture media (Gao et al., 2015a, 2015b). To test this hypothesis, we first tested whether the absence of cystine in the media would induce ferroptosis in our cells. To do that, we combined cystine free RPMI with ferrostatin-1, z-Vad and Nec-1s to test for ferroptotic, apoptotic and necroptotic cell death, respectively. After 48 h of cystine starvation, cell death was fully rescued by ferrostatin-1 but not by z-Vad or Nec-1s, indicating that cystine-deficient media induces ferroptotic cell death in our cellular system **(Figure 18.a,b).** Next, we performed siRNA-mediated silencing of Drp1 under the same conditions. In line with our previous data, silencing Drp1 showed an almost complete rescue of cysteine-deprivation-induced ferroptosis (**Figure 18.c**). To further elucidate whether Drp1 is involved in ferroptosis when GSH levels are depleted as a result of cystine depletion, we next measured the intracellular GSH pool upon erastin and RSL3 treatment and

upon cystine starvation. We made use of Monochloromobimane (MCB), a compound that reacts with low molecular weight thiols, including glutathione, forming a fluorescent conjugate that is quantified by flow cytometry (Briviba et al., 1993). As we expected, both, erastin and cystine-free RPMI efficiently depleted intracellular glutathione levels in our cells (**Figure 18.d,e**). However, RSL3 treatment failed in reducing GSH levels (**Figure 18.f**). Collectively, our data indicate that Drp1 is involved in CDI ferroptosis but not in GPX4 inhibition-induced ferroptosis.

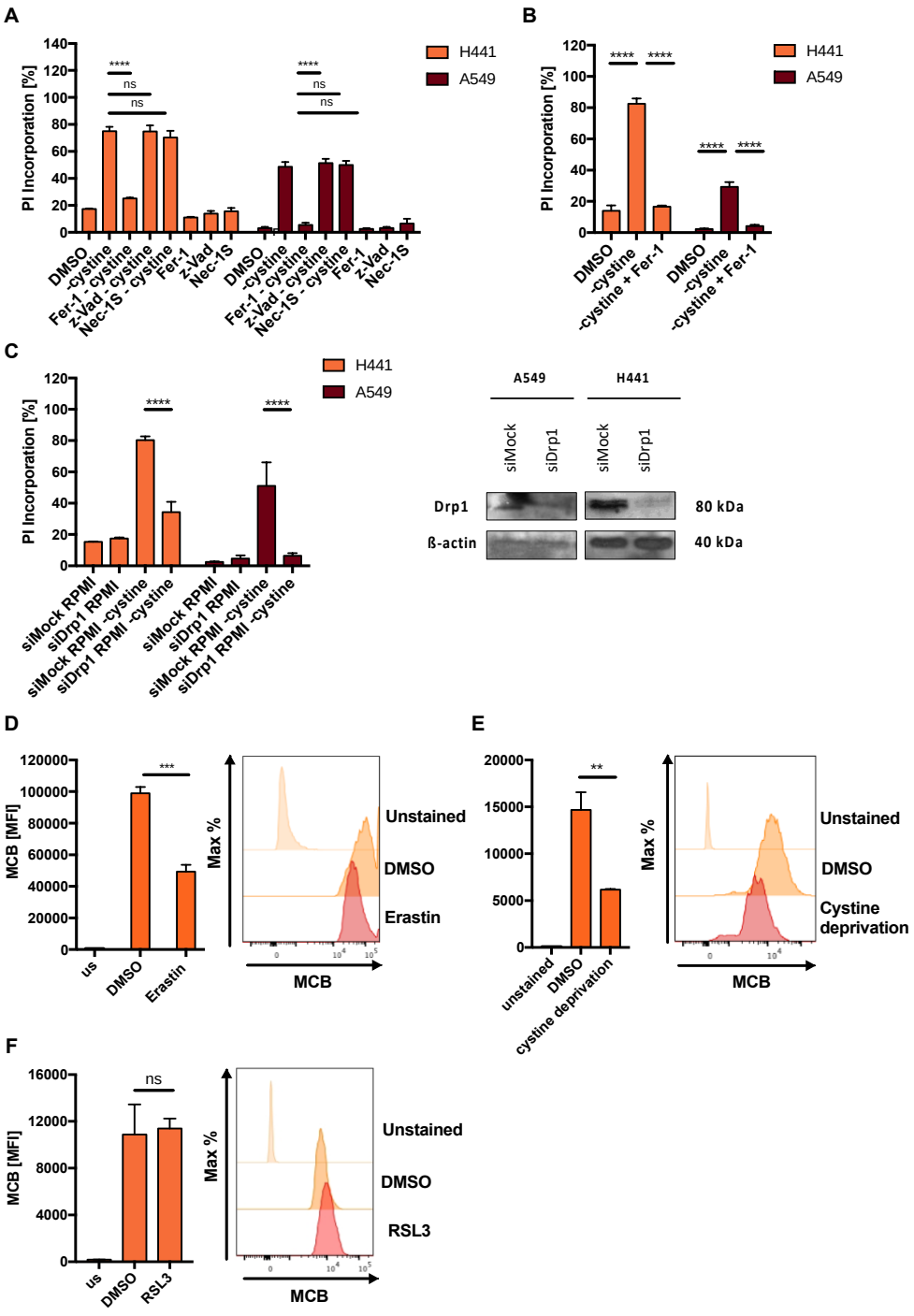

Figure 18. Drp1 participates in cysteine-deprivation-induced (CDI) ferroptosis (**a**). H441 and A549 cells were treated with DMSO, cystine free media, ferrostatin-1 (5 µM), zVAD (20 µM), Nec-1 (20 µM) or the indicated combinations for 48 h. Cell death was quantified by propidium iodide (PI) uptake and flow cytometry (**b**). Cells in ***a*** were treated with DMSO, cystine free media and ferrostatin-1 (5 µM) for 48 h. Cell death was determined as in ***a*** (**c**). The indicated cells were subjected to control or dynamin-related protein 1 (Drp1)-targeting siRNA for 72 h and were treated with DMSO and cystine free media for 48h. Cell death was determined as in ***a*** (**d,e,f**). H441 cells were treated with DMSO, Erastin (10 µM), RSL3 (1 µM) or cystine free RPMI for 16 h, 5h or 24 h respectively. During the last 30 min, MCB was added at 5 µM to each well. Mean fluorescence intensity (MFI) was quantified by flow cytometry. All data are means +/− SEM of three independent experiments. * indicates p<0.05; ** indicates p<0.01; *** indicates p<0.001; **** indicates p<0.0001; ns indicates non-significant differences.

To further validate that Drp1 promotes ferroptosis induced by GSH depletion, we made use of the small molecule Buthionine sulfoximine (BSO). This inhibitor is commonly used to induce glutathione deficiency (Drew and Miners, 1984; Schrieve and Harris, 1986). BSO inhibitis γ-glutamylcysteine synthetase, a key enzyme in glutathione biosynthesis (Dixon et al., 2012, Sun et al., 2016, Xie et al., 2017). In agreement with literature, BSO treatment depleted glutathione levels in our cells (**Figure 19.a**). We next asked whether the direct inhibition of glutathione synthesis might induce ferroptosis in our cells. To test that, we treated H441 cells with BSO alone and in co-treatment with Fer-1, observing that BSO could efficiently induce ferroptosis (**Figure 19.b**). Importantly, silencing of Drp1 by siRNA indeed also impaired BSO-induced ferroptosis (**Figure 19.c**).

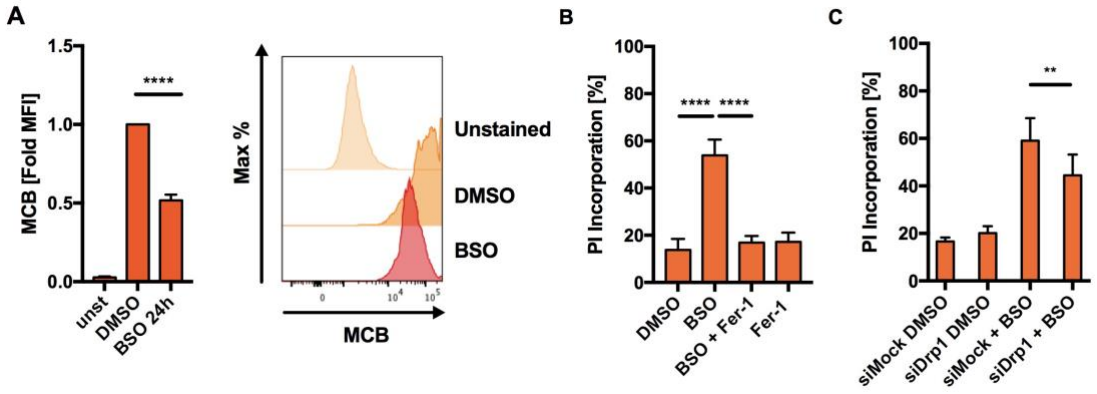

Figure 19. Drp1 regulates BSO-induced ferroptosis (**a**). H441 cells were treated with DMSO and BSO (10 mM) for 24h. During the last 30 min, MCB was added at 5 µM to each well. Mean fluorescence intensity (MFI) was quantified by flow cytometry (**b**). Cells in ***a*** were treated with DMSO, BSO (10 mM) and ferrostatin-1 (5 µM) for 48 h. Cell death was quantified by propidium iodide (PI) uptake and flow cytometry (**c**). Indicated cells were subjected to control or dynamin-related protein 1 (Drp1)-targeting siRNA for 72 h. Cells were treated with DMSO and BSO (10 mM) for 48h. Cell death was determined as in ***b***. All

data are means +/− SEM of three independent experiments. * indicates p<0.05; ** indicates p<0.01; *** indicates p<0.001; **** indicates p<0.0001; ns indicates non-significant differences.

Therefore, these data show that Drp1 promotes ferroptosis induced by glutathione depletion but not by Gpx4 inhibition. Hence, Drp1 implication in ferroptosis is dependent on the context in which ferroptosis is induced.

3.3. Drp1 phosphorylation (Ser616) along with GTPase activity increase upon ferroptosis induction

Drp1 is a cytosolic protein which assembles into small dimers or tetramers but presents with the ability to self-assemble into larger structures that mediate mitochondrial fission (Praefcke et al., 2004). Importantly, the regulation of Drp1 properties such as its mitochondrial translocation or its GTPase activity depend on its posttranslational modifications (Lackner et al., 2009; Santel et al., 2008). Amongst all PTMs, phosphorylation of Drp1 is the most studied so far (Chang et al., 2007; Taguchi et al., 2007). Increasing evidence revealed that phosphorylation of Drp1 at serine 616 or dephosphorylation at serine 637 play a critical role in activation or inactivation of its GTPase activity, respectively (Chang et al., 2007; Taguchi et al., 2007; Archer et al., 2013). To further investigate the molecular and cellular mechanisms behind the regulation of Drp1 activation during ferroptosis, we next studied the phosphorylation state of Drp1 upon ferroptosis induction. First, we performed Western blotting analysis of phospho-S616-Drp1 protein levels from cells treated with erastin for 3, 6 and 10 hours. We could detect an increase in P-S616-Drp1 after 3 hours treatment which remained elevated for the full duration monitored (**Figure 20.a**). Because Drp1 phosphorylation at serine 616 has been shown to elevate its GTPase activity (Chang et al., 2007; Taguchi et al., 2007; Archer et al., 2013), we next elucidated whether during erastin-induced ferroptosis Drp1 GTPase activity is stimulated. For that, we immunoprecipitated Drp1 from control and erastin-treated cells alone and in co-treatment with Mdivi-which was chosen as a negative control- (**Figure 20.b**). Isolated Drp1 was incubated with GTP at 30°C for 30 minutes. The released free phosphate was quantified using a High Throughput Colorimetric GTPase assay kit according to the manufacturer's specified protocol. Strikingly,

the GTPase activity of Drp1 was significantly increased during erastin treatment and inhibited by Mdivi treatment (**Figure 20.c**). Taken together, these data indicate that Drp1 is phosphorylated on its activatory serine 616 site and its GTPase activity increases during erastin-induced ferroptosis.

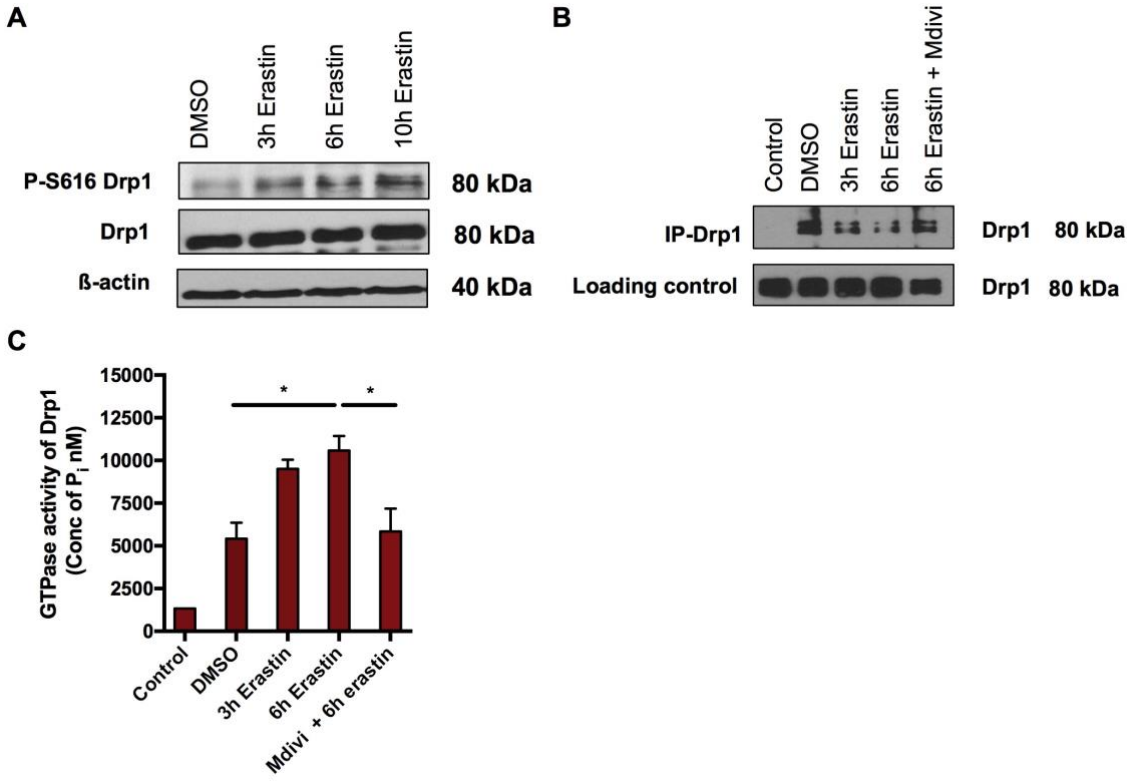

Figure 20. Ferroptosis induces Drp1 phosphorylation at Ser616 and stimulates Drp1 GTPase activity (**a**). A549 cells were treated with erastin (10 µ) for 3, 6, 10 h. Total expression levels of PS616-Drp1 were determined by Western blotting (**b**). Drp1 was immunopurified from A549 cells treated with DMSO, erastin (10 µM) for 3 and 6 h alone and in co-treatment with Mdivi (75 µM) as indicated. A representative blot of immunoprecipitated Drp1 is shown (**c**). A549 cells were treated as in ***b***. GTPase activity was measured by quantifying the released free phosphate using a High Throughput Colorimetric GTPase assay kit according to the manufacture´s specified protocol. All data are means +/− SEM of three independent experiments or representative images where applicable. * indicates $p<0.05$; ** indicates $p<0.01$; *** indicates $p<0.001$; **** indicates $p<0.0001$.

3.4. Calcium/calmodulin-dependent protein kinase II-α (CaMKIIα) promotes CDI-ferroptosis and regulates the phosphorylation of Drp1 at Ser616

Since we observed phosphorylation of Drp1 upon induction of ferroptosis, we next aimed to address whether a putative kinase may be activated during ferroptosis which may mediate this phosphorylation. Recently, a kinome screen for ferroptosis regulators triggered during cystine deprivation revealed 34 essential kinases involved in promoting or inhibiting ferroptosis (Chen at al., 2020). Therefore, we probed this list of candidates against known Drp1-phosphorylating kinases in other contexts. Strikingly, we found that Ca^{2+}/calmodulin-dependent protein kinase-α (CaMKIIα) was both, part of this list of candidates and had previously been shown to phosphorylate Drp1 at S616 during chronic ß-AR stimulation (Xu et al., 2016). Therefore, we hypothesised that CaMKIIα may be responsible for Drp1 phosphorylation at serine 616 during ferroptosis.

3.4.1. Inhibition and silencing of CaMKIIα partially impairs CDI-ferroptosis

To test this hypothesis, we first made use of the CaMKIIα small molecule inhibitor KN-93, and we triggered ferroptosis by erastin treatment. Interestingly, erastin-induced ferroptosis was prevented by KN-93 after 48 h treatment (**Figure 21.a**). In parallel, we investigated whether the absence of the protein might also influence ferroptosis execution. To this end, we performed siRNA-mediated silencing of CaMKIIα followed by erastin treatment (**Figure 21.b**). Indeed, suppression of CaMKIIα could render cells partially resistant to erastin-induced ferroptosis (**Figure 21.b**). In line with what is already published (Chen at al., 2020), our data also suggest that CaMKIIα might be required for CDI ferroptosis.

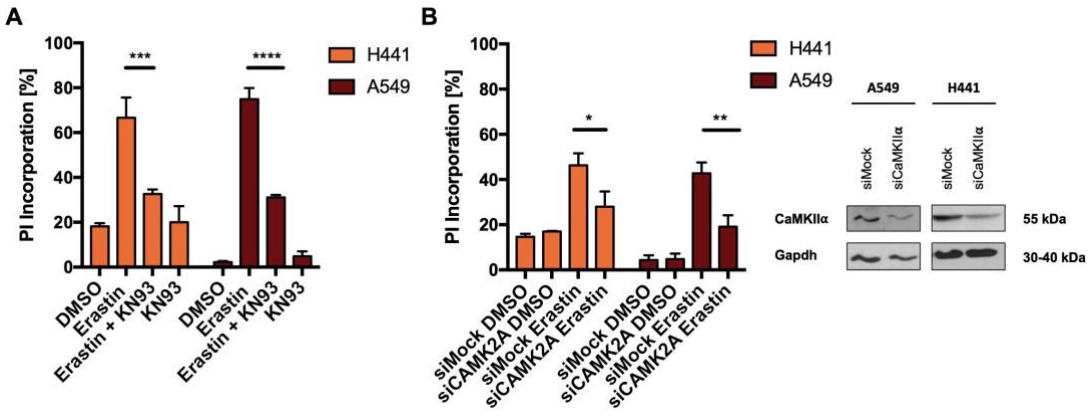

Figure 21. Inhibition and silencing of CaMKIIα impairs cysteine-deprivation-induced-ferroptosis (**a**). H441 and A549 cells were treated with DMSO, erastin (10 µM) and KN-93 (10 µM) for 48 h as indicated. Cell death was quantified by propidium iodide (PI) uptake and flow cytometry (**b**). Indicated cells were subjected to control or Ca2+/calmodulin-dependent kinase-α (CaMKIIα) targeting siRNA for 72 h, a representative blot is shown. Cells were treated with erastin (10 µM) for 48h. Cell death was determined as in ***a***. All data are means +/− SEM of three independent experiments or representative images where applicable. * indicates p<0.05; ** indicates p<0.01; *** indicates p<0.001; **** indicates p<0.0001.

3.4.2. CaMKIIα binds to Drp1 and promotes its phosphorylation at S616

CaMKIIα has many protein targets, including Drp1. However, Drp1 has been shown to also be phosphorylated at S616 by other kinases including CDK1/cyclin B, MAP kinase ERK1/2 and protein kinase C δ (PKCδ) (Qi et al., 2011; Yu et al., 2011; Bo et al., 2018). Since we had established that CaMKIIα indeed promotes ferroptotic cell death in our system, we next determined whether CaMKIIα might be the kinase responsible for Drp1 S616 phosphorylation and activation when ferroptosis is triggered by cysteine deprivation. First, we performed a kinetic assay where we treated A549 cells with erastin for 3, 6 and 9 hours alone, and in co-treatment with the CaMKIIα inhibitor KN-93. Interestingly, we observed that P-S616-Drp1 protein levels did not undergo an increase upon erastin treatment when cells were co-incubated with the inhibitor, whereas, in line with our previous data, erastin treatment by itself, could elevate P-S616-Drp1 levels after 3 h treatment (**Figure 22.a**). Moreover, silencing of CaMKIIα by siRNA almost completely abolished basal phosphorylation of Drp1 at Ser616 (**Figure 22.b**). To further support our data, we studied whether CaMKIIα can directly bind Drp1. For that, we immunoprecipitated CaMKIIα under non-stimulated and erastin-stimulated

conditions. Indeed, Western blotting analysis showed that endogenous Drp1 co-precipitated with CaMKIIα, yet in both, control and treated cells (**Figure 22.c**). While these data show that Drp1/ CaMKIIα interaction is not stimulation dependent, they suggest a constitutive interaction of at least a subset of both proteins. Collectively, our data propose that CaMKIIα promotes Drp1 phosphorylation at S616 upon ferroptosis induction.

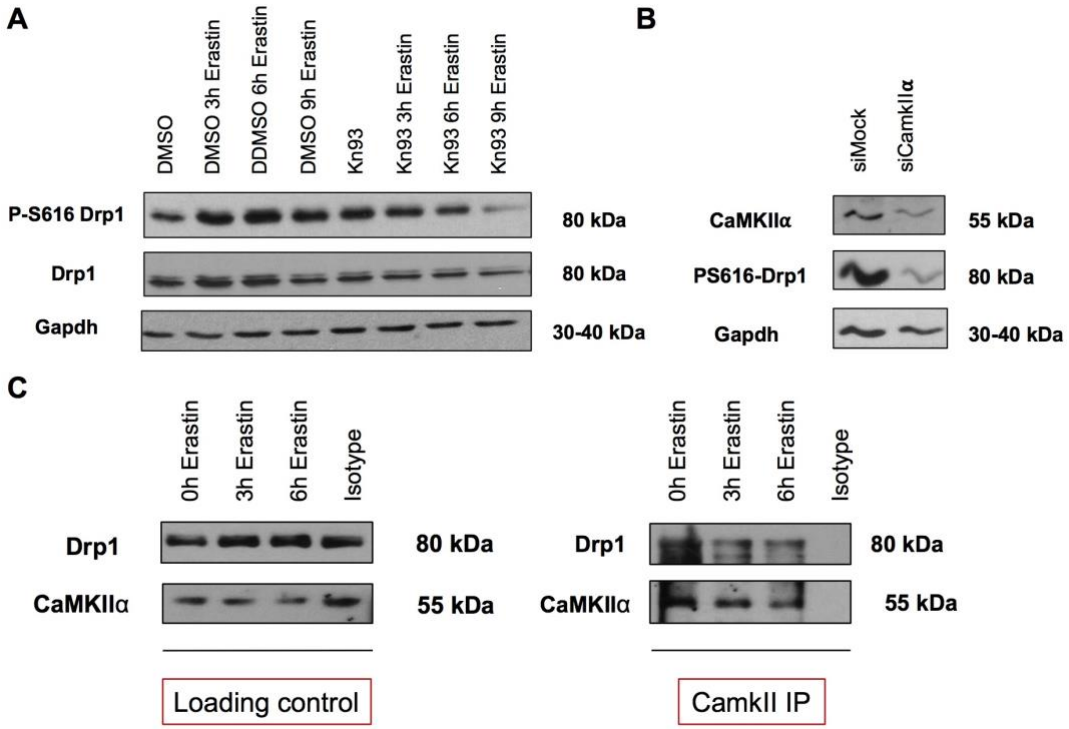

Figure 22. CaMKIIα binds to Drp1 and promotes its phosphorylation at S616 (**a**). A549 cells were treated with erastin (10 μM) for 3, 6, 10 h alone or in combination with KN-93 (10 μM). Total expression levels of P-S616-Drp1, Drp1 and Gapdh were determined (**b**). Total expression levels of PS616-Drp1, Drp1 and Gapdh were determined in A549 cells subjected to control or CaMKIIα-targeting siRNA for 72 h (**c**). Indicated cells were treated with DMSO and erastin (10 μM) for 3 and 6 h. An anti-CaMKIIα antibody specific for immunoprecipitation was pre-incubated with protein G beads. After pre-incubation, protein lysates from indicated cells were incubated with the beads-antibody mixture and supernatants were discarded after incubation. The co-immunoprecipitated samples were used for Western blotting. An anti-Drp1 antibody was used for determining the *in vitro* interaction between CAMKIIα and Drp1. Supernatants from total cell lysates were taken before co-immunoprecipitation and used as loading controls to show total expression levels of Drp1 and CAMKIIα. All data are representative examples from three independent experiments.

3.4.3. Intra- and extracellular calcium are required for ferroptosis execution

We and others could show that CaMKIIα participates in CDI- and erastin-induced ferroptosis (Chen at al., 2020). Of note, CaMKIIα is a kinase regulated by calcium ions (Takemoto-kimura et al., 2017; Lu et al. 2003). Moreover, our lab recently contributed to a study showing that activation of the ferroptosis pathway triggers an increase of cytosolic Ca^{2+} levels that precedes final cell bursting (Pedrera et al., 2020). Therefore, we next aimed to investigate whether calcium may influence the execution of ferroptosis. To this end, we first pre-incubated cells with both, extra and intra-cellular calcium chelators Bapta and Bapta-AM, respectively. Whereas extracellular calcium chelation did not alter ferroptosis induction significantly (**Figure 23.a**), intracellular calcium chelation impaired ferroptosis (**Figure 23.b**). Moreover, the combination of both chelators showed a stronger effect in impairing ferroptosis (**Figure 23.c**). Lastly, we made use of a calcium-free media with or without erastin for 48 h. In support of a requirement for calcium in ferroptosis execution, cells under calcium deprivation were more resistant to ferroptosis than the ones treated with regular media (**Figure 23.d**). Strikingly, in A549 cells, calcium-free media blocked erastin-induced ferroptosis as efficiently as blockade by Fer-1 (**Figure 23.d**). Taken together, these data support the requirement of calcium in ferroptosis (Reviewed in Maher et al., 2018) and point towards a possible mechanism of activation of CaMKIIα which remains to be further validated under ferroptosis conditions.

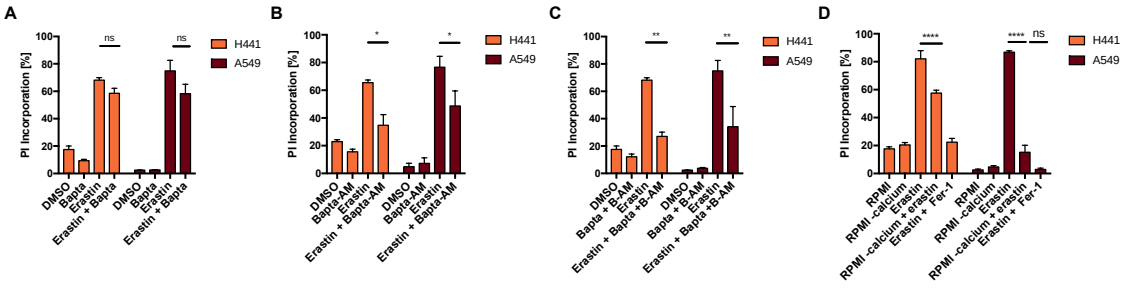

Figure 23. Intra and extracellular calcium are required for ferroptosis (**a**). H441 and A549 cells were treated with DMSO, erastin (10 µM) and Bapta (10 µM) for 48 h as indicated. Cell death was quantified by propidium iodide (PI) uptake and flow cytometry (**b**). Indicated cells were treated with DMSO, erastin (10 µM) and Bapta-AM (10 µM) for 48 h as indicated. Cell death was determined as in ***a*** (**c**). H441 and A549 cells were treated with DMSO, erastin (10 µM) and a combination of Bapta (10 µM) and Bapta-AM (10 µM) for 48 h as indicated. Cell death was quantified by propidium iodide (PI) uptake and flow cytometry

(**d**). Indicated cells were treated with DMSO, calcium free media, erastin (10 µM) and Fer-1 (5 µM) for 48 h as indicated. Cell death was quantified as in ***a.*** All data are means +/− SEM of three independent experiments. * indicates p<0.05; ** indicates p<0.01; *** indicates p<0.001; **** indicates p<0.0001; ns indicates non-significant differences.

3.5. Drp1 drives mitochondrial fragmentation during erastin-induced ferroptosis

During the last decade it has been highlighted an important and decisive role for mitochondrial fragmentation in apoptosis, oxidative-cell death and necrosis, which has been related to Drp1 function (Wang et al., 2012; Cereghetti et al., 2010; Zhou et al., 2017). As mentioned before, phosphorylation of Drp1 at Serine 616 is known to regulate its GTPase activity and to trigger its translocation to mitochondria. Based on this, we next aimed to elucidate whether the function of Drp1 in ferroptosis is mitochondrial dependent.

3.5.1. Drp1 translocates to mitochondria during erastin-induced ferroptosis

We observed that during ferroptosis induction Drp1 was phosphorylated at S616 and its GTPase activity increased in a stimulation-dependent manner. Since activated Drp1 is known to translocate to the mitochondria in other contexts, we first isolated mitochondrial and cytosolic extracts from control and erastin-treated cells at different time points. As expected, erastin treatment increased P-S616-Drp1 levels in the cytosolic fraction after 3 h treatment (**Figure 24.a**). Importantly, Drp1 levels significantly increased in the mitochondrial fractions after 3 h and 6 h of erastin suggesting ferroptosis-stimulated mitochondrial translocation of Drp1 (**Figure 24.a**). To further corroborate these data, we next studied the co-localisation of Drp1 and mitochondria by confocal microscopy upon erastin treatment. Interestingly, immunofluorescence analysis revealed perinuclear localisation of Drp1 without stimulation and a significant increase in mitochondrial co-localisation in erastin-treated cells (**Figure 24.b,c**)**.** Accordingly, our data reveal that upon ferroptosis induction, Drp1 translocates to mitochondria and might triggers their fragmentation (**see figure 14**).

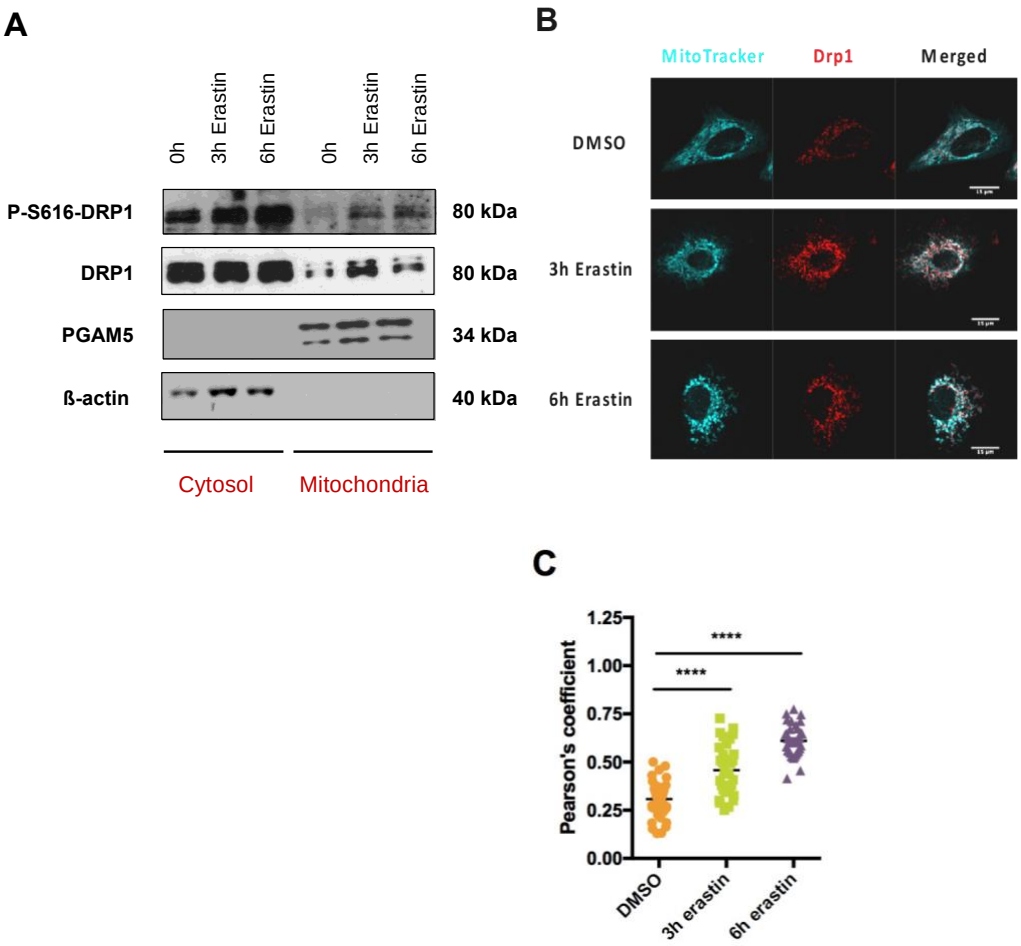

Figure 24. Drp1 translocates to mitochondria upon erastin treatment (**a**). A549 cells were treated with DMSO and erastin (10 µM) for 3 and 6 h. Mitochondrial and cytosolic fractions were isolated using a commercial kit (Mitochondrial Isolation Kit for Cultured Cells from Abcam) according to the manufacture´s specified protocol. The expression levels of PS616-DRP1, Drp1, PGAM5 and ß-actin were determined in both fractions as indicated by Western blotting. PGAM5 was used as a mitochondrial marker, whereas ß-actin was selected as an indicator for the cytosolic extraction. A representative blot from three independent experiments is shown (**b-c**). The co-localisation of Drp1 (red) and mitochondria (cyan) was examined using confocal microscopy. A549 cells were treated with DMSO and erastin (10 µM) for 3 and 6 h. Drp1 was stained with a primary antibody specific for Drp1 and a secondary antibody anti-rabbit-AlexaFluor488 following a regular immunofluorescence protocol. Mitochondria were stained with MitoTracker deep Red (150 nM) which was added to the cells during the last 30 min of the treatment. Scale bars: 15 µM. Co-localisation of Drp1 and mitochondria was quantified by the JaCob plugin in ImageJ. 50 cells from three independent experiments were analysed. All data are means +/− SEM of three independent experiments or representative images where applicable. * indicates $p<0.05$; ** indicates $p<0.01$; *** indicates $p<0.001$; **** indicates $p<0.0001$; ns indicates non-significant differences.

3.5.2. Silencing of the mitochondrial adaptor proteins MiD49 and MiD51 impairs ferroptosis execution

When Drp1 is recruited to the outer mitochondrial membrane (OMM) it needs protein adaptors to be anchored to the mitochondrial membrane and mediate mitochondrial fission (Otera and Mihara, 2011). In mammals, the OMM proteins mitochondrial fission factor (Mff), mitochondrial fission 1 protein (Fis1), mitochondrial dynamics of 49 kDa (MiD49) and mitochondrial dynamics of 51 kDa (MiD51) (Osellame et al., 2016) are described to be adaptors of Drp1 (Otera et al, 2010; Palmer et al., 2011; Zhao et al., 2011). However, while Fis1 and Mff are also localised in other organelles such us peroxisomes, MiD49 and MiD51 are exclusively found in mitochondria (Palmer et al., 2011). Interestingly, Drp1-dependent mitochondrial fission enabled by binding to MiD49 and MiD51, is required for cytochrome-c release during the early phase of intrinsic apoptosis (Otera et al., 2016). To investigate whether its mitochondrial localisation during ferroptosis was required for Drp1-mediated ferroptotic cell death promotion, we decided to impair Drp1 anchoring to the OMM. We performed siRNA-mediated silencing of MiD49 and MiD51 proteins in A549 cells (**Figure 25.a**) and induced ferroptosis by erastin treatment. Similar to Drp1 knockdown results, suppression of MiD49 and MiD51 rendered cells more resistant to ferroptosis (**Figure 25.b**). Hence, mitochondrial adaptors promote ferroptotic cell death.

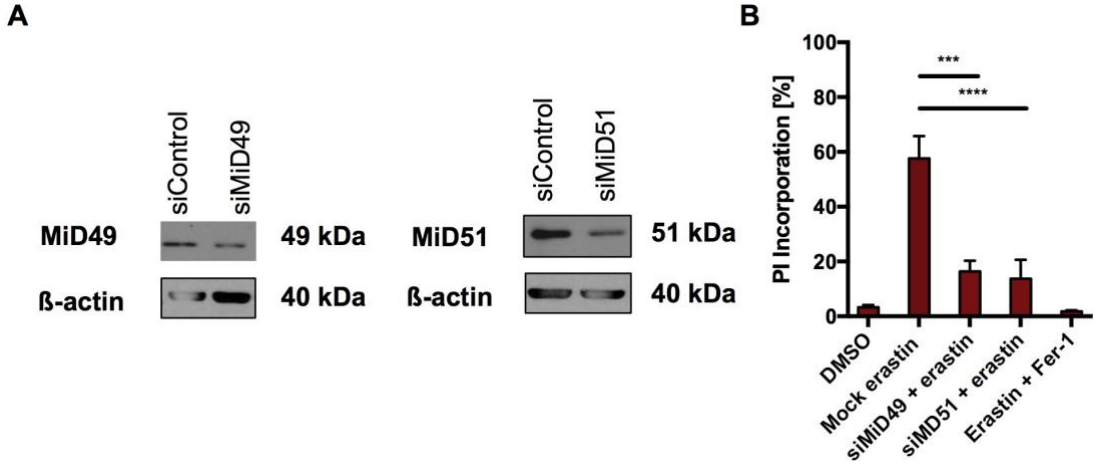

Figure 25. Inhibition of MiD49 and MiD51 impairs ferroptosis execution (**a**). A549 cells were subjected to control or MiD49/MiD51-targeting siRNA for 72 h, a representative blot is shown (**b**). The indicated cells were treated with DMSO, erastin (10 µM) and ferrostatin-1 (5 µM) for 48 h as indicated. Cell death was determined by propidium iodide (PI) uptake and flow cytometry. All data are means +/− SEM of three independent experiments or

representative images where applicable. * indicates p<0.05; ** indicates p<0.01; *** indicates p<0.001; **** indicates p<0.0001.

3.5.3. The phosphoglycerate mutase family member 5 (PGAM5) participates in the activation of Drp1 on mitochondria during ferroptosis

Once Drp1 binds to mitochondria, it assembles into spirals at scission sites around the OMM to mediate mitochondrial fission (Smirnova et al, 2001). The activity of Drp1 is not only increased by phosphorylation at Ser616 but also by dephosphorylation of the inhibitory serine 637 site (Chang and Blackstone, 2007; Cribbs and Strack, 2007). PGAM5, which uses alternative catalytic activity to function as a Ser/Thr phosphatase is located on the OMM (Takeda et al., 2009; Lo and Hannik, 2008). Interestingly, it has been shown that, upon both, intrinsic and extrinsic necrosis induction, PGAM5 recruits Drp1 to mitochondria and participates in the activation of its GTPase activity by dephosphorylating it at Ser637 (Wang et al., 2012). Given its role in other necrotic types of cell death and known Drp1 activatory function on mitochondria, we next aimed to elucidate whether the phosphatase PGAM5 could also participate in the complete activation of Drp1 during ferroptosis. To investigate that, we made use of three different HEK cell lines (kindly provided by Prof. Dr. Thomas Langer)-wildtype, *pgam5* KO and, *pgam5* KO that upon tetracyclin treatment re-express the wildtype form of the protein. First, we studied whether the absence of PGAM5 would render cells more resistant to CDI-ferroptosis. Indeed, we found that *pgam5* knockout cells were more resistant to erastin and cysteine-deprivation treatments in comparison to wildtype control cells (**Figure 26.a,b**). Moreover, upon *pgam5* reconstitution in the knockout cell line, this effect was fully rescued (**Figure 26.c**). In order to test whether the resistance of *pgam5* knockout cells to ferroptosis was related to Drp1 activation, we checked P-S637-Drp1 levels. Strikingly, P-S637-Drp1 levels were increased in the knockout cells in comparison to the wildtype control, and these levels were decreased upon *pgam5* re-expression (**Figure 26.d**). Taken together, all our data suggest that the phosphatase PGAM5 might be required for the full activation of Drp1 on mitochondria during ferroptosis induction. Thus, these data

further corroborate a mitochondrial localisation of Drp1 to be important for Drp1-mediated ferroptosis promotion.

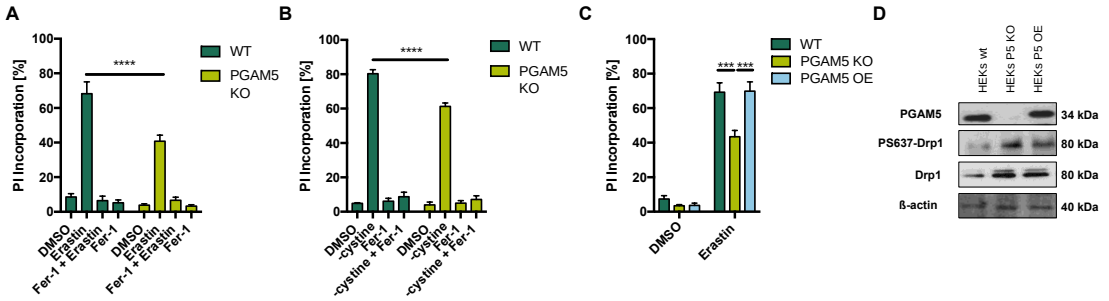

Figure 26. PGAM5 contributes to the activation of Drp1 on mitochondria during ferroptosis (**a**). *pgam5* KO HEK cells and wildtype HEK cells were treated with DMSO, erastin (10 µM), ferrostatin-1 (5 µM), and a combination of both for 48 h. Cell death was determined by propidium iodide (PI) uptake and flow cytometry (**b**). HEKs cells were treated with DMSO, cystine free media, ferrostatin-1 (5 µM), and a combination of both for 48 h. Cell death was determined as in ***a*** (**c**). *pgam5* knockout cells were pre-treated during 48 h with tetracyclin (100ng/mL) to induce *pgam5* re-expression. After pre-treatment, cells were treated as in ***a***. Cell death was determined by propidium iodide (PI) uptake and flow cytometry (**d**). HEK cells were subjected to protein isolation and western blotting. The expression levels of P-S637-Drp1, PGAM5 and ß-actin were determined. A representative blot from three independent experiments is shown. All data are means +/− SEM of three independent experiments or representative images where applicable. * indicates p<0.05; ** indicates p<0.01; *** indicates p<0.001; **** indicates p<0.0001.

3.5.4. Drp1 mediates mitochondrial fragmentation during ferroptosis

Despite the important role of mitochondria in oxidative metabolism, its implication in ferroptosis is still controversial. This type of iron-dependent cell death is associated with morphological changes of mitochondria, including mitochondrial fragmentation (Dixon et al., 2012; Doll et al., 2017). However, it remains unknown the underlying mechanisms responsible for this fragmentation. Since Drp1 has been described to mediate mitochondrial fragmentation in other types of regulated-cell death and we have demonstrated that it translocates to mitochondria upon cysteine-deprivation-induced-ferroptosis, we next hypothesised that Drp1 might be the protein that drives mitochondrial fragmentation in ferroptosis. To validate it, we performed confocal microscopy and we studied mitochondrial fragmentation by MitoTracker deep red stainig. A549 cells were treated with erastin alone and in combination with ferrostatin-1 and Mdivi for 24 h. Of note, after 24 h erastin treatment

mitochondria were completely fragmented (**Figure 27; also see Figure 14**). Strikingly, Mdivi treatment could avoid mitochondrial fragmentation whereas the ferroptosis inhibitor Fer-1 did not prevent it (**Figure 27**). The fact that ferrostatin-1 could not prevent mitochondrial fragmentation suggests that sort-term, cells survive regardless their mitochondrial network status. Long-term studies must be done to elucidate whether cells are able to renovate the mitochondrial network or whether they finally die. Collectively, these data reveal that Drp1 drives mitochondrial fragmentation during erastin-induced ferroptosis.

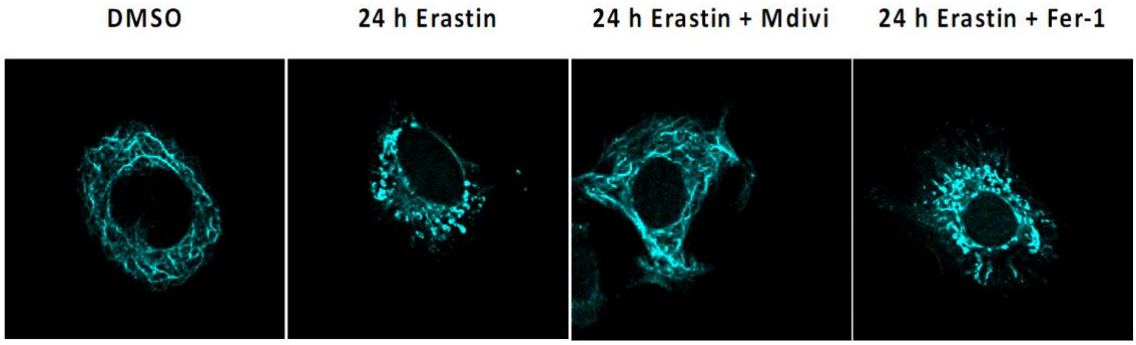

Figure 27. Drp1 drives mitochondrial fragmentation in ferroptosis. Mitochondrial fragmentation was studied by confocal microscopy. A549 cells were treated with DMSO, erastin (10 µM), ferrostatin-1 (5 µM) and Mdivi (75 µM) for 24 h. Mitochondria were stained with MitoTracker deep Red (150 nM) which was added to the cells during the las 30 min of the treatment. Scale bar: 15 µM. 50 cells from three independent experiments were analysed.

4. DISCUSSION

The research that has been carried out for this PhD thesis has revealed two novel important facts for the ferroptosis field. On the one hand, a new potent and efficient ferroptosis inhibitory activity has been described for dynasore. Importantly, dynasore is not only a dynamin 1 and 2 inhibitor but also a ROS scavenger agent in cell-free assays. This finding may allow researchers to use dynasore as a candidate molecule to block oxidative-stress induced cell death pathways such as ferroptosis. On the other hand, this work has shown the involvement of a kinase (CaMKIIα) in cysteine-deprivation induced ferroptosis, as well as its target (Drp1), which is essential for the pathway. Below, these new findings will be further discussed.

4.1. Dynasore inhibits ferroptosis through modulation of iron uptake via CD71 (Tf)-Tf-Receptor and ROS scavenging (Adapted from Prieto-Clemente et al., 2020)

Recently, ferroptosis was described as an iron and ROS-dependent form of regulated cell death (Dixon et al., 2012; reviewed in Bebber....Prieto-Clemente et al., 2020). Ferroptosis has been related to promote tissue injury in various human pathologies such as neurodegeneration of motor neurons in amyotrophic lateral sclerosis (ALS) (Devos et al., 2019; Chen et al., 2015) and Huntington´s disease (Ong et al., 2015). Moreover, ferroptosis was linked to mediate ischemia-reperfusion injury (Gao et al., 2016) and to participate in several other malignancies, including carcinogenesis or stroke (Ong et al., 2015; Stockwell et al., 2017).

Here, we have identified a novel functionality of the dynamin 1 and 2 inhibitor dynasore in blocking ferroptosis. The GTPases dynamin 1 and 2 mediate transferrin uptake by regulating earlier rate-limiting steps of clathrin-coated vesicle formation during endocytosis (Harding et al., 1983). In agreement with this regulation, both, dynasore treatment and silencing of dynamin 1 and 2 expression led to surface increase of transferrin receptor (CD71). However,

regardless of depleting intracellular iron levels, we surprisingly found that silencing of dynamin 1 and 2 expression did not rescue cells from ferroptosis nor lipid ROS accumulation, whereas treatment with the small molecule dynasore did. These data suggested that, at least in the short term, a reduction of intracellular iron levels is less important for the execution of ferroptosis than previously thought. Strikingly, the iron chelating agent DFO, has been shown to act as a high affinity radical scavenger in cell-free assays (Morel et al., 1992). Based on the fact that peroxyl radicals propagate lipid peroxidation within membranes during ferroptosis (Conrad et al., 2019), it is tempting to speculate that the radical scavenging activity of DFO may be responsible, together with its iron chelating ability, for blocking ferroptosis. Due to the fact that dynasore effectively blocked extracellular iron uptake but this activity was insufficient to inhibit cell death, our data suggest that intracellular iron storage compartments may be more important for iron-fueled hydroxyl radical formation than CD71-TfR endocytosis. Alternatively, the divalent metal-ion transporter-1 (DMT1), a transferrin-independent iron transporter, might be sufficient to support ferroptosis in the cellular systems studied here (Yanatori et al., 2015; Lane et al., 2015).

One of the hallmarks of ferroptosis is the accumulation of lipid ROS (Dixon et al., 2012). Our data showed that dynasore can counteract this accumulation, as well as general cellular ROS, acting as a radical trapping agent in cell-free assays. ROS are mainly produced as a result of mitochondrial OXPHOS, but they can also be released from cytosolic enzymes such as NADPH oxidases (NOX). Interestingly, hydroxyl radicals are generated from iron and H_2O_2 via the Fenton and Haber–Weiss reactions (Kajarabille et al., 2019). Of note, dynasore has been proposed as an inhibitor to treat mitochondrial disorders characterised by aberrant accumulation of mitochondrial ROS (Devos et al,. 2019; Reddy et al., 2014). Moreover, in human corneal epithelial cells, dynasore prevented oxidative stress-induced cell damage through a non-described mechanism independent of dynamin 1 and 2 inhibition (Webster et al., 2018). It is tempting to speculate that, the radical-trapping activity described in our study may underlie such tissue protection. In addition, the chemical structure of dynasore might explain that it functions as a direct ROS scavenger via its phenol or amine moiety (Kareem et al., 2015). Dynole 34-2 is another dynamin 1 and 2 inhibitor which directly targets

the GTPase domain (Robertson et al., 2014). Our data showed that Dynole 34-2 blocked ferroptosis as efficiently as dynasore. Given that dynamin 1 and 2 silencing was, however, insufficient to block cell death, the fact that Dynole 34-2 is structurally similar to dynasore also points towards a ROS scavenging activity for Dynole 34-2. While abnormal accumulation of ROS can cause DNA damage, protein denaturation and lipid peroxidation, certain amounts of ROS are essential to maintain cellular homoeostasis (Dixon et al., 2012; Dixon et al., 2014; Kajarabille et al., 2019). This might explain the slight cytotoxic effects of prolonged dynasore treatment observed in our cellular system.

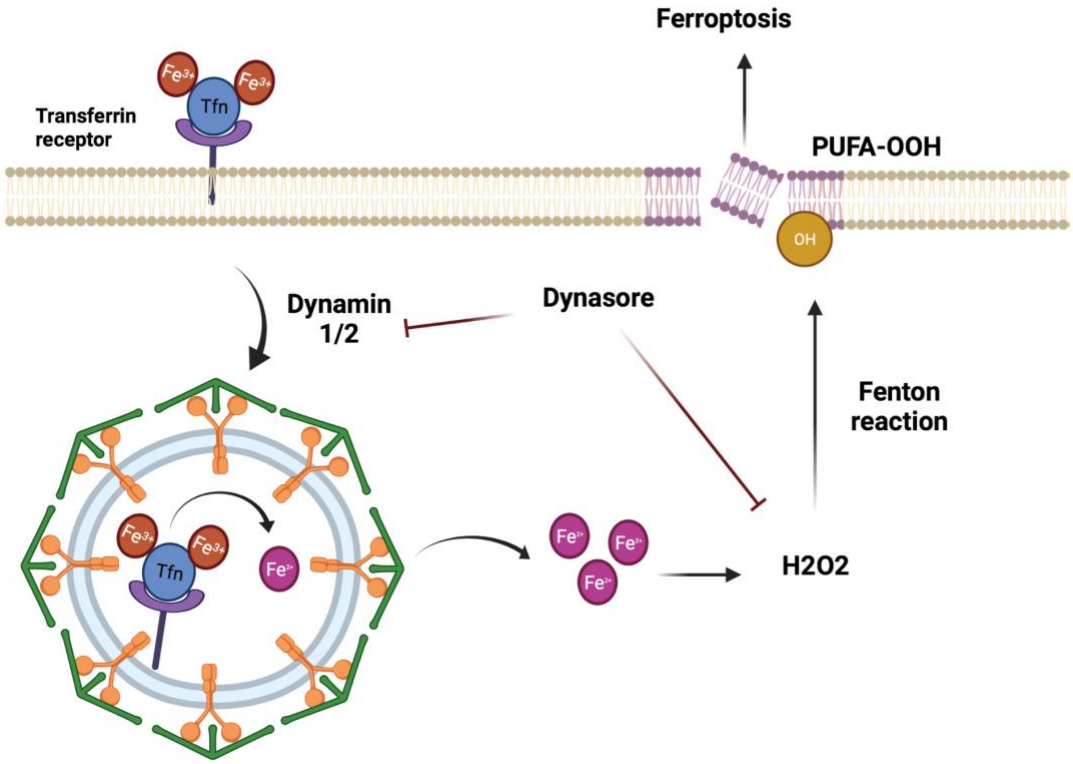

Figure 28. Dynasore inhibits ferroptosis through combined modulation of iron uptake via CD71 (Tf)-Tf-Receptor and ROS scavenging. This figure was created using a licensed version of Biorender.com.

Based on the fact that DFO does not rescue H_2O_2-induced cell death (Dixon et al., 2012) and it has been shown to directly scavenge peroxyl radicals (Morel et al., 1992), we propose that dynasore scavenges general radicals, explaining its inhibition of H_2O_2-induced cell death. In addition, in collaborative work with the Culmsee laboratory, we also found that dynasore inhibits mitochondrial respiration in neuronal cells, limiting cellular H_2O_2 and iron availability (Data not

shown, see Prieto-Clemente et al., 2020). Taken together, our findings propose two mechanisms by which dynasore functions as a potent blocker of ferroptosis. On the one hand, the combined inhibition of CD71-iron uptake and mitochondrial respiration prevent lipid peroxidation and ferroptosis. On the other hand, dynasore acts as a direct radical-trapping agent that blocks H_2O_2-induced cell death (**Figure 28**). These novel findings suggest that dynasore can be used as a new potent combined ROS blocker and lipid ROS-induced cell death inhibitor for *in vivo* studies.

4.2. Drp1 activation promotes cysteine-deprivation-induced (CDI) ferroptosis

Ferroptosis strongly relies on high ROS levels (Dixon et al., 2012). Among the different sources of ROS, mitochondrial oxidative metabolism represents the most important one for CDI-ferroptosis (Gao et al., 2019). Mitochondrial homeostasis is preserved by a balance between mitochondrial fission and fusion events (Praefcke et al., 2004). Interestingly, mitochondrial fragmentation and morphological changes of mitochondria have been observed when this balance is disrupted, being characteristic phenotypic steps for a wide variety of programmed cell death pathways, including ferroptosis (Cereghetti et al., 2010; Xie et al., 2018). In line with this, our data showed that upon ferroptosis induction, cells present with a disrupted mitochondrial network. Mitochondrial fission and, along with that, fragmentation, is known to be mainly regulated by the dynamin superfamiliy member Drp1 (Xie et al., 2018). Of note, during autophagy, Drp1 can disturb mitochondrial homeostasis and along with that, impair mitochondrial function, leading to mitochondrial fragmentation and activating autophagic cell death (Dubois et al., 2016). Moreover, Drp1 mediated-mitochondrial fission is considered to be a crucial prerequisite for apoptosis (Karbowski et al., 2002). In support of this, overexpression of a dominant negative Drp1 mutant (Drp1K38A) slows down apoptosis kinetics (Frank et al., 2001), which suggests that Drp1 might be essential for the release of mitochondrial components such us cytochrome C. Even though Drp1 is the main described regulator of mitochondrial fission, it has become a major point of controversy. The argument focuses on whether Drp1 directly regulates cell death, and if involved, whether it is a boost

or a negative mediator of the pathway. It has been shown that loss of Drp1 induce cell death in mice embryos (Ashrafian et al., 2010). Indeed, cardiac-specific *drp1* knockout in mice impaired the ventricular function and induced cell death (Ikeda et al., 2015). Moreover, *drp1*-null mice were unable to undergo developmentally regulated apoptosis during neural tube formation, which resulted in embryonic death (Wakabayashi et al., 2009). On the other hand, overexpression of Drp1 in mouse cell lines led to an inhibition of muscle growth (Touvier et al., 2015). In addition, recent studies have demonstrated that mutations of Drp1 result in disruption of mitochondrial fission and lead to a wide variety of diseases. For example, the hyper-phosphorylation of Drp1 at Ser637 induces a misbalance between mitochondrial fusion and fission in spastic paraplegia patients (Lavie et al., 2016). Moreover, cells from patients with Charlevoix Saguenay, presented reduced ability to recruit Drp1 to mitochondria and poor mitochondrial health (Bradshaw et al., 2016). Intriguingly, mitochondrial fission plays an important role in multiple tumors (Varadarajan et al., 2013). The inhibition of Drp1 activity in brain-tumor cells attenuated their tumorigenicity *in vitro* (Xie et al., 2015). Moreover, blocking Drp1 activity also killed thyroid cancer cells by modifying the migration and invasion ability of tumor cells (Xie et al., 2015; Ferreira-da-Silva et al., 2015). Here, we have shown for the first time that both, the inhibition and silencing of Drp1 expression impaired erastin-induced ferroptosis. Interestingly, whereas homozygous knockout mice for *drp1* are embryonically lethal (Ishihara et al., 2009; Wakabayashi et al., 2009), heterozygous *drp1* knockout mice survive and present with lower levels of H_2O_2 and lipid peroxides in tissues in comparison to wild type littermates (Manczak et al., 2012). It is tempting to speculate that this decrease in lipid ROS levels is linked to an impairment of ferroptosis due to the partial absence of Drp1. Indeed, a misbalance between mitochondrial fission and fusion together with an alteration of mitochondrial quality control, leads to ischemia/reperfusion injury, a condition which is mainly conducted by ferroptosis (Ikeda et al., 2015). Our data showed that *drp1* knockout cells generated by CRISPR/Cas9 can undergo ferroptosis as efficiently as wildtype cells. However, in line with our results obtained through transient silencing of Drp1, the conditional deletion of *drp1* reduced CDI-ferroptosis. Mitochondria are highly dynamic organelles that are characterised by their plasticity, which is a key factor in metabolic adaptation to different stimuli (Romanello and Sandri., 2013).

Indeed, alterations in the mitochondrial content, function or shape are associated with over- or underexpression of the mitochondrial fission and fusion machineries (Romanello and Sandri., 2013; Touvier et al., 2015; Tezze et al., 2017). This regulation also occurs in several diseases such as cancer cachexia, where *drp1* expression was shown to be dramatically reduced (Barreto et al., 2016; van der Ende et al., 2018; Brown et al., 2017). Consistently, we propose that the generation of a stable knockout of *drp1* might influence the regulation of the mitochondrial shape and function, leading to an adaptation of the knockout status which may not interfere with the ferroptosis pathway. A conditional *drp1* knockout or siRNA-mediated transient silencing in turn, might not leave enough time for this adaption to occur, which could explain the partial ferroptosis resistance that is cause by these two experimental set-ups.

Ferroptosis is triggered by an iron-dependent accumulation of ROS that exceeds cellular redox buffering by intracellular GSH levels together with the phospholipid hydroperoxidases that use it as a cofactor (Dixon et al., 2012; Yang and Stockwell., 2016). *In vitro*, ferroptosis can be triggered via two currently known distinct strategies. On the one hand, the synthetic small molecule erastin can induce ferroptosis by inhibiting the activity of system xc-, causing a depletion of intracellular GSH levels (Dixon et al., 2012). On the other hand, the pharmacological inactivation of GPX4 by the small molecule RSL3 can trigger ferroptosis without affecting GSH levels (Friedmann Angeli et al., 2014; Yang et al., 2014). Furthermore, cystine-deprivation from cell culture media can also induce ferroptosis by depleting GSH levels, mimicking the erastin effect, albeit representing a more physiological scenario (Gao et al., 2015a, 2015b). In agreement with this regulation, both, cystine deprivation and the inhibition of the GSH synthesis pathway induced ferroptosis in our cellular system. Interestingly, silencing of Drp1 expression could efficiently block all types of CDI ferroptosis. However, upon elimination and inhibition of GPX4, cells underwent ferroptosis irrespective of Drp1 presence or absence. When cells are deprived of cystine, intracellular GSH levels decrease rapidly, contributing to subsequent aberrant ROS and lipid ROS accumulation and induction of ferroptosis (Gao et al., 2019). We found that upon GPX4 inhibition GSH levels remain normal. Based on our data, it is tempting to speculate that (**i**) when GPX4 is inhibited or depleted, the

low amount of basal lipid ROS are quickly amplified due to the lack of its activity, leading to ferroptosis even when Drp1 is absent; (**ii**) due to the fact that GPX4 is located downstream in the ferroptosis pathway, Drp1 may regulate earlier steps that do not interfere with the regulation of GPX4 activity and (**iii**) Drp1 implication/activation in the pathway is triggered by the depletion of the GSH content, thereby is not involved in GPX4 inhibition induced-ferroptosis. Future research is required to further investigate the hypothesis that the implication of Drp1 in ferroptosis is dependent on the specific ferroptosis activation route.

Drp1 is a cytosolic protein which is recruited to mitochondria to regulate mitochondrial fission (Praefcke et al., 2004). The regulation of the Drp1 GTPase activity and its mitochondrial translocation is mediated by different posttranslational modifications (Lackner et al., 2009; Santel et al., 2008). Importantly, phosphorylation and dephosphorylation events are the best characterized PTMs described for Drp1 so far (Chang et al., 2007). Whereas phosphorylation of Drp1 at Ser616 is linked to increased GTPase activity and Drp1-dependent mitochondrial fission, phosphorylation at Ser637 inhibits mitochondrial division and GTPase activity (Chang et al., 2007; Taguchi et al., 2007; Archer et al., 2013). However, some studies revealed that P-Ser616 does not necessarily influence Drp1 GTPase activity (Chang et al., 2007; Taguchi et al., 2007). Our own data support that upon erastin treatment, Drp1 phosphorylation at Ser616 is increased along with an increase in its GTPase activity pointing towards an activatory function of Ser616 in our experimental context. Interestingly, increased levels of Drp1 (Ser616) were observed during early stages of ischemic injury (Chenyang et la., 2020; Gao et al., 2013), a type of tissue injury previously associate with ferroptosis. Moreover, phosphorylation of Drp1 at serine 616 or dephosphorylation at serine 637 are known to positively regulate Drp1 GTPase activity and to induce its mitochondrial translocation (Chang et al., 2007; Taguchi et al., 2007; Archer et al., 2013). In agreement with these regulations, we propose that Drp1 phosphorylation (Ser616) along with GTPase activity, increase upon CDI-ferroptosis (**Figure 29**).

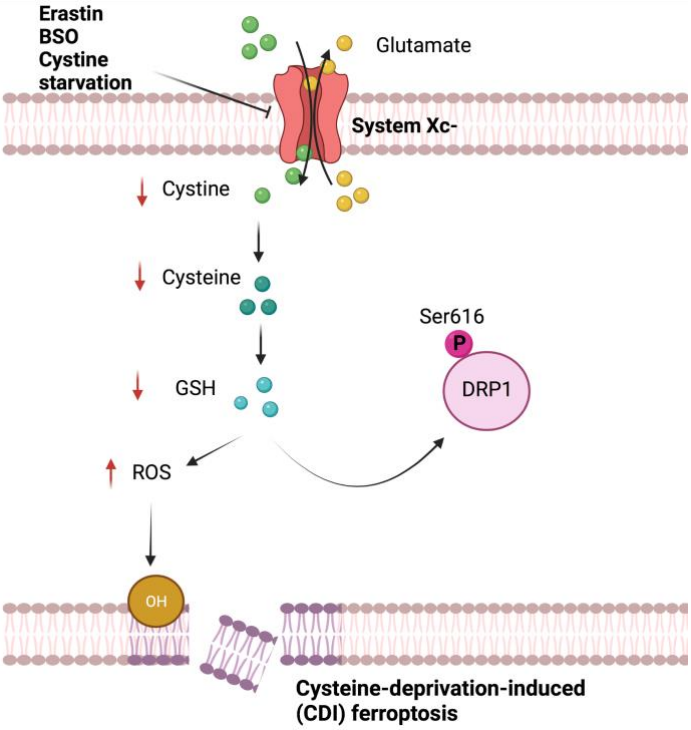

Figure 29. Cysteine starvation triggers ferroptosis via Drp1 activation. This figure was created using a licensed version of Biorender.com.

4.3. CaMKIIα promotes CDI-ferroptosis and regulates phosphorylation of Drp1 (Ser616)

Protein kinases phosphorylate their targets via catalyzing the transfer of γ-phosphate from ATP to the phospho-residues (tyrosine, threonine or serine), which differ among the different targets (Zhang et al., 2009). Considering the increase in Drp1 Ser616 levels upon ferroptosis induction, we assumed the implication of a kinase in the pathway. Interestingly, based on the critical role of kinases in apoptosis or necroptosis, a study performed a kinome screen against CDI-ferroptosis. The screen identified 34 essential kinases, and investigated a role for ATM (Mutated in Ataxia-Telangiectasia) in promoting ferroptosis. However, among the list of potentially positive regulators of ferroptosis, Ca^{2+}/calmodulin (CaM)-dependent protein kinase II (CaMKII) was found to be crucial for CDI-ferroptosis (Chen et al., 2019). CaMKIIα has been shown to indirectly mediate mitochondrial fission by phosphorylation of Drp1 (Ser616) (Bo et al., 2017). Interestingly, we found that both, the inhibition and silencing of CaMKIIα expression partially impaired CDI-ferroptosis and reduced ferroptosis-

induced phosphorylation of Drp1 (Ser616). Furthermore, silencing of CaMKIIα expression dissipates Drp1-dependet mitochondrial fission in apoptosis (Hu et al., 2019). Interestingly, CaMKII has been implicated in oxidative stress-induced mitochondrial fragmentation and apoptosis in rat hepytocytes (Toledo et al., 2013). Moreover, oxidized-CaMKII was identified as an essential component for promoting ischemia-reperfusion injury by ROS induction (Wu et al., 2019). Based on our data and current literature, it is tempting to speculate that CaMKIIα is the kinase which phosphorylates Drp1 (Ser616) upon CDI-ferroptosis.

Even though CaMKII is mainly expressed in the brain, is a ubiquitous protein involved in mediating cellular Ca^{2+} signals (Bayer et al., 1999; Cook et al., 2018). The activity of CaMKII is triggered by the binding of Ca^{2+}/Calmodulin (Ca^{2+}/CaM) to its regulatory domain. This combination relieves an autoinhibitory block of the domain, which mainly regulates substrate access and nucleotide binding. Calcium ions are fundamental second messengers that regulate a variety of cellular functions including oxidative stress-induce cell death pathways such as oxytosis or ferroptosis (Maher et al., 2017). Even though the role of calcium in ferroptosis has not been fully explored, our laboratory has demonstrated that ferroptosis induction is characterised by an early and sustained increase of cystosolic Ca^{2+} levels (Pedrera et al., 2020). In line with this regulation, we found that ferroptosis was impaired upon either calcium chelation or deprivation from the cell culture media. Based on our finding that CaMKIIα promotes CDI-ferroptosis and that upon ferroptosis induction there is an increase in cytosolic calcium we propose a model in which Ca^{2+} influx may activate CaMKIIα, which would later in turn phosphorylate Drp1 downstream in the pathway.

The Ca^{2+} signaling network connects with other cellular signaling systems such as ROS. Although initially ROS were considered potentially dangerous for cells, at balanced levels, they serve as signaling molecules that are important for various cellular processes including cell death (Ermak et al., 2002; Holmström et al., 2014). Various studies have shown evidence that suggest that ROS and calcium can interact in a bidirectional way (Gordeeva et al., 2003). Of note, the voltage-dependent Ca^{2+} channels (VDCC) from the plasma membrane are redox

sensitive (Hudasek et al., 2004; Mikami et al., 1989). Specifically, the activated or inhibited redox status of these channels modulates their activity, expression and opening-time (Trebak et al., 2010; Bogeski et al., 2010). Interestingly, ROS and H_2O_2 were shown to stimulate Ca^{2+} entry *in vitro* (Hudasek et al., 2004; Tabet et al., 2004). In addition, a variation in the ratios of the GSH/GSSG redox pair can also regulate the ryanodine calcium receptors (RyR) and the inositol 1,4,5-triphosphate calcium receptors (IP_3R) from the sarcoplasmic/endoplasmic reticulum (SR/ER) (Hidalgo et al., 2005). When both types of calcium channels are oxidized their activity is increased, which leads to a release of Ca^{2+} ions to the cytosol (Terentyev et al., 2008; Yan et al., 2008). Considering this regulation, we propose a working model in which triggering ferroptosis by cystine deprivation leads to a decrease in the glutathione levels, which are unable to preserve sub-toxic levels of ROS. As a consequence, subsequent elevated ROS levels may oxidize calcium channels from the plasma membrane and from the SR/ER, which elevate the cytosolic calcium levels. Following this increase, CaMKIIα is activated by calcium binding and later on, it phosphorylates Drp1 (Ser616), which promotes CDI-ferroptosis (**Figure 30**).

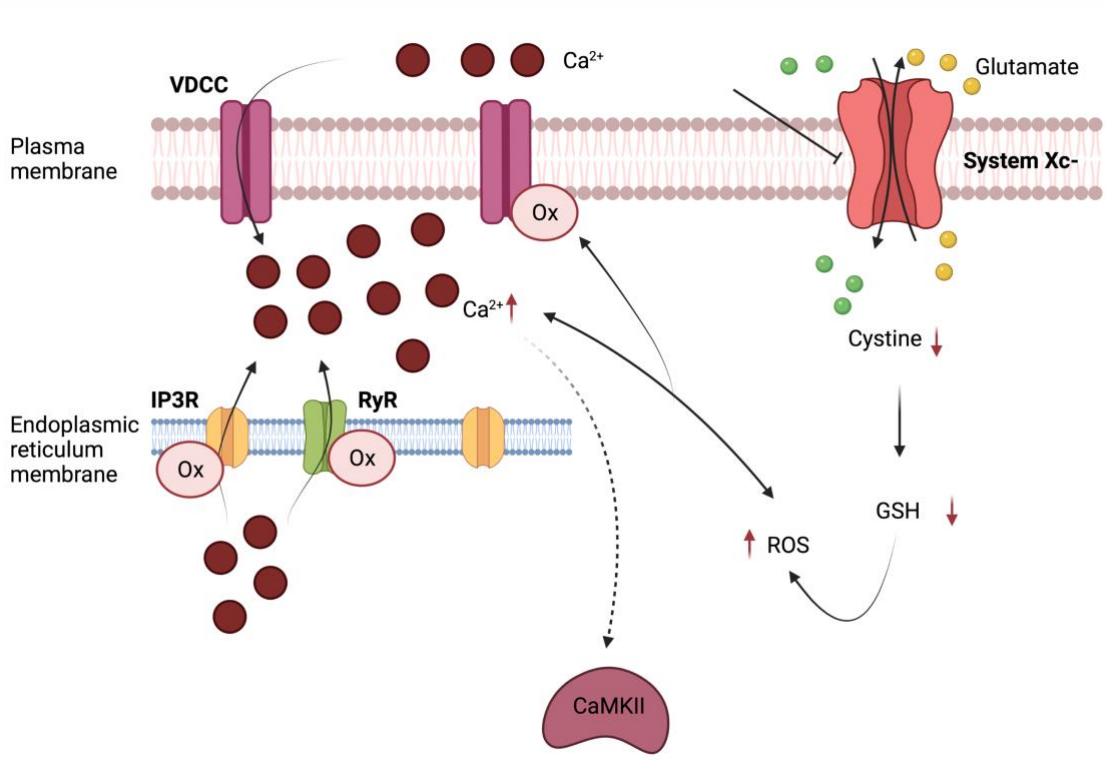

Figure 30. CaMKIIα promotes CDI-ferroptosis and might phosphorylate Drp1 (Ser616). This figure was created using a licensed version of Biorender.com.

4.4. Drp1 and mitochondria are essential for CDI-ferroptosis

Homozygous *drp1* knockout mice are embryonically lethal due to severe developmental abnormalities related to defective mitochondrial fission and metabolism (Ishihara et al., 2009; Wakabayashi et al., 2009). However, heterozygous *drp1* knockout mice, survive and present with low levels of lipid peroxides in tissues (Manczak et al., 2012). Interestingly, *in vitro* acetaldehyde treatment induces Drp1 phosphorylation and mitochondrial fragmentation by increasing intracellular ROS and Ca^{2+} levels (Yan and Zhao., 2019). The mitochondrial electron transport chain (ETC) is known to be the main source of ROS. When the ETC is impaired or damaged, ROS are overproduced and aberrant amounts accumulate leading to lipid peroxidation and cell death (Apostolova et al., 2015; Arena et al., 2018). However, regardless of inhibiting CID-ferroptosis, silencing of Drp1 expression neither affected lipid ROS nor general ROS accumulation upon erastin treatment (data now shown) suggesting that it is less likely to regulate the ETC during ferroptosis. Mitochondrial fission is mediated by Drp1, which is recruited to the outer mitochondrial membrane upon phosphorylation (Ser616) to form active GTP-dependent mitochondrial fission sites (Smirnova et al., 2001; Xie et al., 2018). In line with this regulation, we found that Drp1 is recruited to mitochondria during erastin-induced ferroptosis. Based on our data, it is tempting to speculate that the function of Drp1 in ferroptosis is related to mitochondria instead of modulating general ROS and Lipid ROS levels.

Unlike other dynamin family members, Drp1 does not present a lipid-binding domain. After being recruited to mitochondria, Drp1 needs protein anchors to oligomerise around the scission sites in the outer mitochondrial membrane (Otera and Mihara, 2011). In mammals, Drp1 makes use of 4 adaptor proteins; Fis1, Mff, MiD49 and MiD51 (Otera et al, 2010; Palmer et al., 2011; Zhao et al., 2011). Nonetheless, these protein adaptors are not only localised on mitochondria but also on other organelles such as the ER or peroxisomes (Ji et al., 2017). Interestingly, even though poly-unsaturated fatty acids (PUFAs) are the main target of peroxidation, recently, long-chain saturated fatty acids (SFA) have been described to be implicated in ferroptosis. Strikingly, SFA-mediated ferroptosis is

dependent on peroxisome driven ether phospholipid biosynthesis (Cui et al., 2021). Distinct from Fis1 and Mff, MiD49 and MiD51 are confined to mitochondria (Palmer et al., 2011). Thus, MiD49 and MiD51 are key proteins in the regulation of mitochondrial fission due to their function in tethering Drp1 to mitochondria (Palmer et al., 2011). Interestingly, we found that silencing of MiD49 and MiD51 expression impaired erastin-induced ferroptosis to similar levels as Drp1 silencing. These data suggest that the role of Drp1 in ferroptosis is dependent on mitochondrial recruitment of Drp1. Nevertheless, more research is needed to completely discard the requirement of other organelles such as the ER or peroxisomes in the Drp1-regulated ferroptosis pathway. Of note, mitochondrial membrane fission occurs at inter-ER contact sites where Drp1 oligomerises, which proposes that the ER could also contribute to mitochondrial fission (Friedman et al., 2011; Korobova et al., 2013; Lewis et al., 2016). Indeed, a recent study showed that the ER protein STING1 (Stimulator of interferon genes 1) promotes ferroptosis in human pancreatic cancer cells by triggering Mfn1/2-dependent mitochondrial fusion (Li et al., 2021). This finding points towards a crosstalk between subcellular organelles, such us mitochondria and ER, in the regulation of ferroptosis.

Besides phosphorylation of Drp1 at Ser616, its activity is also regulated by dephosphorylation events at Ser637 (Chang and Blackstone, 2007). The phosphatase PGAM5 is located on the outer mitochondrial membrane (Takeda et al., 2009; Lo and Hannik, 2008). Interestingly, upon both, intrinsic and extrinsic necrosis induction, PGAM5 was shown to recruit Drp1 to mitochondria participating in its activation by dephosphorylating Drp1 at Ser637 (Wang et al., 2012). In agreement with this modulation, we found that *pgam5* KO cells demonstrated increased constitutive Drp1 phosphorylation at Ser637 and were partially resistant to CDI-ferroptosis. Because PGAM5 is placed at the constriction sites of mitochondrial fission, it is tempting to speculate that Drp1 might be fully activated *in situ* in these sites.

Drp1-mediated mitochondrial fission, and along with that, fragmentation, seems to be a phenotypic feature of apoptosis, necrosis and ferroptosis. During apoptosis, Drp1 is known to drive crucial steps for mitochondrial fission and

fragmentation, which enable the release of mitochondrial apoptosis-regulatory components such us cytochrome c and Smac from mitochondria into the cytosol (Jiang and Wang, 2004; Wang et al., 2001). For necrosis, mitochondria fragment and aggregate around nuclei before the rupture of the plasma and nuclear membrane (Wang et al., 2012). Lastly, for CDI-ferroptosis the canonical metabolic function of mitochondria enriches lipid ROS generation (Gao et al., 2019). Yet, neither cytochrome c is released from mitochondria during ferroptosis nor fragmented mitochondria are observed to cluster around the nuclei, which suggests that the downstream event following fragmentation might be different amongst the three distinct types of cell death. Interestingly, upon glutamate toxicity, Drp1 has been described to be a key factor mediating mitochondrial fragmentation, loss of mitochondrial membrane potential (MMP) and neuronal cell death (Grohm et al., 2012). Moreover, mitochondria are the main target in hypoxic/ischemic reperfusion injury, a type of tissue injury that is blocked by the ferroptosis inhibitor ferrostatin-1 (Li et al., 2019; Linkermann et al., 2014). In addition, the mitochondrial dysfunction which occurs after ischemia/reperfusion has been linked to Drp1 function (Favaro et al., 2019). Consistently, our results showed that erastin treatment affects mitochondrial shape and induces mitochondrial fragmentation, which is abolished by pharmacological inhibition of Drp1 activity. These data suggest that Drp1 drives mitochondrial fragmentation during ferroptosis, and the impairment of the GTPase activity of Drp1 by its pharmacological inhibition preserves mitochondrial integrity and blocks cell death. Interestingly, the ferroptosis inhibitor ferrostatin-1 could rescue cells from death but was unable to preserve a healthy mitochondrial network. Mitochondrial fission has been described to eliminate mitochondrial damage (Youle and van der Bliek, 2012), which suggests that endogenous Drp1 maintains healthy mitochondria. However, an excess in Drp1 activity leads to mitochondrial fragmentation (Hemachandra Reddy, 2015). Whereas pharmacological inhibition of Drp1 could both, block ferroptosis and maintain a healthy mitochondrial network, ferrostatin-1 treatment impaired cell death but failed to inhibit mitochondrial fragmentation. The importance of these studies is highlighted by the finding that ferroptosis can be blocked independently of the status of the mitochondrial network in the cell, together with the fact that Drp1 drives the mitochondrial fragmentation observed during ferroptosis. Based on all obtained

results, it is tempting to speculate that Drp1 is activated upon CDI-ferroptosis induction and translocates to mitochondria where it drives mitochondrial fission and, along with that, fragmentation, most likely as a consequence of an excess of Drp1 activation. Short-term, ferrostatin-1 can block ferroptosis *in vitro* even when the mitochondrial network is fragmented. However, long-term experiments must be performed to elucidate whether fragmentated mitochondria could be eliminated upon mitophagy, allowing cells to restore a new and healthy mitochondrial network. Yet, how mitochondrial fragmentation driven by Drp1 promotes ferroptosis mechanistically it still not clear and remains to be fully elucidated.

In summary, here we have demonstrated that cystine depletion and subsequent glutathione reduction induces ferroptosis that is promoted by Drp1. We propose that, the induction of CDI ferroptosis may elevate intracellular Ca^{2+} levels, that activate the Ca^{2+}-dependent kinase CaMKIIα. Erastin treatment increases the interaction between CaMKIIα and Drp1, suggesting that the kinase might phosphorylate it at Ser616 inducing its mitochondrial translocation. Our working model proposes that Drp1 is fully activated on mitochondria by dephosphorylation (Ser616) by PGAM5, driving excessive mitochondrial fission and fragmentation. This might lead to an increase in mitochondrial ROS production, feeding into the mitochondrial lipid peroxidation pool. However, the challenge remains to further investigate biochemical steps that are crucial for ferroptosis execution downstream of Drp1 (**Figure 31**).

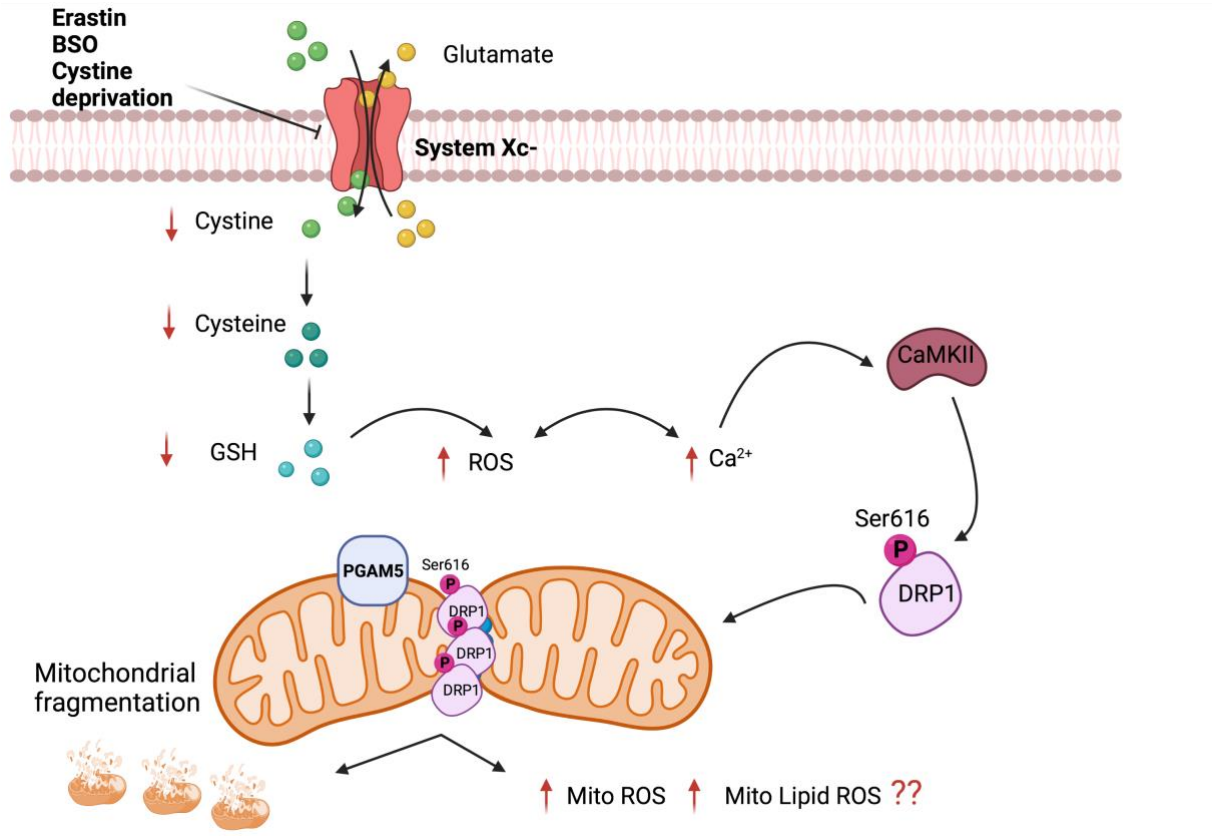

Figure 31. Cysteine starvation triggers ferroptosis via CaMKII-mediated Drp1 activation and mitochondrial fragmentation. This figure was created using a licensed version of Biorender.com.

5. CONCLUDING REMARKS AND FUTURE PERSPECTIVE

Experimental work undertaken for this doctoral dissertation set out to: (1) Investigate the impact of iron uptake regulation by dynamin 1 and 2 on ferroptosis; (2) Study the implication of dynamin-related protein 1 in ferroptosis; (3) Mechanistically define and characterise the early crucial steps involved in Drp1 activation during ferroptosis; (4) Elucidate the functional consequence of Drp1 activation in its ferroptosis-induced activation. Here, we have revealed the following key findings:

1. Dynamin 1 and 2 regulate CD71 turnover and iron uptake but are dispensable for acute induction of ferroptosis. However, we have shown for the first time that the widely used classical dynamin 1 and 2 inhibitor dynasore, is a new and highly effective inhibitor of ferroptosis through additional activities. Our findings propose two combined mechanisms by which dynasore functions as a potent blocker of lipid ROS- (ferroptosis) and ROS-driven cell death, respectively. First, inhibition of CD71-iron import limits lipid peroxidation and ferroptosis, and second, direct radical-trapping activity of dynasore broadly blocks ROS-driven types of cell death. These unexpected and novel findings suggest that dynasore may be used as a new potent combined ROS blocker and lipid ROS-induced cell death inhibitor for *in vivo* studies. At the same time, our results propose that urgent re-interpretation is warranted of studies making use of dynasore to block dynamin 1 and 2-mediated effects *in vitro* and *in vivo*.
2. We find that loss of Drp1 impairs cysteine-deprivation-induced (CDI) ferroptosis. Strikingly, cells can commit ferroptosis triggered by both, genetic depletion or pharmacological inhibition of GPX4 regardless of Drp1 absence. These data propose that “canonical” induction of ferroptosis via direct inhibition or depletion of GPX4 might bypass mitochondrial regulation while CDI ferroptosis cannot. On the one hand, ferroptosis can be triggered by cystine deprivation and the subsequent glutathione depletion. On the other hand, cells undergo ferroptosis upon GPX4 inhibition. In the latter scenario, glutathione levels remain unperturbed, and the basal amount of lipid ROS are quickly amplified leading to a potent ferroptosis response. In agreement with what is

published, our data suggest that Drp1 promotes ferroptosis when GSH is depleted and therefore, its implication in ferroptosis is likely context-dependent. Hence, interesting future research pathways of canonical and non-canonical induction of ferroptosis to clarify mitochondrial involvement in one versus the other pathway.

3. While apoptosis is characterised by caspase activation (Li and Yuan., 2008) and during necroptosis the kinase RIPK1 is essential for its execution (Yuan et al., 2018) a potential function for kinases in the execution of ferroptosis has been poorly explored. We find that Calcium-calmodulin kinase II-α (CaMKIIα) promotes cysteine-deprivation-induced-ferroptosis and regulates phosphorylation of Drp1 at Ser616. Moreover, the elimination of CaMKIIα renders cells resistant to ferroptosis. This result, highlights the importance of kinases in programmed cell death pathways. Importantly, we found that CaMKIIα constitutively binds Drp1, which proposes that Drp1 might be a phosphorylation target of CaMKIIα. In support of this notion, absence of CaMKIIα reduced phosphorylated Drp1 (Ser616) protein levels. In accordance with work published by us and others, Ca^{2+} and ROS are required for ferroptosis (Maher et al., 2017; Pedrera et al., 2020) and might be responsible for CaMKIIα and Drp1 activation. Nevertheless, further research is needed to clarify the exact mechanism as well as the kinetics involved in CaMKIIα-Drp1 regulation.
4. We identify that upon cystine starvation, P-Ser616-Drp1 translocates to mitochondria where Drp1 promotes mitochondrial fragmentation during ferroptosis. Our data support a role of Drp1 mediating mitochondrial fission and, along with that, fragmentation during ferroptosis, which is observed during other programmed cell death pathways such as apoptosis or necroptosis (Jiang and Wang, 2004; Wang et al., 2001; Wang et al., 2012). Future research is needed to elucidate whether Drp1 could be also involved in modulating mitochondrial ROS or mitochondrial lipid ROS, and thereby regulate mitochondrial ferroptosis.
5. Taken together, this doctoral thesis proposes a model for ferroptosis where Drp1 promotes the execution of this new type of programmed cell death with the following working model: Upon cysteine-deprivation, GSH

levels decrease causing an increase in general ROS levels. Both, induce the release of Ca^{2+} to the cytosolic compartment which contributes to CaMKIIα activation. This kinase might phosphorylate its target, Drp1, at Serine616, promoting Drp1 translocation to mitochondria. There, Drp1 requires its adaptors MiD49 and MiD51 to be anchored to the outer mitochondrial membrane. Moreover, the phosphatase PGAM5 contributes to the full activation of Drp1 by dephosphorylation at Serin637. Finally, Drp1 mediates mitochondrial fission which results in mitochondrial fragmentation due to an increase in Drp1 activity. As Drp1 plays an essential role in neurodegenerative diseases (Itoh et al., 2013) and ischemia/reperfusion injury (Favaro et al., 2019) and we identify a role for Drp1 in regulating ferroptosis, amelioration of these diseases may be brought about by blocking Drp1 and thereby exacerbated ferroptosis.

6. MATERIALS AND METHODS

6.1. Materials

6.1.1. Chemicals and Reagents

Chemicals/Reagents	Supplier	Catalog number
2-Isoropanol	AppliChem GmbH	1310901212
3-(4,5-dimethylthiazol-2-yl)-2,5-diphenyltetrazolium bromide **(**MTT)	Sigma Aldrich	298-93-1
Acetic acid 100%	VRW	1.000.631.011
Agarose	Biozym	840004
Ampicilin	Sigma aldrich	A0166
Antimycin-a	Sigma aldrich	A8674
Bapta	Caymanchem	11706
Bapta-AM	Caymanchem	15551-5
BODIPY-C11	Invitrogen	D3861
BSA	Hyclone	K41-001
Buthionine sulfoximine (BSO)	Caymanchem	14484-250
Cell titer blu	Promega	G8081
Classico Western solution	Milipore	WBLUC0500
Compelete mini EDTA-free Protease Inhibitor Cocktail	Sigma Aldrich	4693159001
Complete mini Phosphatase Inhibitor	Sigma Aldrich	4906837001
D-Mannitol	Sigma Aldrich	MA125
Dharmafect Reagent I	Dharmacon	T-2001-01
Dimethyl sulfoxide (DMSO)	PAN Biotech	P60-36720100
DNA ladder (100 bp/1kb)	NEB	N3231S
DNA Loading dye (6x)	Thermo Fisher	R0611
DRAQ7	Biolegend	424001
DTT	VWR	441496P
Dulbecco´s modified eagle´s medium (DMEM)	Thermo Fisher	41966052

Dynasore	Sigma Aldrich	324410
Ecl^{tm} wb Prime	GE Healthcare	RPN2232
Erastin	Biomol	Cay17754-5
Ethanol	VRW	20821330
Ferrostatin-1	Sigma Aldrich	SML0583
Fetal bovine serum (FCS)	Sigma Aldrich	0599P
Formaldehyde (FA)	VRW	1039992500
Glycerin	VRW	24388238
H2DCFDF	Invitrogen	D399
H2O2 30%	Sigma Aldrich	H1009
Hepes	Sigma Aldrich	H3375
Kanamycin	Bio Techne	5505
KCL	VRW	MFCD00011360
KN-93	Merck	422708
L-Glutamine	Sigma Aldrich	G7513
LDS sample buffer (4x)	Thermo Fisher	NP0008
Lipofectamine 2000 reagent	Invitrogen	S1111-6001
Methanol	Sigma Aldrich	34860
$MgCl_2$	Sigma Aldrich	M8266
Milk powder	Merck	70166
Mitochondrial division inhibitor 1 (Mdivi)	Sigma Aldrich	M0199
Monochlorobimane (MCB)	Sigma aldrich	69899
NaCl	VWR	1064045000
Necrostatin-1s	Abcam	ab221984
Nuclease free water	NEB	B1500L
OPTI-MeM	Gibco	31985062
Page ruler Prestained Protein Ladder	Thermo Fisher	815-968-0747
PBS 1x	Thermo Fisher	10010056
Penicilin/Streptomycin (P/S)	Sigma Aldrich	P4333
Phen green SK diacetate	Thermo Fisher	25393

Polybrene Transfection Reagent	Milipore	TR-1003-G
Ponceau S	Sigma Aldrich	P3504
Propidium iodide (PI)	Sigma Aldrich	P4170
Protein G-Agarose beads	Santa Cruz	sc-2002
Puromycin	Sigma Aldrich	P8833
Red taq 2X Mastermix	VWR	733-2546
RIPA Lysis Buffer	Thermo Fisher	89901
RMPI (1x) (-) Calcium	MybioSource	MBS652645
RMPI (1x) (-) cystine	Sigma Aldrich	R7513
RPMI 1640	Thermo Fisher	21875091
RSL3	Selleckchem	S8155
Sodium dodecyl sulfate (SDS) ultra-pure	Sigma Aldrich	L3771
SyBr safe DNA gel stain	Invitrogen	S33102
Tamoxifen 4-OH	Sigma Aldrich	T5648
Tetracyclin	Sigma Aldrich	87128
Triton x-100	VWR	1086031000
Trizma hydrochloride (tris-HCl)	VWR	648313-250
Trypsin-EDTA free	Thermo Fisher	745065
Tween 20	VWR	0777
zVad	Enzo	BML-P416-0005

Table 3. Chemical and reagents used in this study.

6.1.2. Kits

Kits	Supplier	Catalog number
Bicinchoninic acid (BCA) protein assay	BioRad	774985
High Throughput Colorimetric GTPase assay	Abcam	ab270553

Mitochondrial Isolation Kit for Cultured Cells	Abcam	ab110171

Table 4. Kits used in this study.

6.1.3. Antibodies

Antibodies	Applications				Supplier	Catalog number
	WB	**IF**	**FACs**	**IP**		
CaMKIIα	1:1000				Thermo Fisher	13-7300
CaMKIIα				0,01 µg/µl	Abcam	Ab50202
CD71	1:2000				Santa Cruz	Sc-65882
CD71 (Transferrin Receptor) Monoclonal Antibody (OKT9)			FITC (0,125 µg/test)		Thermo Fisher	11-0711-82
Drp1 (DNML1)	1:1000				Cell Signaling	14647S
Drp1 (DNML1)		1:50		0,01 µg/µl	Cell Signaling	8570S
Dynamin-1 (DNML1)	1:1000				Cell Signaling	4565S
Dynamin-2 (DNM2)	1:1000				Sigma Aldrich	HPA054246
GAPDH	1:2000				Cell signaling	97166S
GPX4	1:2000				Abcam	Ab37185

Horse radish peroxidase (HRP)-coupled secondary antibodies (Mouse/ Rabbit)	1:10000				Biotium	ADI-40126-200
MiD49 (SMCR7)	1:1000				Thermo Fisher	PA5-46624
MiD51 (SMCR7L)	1:1000				Thermo Fisher	PA5-43348
Mouse IgG1 kappa Isotype Control			FITC (1 µg/test)		Thermo Fisher	P36281
P-S616-Drp1	1:1000				Cell Siganling	3455S
P-S637-Drp1	1:1000				Cell Signaling	4867
PGAM5	1:1000				Sigma Prestige	HPA036978
ß-actin	1:20.000				Sigma Aldrich	A1978

Table 5. Antibodies used in this study

6.1.4. Oligonucleotides and vectors

6.1.4.1. Small Interfering RNA (siRNAs)

siRNA	Supplier	Catalog number
CaMKIIα	Dharmacon	L-004942-00-0005
Drp1/DNM1L	Dharmacon	L-012092-00-0005

Dynamin 1	Dharmacon	L-003940-00-0005
Dynamin 2	Dharmacon	L-004007-00-0005
MiD49	Dharmacon	L-017272-02-0005
MiD51	Dharmacon	L-015938-01-0005

Table 6. siRNAs used in this study.

6.1.4.2. CRISPR RNA guides

gRNAs	Sequence (5´-3´)	Annealing tem (C°)
Drp1_sg1_F	CACCGCGTCCTGCTTTATTTGTGCC	54.2
Drp1_sg1_R	AAACGGCACAAATAAAGCAGGACGC	54.2
Drp1_sg2_F	CACCGGCTGCCTCAAATCGTCG	53.1
Drp1_sg2_R	AAACCGACGATTTGAGGCAGCC	53.1
Drp1_sg3_F	CACCGAAATCAGAGAGCTCATTCTT	48.3
Drp1_sg3_R	AAACAAGAATGAGCTCTCTGATTTC	48.3

Table 7. CRISPR RNA guides used in this study.

6.1.4.3. Plasmids

Plasmids	Supplier	Catalog number
LentiCas9-Blast (CRISPR Control plasmid)	Addgene	52962

Table 8. Plasmids used in this study.

6.1.4.4. Virus strain

Virus strain	Supplier	Catalog number
AdenoCre virus	Vectors Uniowa	Ad4364

Table 9. Virus strain used in this study.

6.1.5. Cell lines

Cell lines	Cell type	Provider/Source
A549	NSCLC	Prof. Dr J. Downward
H272	NSCLC	Prof. Dr J. Downward
H332m	NSCLC	Prof. Dr J. Downward
H441	NSCLC	Prof. Dr J. Downward
H520	NSCLC	Prof. Dr J. Downward
H460	NSCLC	Prof. Dr J. Downward
H82	SCLC	Prof. Dr. Roman Thomas
HEKs	– PGAM5 KO – PGAM5 KO OE	Prof.Dr T.Langer
	– DRP1 KO	Generated by L. Prieto Clemente
MEFs	– Inducible DRP1 KO	Prof. Dr. L. Scorrano
	– Inducible GPX4 KO MEFs (Pfa-1 Cells)	Prof.Dr.JP.Friedmann Angeli

Table 10. Cell lines used in this study.

6.2. Methods

6.2.1. Cell lines and cell culture conditions

Human non-small cell lung cancer (NSCLC) cell lines (H441, A549, H460, H727, H520, H332m) were kindly provided by Prof. Julian Downward and the small cell lung cancer cell line (SCLC) H82 was kindly provided by Prof. Dr. Roman Thomas. They were cultured in a humidified 37 °C atmosphere containing 10% CO_2 in RPMI 1640 medium supplemented with 10% fetal calf serum (FCS) and 1000 U/mL of both penicillin and streptomycin (P/S). Human embryonic kidney 293 (HEK) cell lines (WT, *pgam5* KO, *pgam5* KO overexpression (OE)) were

kindly provided by Prof. Dr. Roman Thomas. They were cultured in a humidified 37 °C atmosphere containing 10% CO_2 and grown in Dulbecco's modified Eagle's medium (DMEM) supplemented with 10% FCS, 1000 U/mL of both penicillin and streptomycin and 2 mM L-glutamine. To reconstitute PGAM5 in the *pgam5* KO OE cell line, cells were treated with tetracyclin 100ng/mL for 48 h. Pfa-1 cells were kindly provided by Prof. Dr. JP. Friedmann Angeli. Cells were cultured in a humidified 37 °C atmosphere containing 10% CO_2 and grown in DMEM supplemented with 10% FCS, 1000 U/mL of both penicillin and streptomycin and 2 mM L-glutamine. To induce the *gpx4* KO, cells were treated with tamoxifen 1 µM for 72 h. All cell lines were tested for mycoplasma at regular intervals. Lastly, inducible *drp1* KO floxed MEFs were kindly provided by Prof. Dr. L. Scorrano and were cultured in a humidified 37 °C atmosphere containing 10% CO_2 and grown in DMEM supplemented with 10% FCS, 1000 U/mL of both penicillin and streptomycin.

6.2.2. Compound preparation for *in vitro* experiments

All compounds were resuspended and dissolved in DMSO, filtered, and added to the culture medium to make a working solution at designated concentration.

6.2.3. Cell Viability Assays

To determine viability 10,000 cells were plated in 100 µL media in each well of a 96-well plate. Compounds were added 1 day post-plating and incubated for 48 h. Then, 5 µl Cell Titer Blu reagent was added to each well and cells were incubated for 1.5 h at 37 °C in atmosphere containing 10% CO_2. The fluorescent substrate was measured using a plate reader (EnSight™ Multimode Microplate Reader, PerkinElmer, Rodgau, Germany). Metabolic activity as an indicator of cell viability was quantified using the MTT assay, as done previously (Neitemeier et al., 2017). Viable and metabolically active cells converted 3-(4,5-dimethylthiazol-2-yl)-2,5-diphenyltetrazolium bromide, which was added at a concentration of 2.5 mg/mL for 1 h at 37 °C to the culture medium, into purple formazan. Absorbance was measured at 570 nm versus 630 nm with FluoStar after dissolving in DMSO.

6.2.4. Fluorescence-Activated Cell Sorting (FACS) Assays

6.2.4.1. PI uptake/cell death assays

To determine cell death, 25,000 cells were plated in 500 µL media in each well of a 24-well plate. Compounds were added 1 day post-plating and cells were incubated for 48 h, followed by staining with propidium iodide (1 µg/mL) in PBS supplemented with 2% FCS. PI-positive cells were quantified by flow cytometry using an LSR-FACS Fortessa (BD Bioscience, Heidelberg, Germany) and FlowJo software (BD Bioscience, Heidelberg, Germany). Propidium iodide was excited at 488 nm and fluorescence emission was detected using a 690 ± 50 nm bandpass filter. Flow cytometry data were collected from at least 5,000 cells with at least three replicates per condition.

6.2.4.2. CD71 staining

To determine CD71 surface levels, 25,000 cells were plated in each well of a 24-well plate. Cells were subjected to treatments as indicated. Cells were washed in PBS and stained for 30–40 min with the CD71 (Transferrin Receptor) Monoclonal Antibody (OKT9 (OKT-9)) (0.125 µg/test) FITC, and the Mouse IgG1 kappa Isotype Control, FITC, (1 µg/test). Mean fluorescent intensity (MFI) was quantified by flow cytometry using an LSR-FACS Fortessa and FlowJo software. Flow cytometry data were collected from at least 5,000 cells with at least three replicates per condition.

6.2.5. Transfection with Small Interfering RNA (siRNA)

For all knockdowns (**Table 6**), 200 µL Opti-MEM and 1.5 µl Dharmafect Reagent I were mixed and used per well of a 6-well plate and were incubated for 5–10 min at room temperature. Next, 2.2 µL per 200 µL of siRNA (stock 20 mM) were added to the mixture and incubated for 30 min at room temperature. Then, 200 µL of the mixture were added to each well of a 6-well plate and 300,000 cells were plated on top in 1 mL media. Knockdowns were incubated for 72 h, as indicated.

6.2.6. Time-Lapse Cell Death Assays

Cells were plated in 24-well plates (25,000 cells/well) a day in advance. The next day, cells were stimulated as indicated. Dead cells were stained by adding 100 nM DRAQ7 to all wells. Cells were imaged for 48 h every 8 h and 3 images per well were captured using the Incucyte live-cell imaging system and automated quantification software (Essen BioScience, Royston, UK).

6.2.7. Western Blotting

After indicated treatments, cells were washed in PBS, lysed in IP-lysis buffer (30 mM Tris-HCl (pH 7.4), 120 mM NaCl, 2 mM EDTA, 2 mM KCl, 1% Triton X-100, 1× COMPLETE protease and phosphatase-inhibitor cocktail) and frozen at −20 °C. After re-thawing, lysate concentrations were adjusted to equal protein concentrations using the bicinchoninic acid (BCA) protein assay. Equal amounts of protein were mixed with a final concentration of 1× reducing sample buffer and 200 mM DTT. Samples were heated to 80 °C for 10 min, separated via gel electrophoresis and transferred to nitrocellulose membranes using the TurboBlotting system. Membranes were blocked in PBS with 0.1% Tween 20 (PBST) with 5% (w/v) dried milk powder for at least 30 min. Next, membranes were incubated overnight at 4 °C with primary antibodies against CD71, β-actin, CaMKIIα, dynamin-1, dynamin-2, dynamin-related protein-1, PS616-Drp1, PS637-Drp1, Gapdh, GPX4, MiD49, MiD51, and PGAM5, all diluted 1:1000 in PBST with 5% bovine serum albumin (BSA) (Table 5). After washing with PBST, membranes were incubated with horse radish peroxidase (HRP)-coupled secondary antibodies (Biotium, California, USA) diluted 1:10,000 for at least 1 h at room temperature. After another washing step, bound antibodies were detected using chemiluminescent Classico Western HRP Substrate and X-ray films.

6.2.8. Relative Intracellular Iron Quantification

Relative levels of intracellular iron were determined using Phen Green SK diacetate. First, 25,000 cells were plated in 500 µL in each well of a 24-well plate. During the last 30 min of treatment incubation, cells were washed at least three times with PBS 1x and Phen Green SK was resuspended in RPMI serum

free and added to each well at 5 µM. Mean fluorescence intensity was determined by flow cytometry using an LSR-FACS Fortessa and FlowJo software. Flow cytometry data were collected from at least 5,000 cells with at least three replicates per condition.

6.2.9. GSH Measurement

Relative levels of glutathione were determined using Monochlorobimane (MCB). First, 25,000 cells were plated in 500 µL in each well of a 24-well plate. During the last 30 min of treatment incubation, MCB was added to each well at 50 µM. Mean fluorescence intensity was determined by flow cytometry using an LSR-FACS Fortessa and FlowJo software. Flow cytometry data were collected from at least 5,000 cells with at least three replicates per condition.

6.2.10. Lipid Reactive Oxygen Species (ROS) Quantification

Lipid ROS levels were quantified by BODIPY-C11 staining. First, 25,000 cells were plated in 500 µL in each well of a 24-well plate. To stain cells, during the last 30 min of incubation BODIPY C11 was added at 5 µM to each well. Mean fluorescence intensity was determined by flow cytometry using an LSR-FACS Fortessa and FlowJo software. Flow cytometry data were collected from at least 5,000 cells with at least three replicates per condition.

6.2.11. General Cellular ROS Quantification

Cellular ROS levels were measured as described before. To stain cells, H2DCFDF was used at 20 µM/well. Flow cytometry data were collected from at least 5,000 cells with at least three replicates per condition.

6.2.12. DPPH Assay

To determine radical scavenging activity via the DPPH assay, dynasore or positive and negative control samples were prepared in 75% ethanol. Ninety microliters of 150 µM DPPH and 10 µL of the sample were incubated for 30 min in a 96-well plate in the dark. Absorbance was measured at 517 nm with a plate reader (SPARK 20M, TECAN, Baden-Württemberg, Germany). Radical scavenging activity was calculated using the following formula: (A0 − A1)/(A0) × 100.

6.2.13. Generation of CRISPR/Cas9-mediated *drp1* KO cells

HEK 293 cells were stably transfected with vector containing one of four different Drp1-targeting gRNAs (for guide generation two primers/guide with specific overhangs were annealed, see CRISPR guides **6.1.4.2. section**, **Table 7**). For transfection, 125 µL Opti-MEM and 3 µl Lipofectamin were mixed and used per well of a 6-well plate and incubated for 5–10 min at room temperature. Next, 125 µL Opti-MEM and 1 µg CRIPSR/Cas9 vector were mixed and used per well of a 6-well plate and were incubated for 5–10 min at room temperature. Following incubation, both mixtures were combined and incubated for 30 min at room temperature. Then, 250-260 µL of the mixture were added to each well of a 6-well plate and 200,000 cells were plated 1 mL media. Transfection was performed in cell culture medium without P/S for 6 h. After incubation, transfection medium was removed and cells were cultured in normal conditions. After 48 h post-transfection, cells were selected with puromycin (A549 100 µg/ml; HEKs 1 µg/µL) for 4 days. Resistant cells were kept in normal cell culture conditions and KO cells were obtained from single cell cloning. Whole cell populations were validated for KO via Western blot.

6.2.14. Transduction with AdenoCre Virus

For the inducible *drp1* knockouts, 250 µL Opti-MEM and 0.75 µl Polybrene Transfection Reagent were mixed and used per well of a 6-well plate. The mixture was incubated for 5–10 min at room temperature. Next, $2x10^8$ UI of AdenoCre virus (**See 6.1.4.4. section ,Table 9**) were added to the mixture. The transduction solution was aggregated to each well of a 6-well plate with 100,000 inducible *drp1* floxed MEFs in 1 mL media. 6-well plates were centrifuged down at 2,500 rpm and 30°C for 45 h. The transduction mixture was incubated for 24 h. After incubation, cells were washed 3 times in PBS 1x and incubated for 24 h more in fresh media before adding the specific treatment.

6.2.15. Immunoprecipitation of Drp1

First, endogenous Drp1 was isolated from A549 cells rather than using recombinant Drp1. Cells were treated with the indicated compounds for the indicated time before isolation of total protein. Protein was extracted as

described in previous sections (**Methods; 6.2.7**). 50 µL of protein G-agarose beads were taken per condition and incubated with 0,01 µg/µL of Drp1 antibody or 1 µg of Isotype control antibody (**See 6.1.3. section, Table 5**) at 4°C overnight (o/n). After incubation, Drp1/Isotype-protein-G-agarose beads mixture was centrifuged and washed three times in RIPA lysis buffer. Whole cell protein from each group was allowed to bind to the Drp1-protein G-agarose beads mixture at 4°C o/n.

6.2.16. GTPase Activity Assay

After incubation with the protein-antibody mixture (Drp1), samples were centrifuged and washed five times with RIPA lysis and extraction buffer and twice with GTPase buffer (50 µM Tris-HCl pH 7.5, 2,5 µM $MgCl_2$) at 30°C for 30 minutes. Isolated Drp1 was incubated with GTP at 30°C for 30 minutes. The released free phosphate was quantified using a High Throughput Colorimetric GTPase assay kit according to the manufacturer´s specified protocol. OD_{620} was measured by a plate Reader.

6.2.17. Immunoprecipitation of CaMKIIα

Endogenous CaMKIIα was isolated from A549. Cells were treated with the indicated compounds for the indicated time before isolation of total protein. Protein was extracted as described in previous sections (**See 6.2.7. section**). 50 µL of protein G-agarose beads were taken per condition and incubated with 1 µg of CaMKIIα antibody or 1 µg of Isotype control antibody (**See 6.1.3. section, Table 5**) at 4°C overnight (o/n). After incubation, CaMKIIα/Isotype-protein-G-agarose beads mixture was centrifuged and washed three times with RIPA lysis buffer. Whole cell protein from each group was allowed to bind to the CaMKIIα/-protein G-agarose beads mixture at 4°C o/n. After incubation with the protein-antibody mixture (CaMKIIα), samples were centrifuged and washed five times with RIPA lysis and extraction buffer and last supernatants were discarded. Pellets were allowed to dry and resuspended in 4× reducing sample buffer and 200 mM DTT. 50 µL from whole cell lysates were taken as loading control and resuspended in 4x reducing sample buffer + DTT. The co-immunoprecipitated samples were used for Western blotting.

6.2.18. Isolation of cytosolic and mitochondrial fractions

Isolation of cytosolic and mitochondrial fractions were performed using cultured A549 cells. $1{,}8x10^6$ cells were plated on 10 cm Petri dishes and treated with DMSO and erastin 10 µM for 3 and 6 hours. Following treatment, cells were centrifuged down and pellets were dried and frozen at -80°C. Mitochondria and cytosol were isolated using a Mitochondrial/Cytosol Fractionation kit according to the manufacturer´s specified protocol.

6.2.19. Immunofluorescence

A549 cells were seeded on Ibidi chambers (12,000 cells/well). Compounds were added 1 day post-plating and cells were incubated for 3, 6 and 24 h. To stain mitochondria, during the last 30 min of incubation MitoTracker Deep red was added at 150 nM to each well. Following staining, cells were washed two times in PBS, fixed with 4% formaldehyde for 20 minutes, permeabilized with 0,1 % Triton X-100 in PBS for 5 min, and then blocked with 0,1 % Triton X-100, 1 % BSA in PBS for 1-2 h at room temperature. Cells were incubated overnight with primary Drp1 antibody at 4°C, washed three times with PBS and followed by incubation with the appropriate secondary antibody at 37°C for 1-2 h at room temperature. Finally, cells were washed five times in PBS and stored at 4°C in 100 µL of PBS per well. The stainings were viewed using a laser-scanning confocal microscope (TCS SP8 gSTED 3X, Leica Microsystems).

6.2.20. Quantification from Fluorescent Microscopy Imaging

All images were analysed by ImageJ software. Jacob Plugin was used for studying co-localization.

6.2.21. Statistical Analysis

Statistical analysis was performed using GraphPad software (GraphPad Software Inc.). One-way ANOVA test was performed for comparison between two conditions, two-way ANOVA and the Tukey´s multiple comparisons post hoc test was used for comparison between multiple samples. Data are presented as mean +/− standard error of the mean (SEM) of at least three representative independent experiments.

REFERENCES

1. Achiriloaie, M., Barylko, B., & Albanesi, J. P. (1999). Essential role of the dynamin pleckstrin homology domain in receptor-mediated endocytosis. *Molecular and cellular biology*, *19*(2), 1410–1415.
2. Adachi, Y., Itoh, K., Yamada, T., Cerveny, K. L., Suzuki, T. L., Macdonald, P., Frohman, M. A., Ramachandran, R., Iijima, M., & Sesaki, H. (2016). Coincident Phosphatidic Acid Interaction Restrains Drp1 in Mitochondrial Division. *Molecular cell*, *63*(6), 1034–1043.
3. Agmon, E., Solon, J., Bassereau, P., & Stockwell, B. R. (2018). Modeling the effects of lipid peroxidation during ferroptosis on membrane properties. *Scientific reports*, *8*(1), 5155.
4. Alexander, C., Votruba, M., Pesch, U. E., Thiselton, D. L., Mayer, S., Moore, A., Rodriguez, M., Kellner, U., Leo-Kottler, B., Auburger, G., Bhattacharya, S. S., & Wissinger, B. (2000). OPA1, encoding a dynamin-related GTPase, is mutated in autosomal dominant optic atrophy linked to chromosome 3q28. *Nature genetics*, *26*(2), 211–215.
5. Anderson, S. L., Carton, J. M., Lou, J., Xing, L., & Rubin, B. Y. (1999). Interferon-induced guanylate binding protein-1 (GBP-1) mediates an antiviral effect against vesicular stomatitis virus and encephalomyocarditis virus. *Virology*, *256*(1), 8–14.
6. Anggono, V. and Robinson, P. J. (2009). *Dynamin.* Encyclopedia of Neuroscience. Edited by Larry R. Squire. Amsterdam, The Netherlands: Elseiver.725-735.
7. Anzell, A. R., Fogo, G. M., Gurm, Z., Raghunayakula, S., Wider, J. M., Maheras, K. J., Emaus, K. J., Bryson, T. D., Wang, M., Neumar, R. W., Przyklenk, K., & Sanderson, T. H. (2021). Mitochondrial fission and mitophagy are independent mechanisms regulating ischemia/reperfusion injury in primary neurons. *Cell death & disease*, *12*(5), 475.
8. Anzell, A. R., Fogo, G. M., Gurm, Z., Raghunayakula, S., Wider, J. M., Maheras, K. J., Emaus, K. J., Bryson, T. D., Wang, M., Neumar, R. W., Przyklenk, K., & Sanderson, T. H. (2021). Mitochondrial fission and mitophagy are independent mechanisms regulating ischemia/reperfusion injury in primary neurons. *Cell death & disease*, *12*(5), 475.
9. Apostolova, N., & Victor, V. M. (2015). Molecular strategies for targeting antioxidants to mitochondria: therapeutic implications. *Antioxidants & redox signaling*, *22*(8), 686–729.
10. Archer S. L. (2013). Mitochondrial dynamics--mitochondrial fission and fusion in human diseases. *The New England journal of medicine*, *369*(23), 2236–2251.
11. Area-Gomez, E., Guardia-Laguarta, C., Schon, E. A., & Przedborski, S. (2019). Mitochondria, OxPhos, and neurodegeneration: cells are not just running out of gas. *The Journal of clinical investigation*, *129*(1), 34–45.
12. Ashrafian, H., Docherty, L., Leo, V., Towlson, C., Neilan, M., Steeples, V., Lygate, C. A., Hough, T., Townsend, S., Williams, D., Wells, S., Norris, D., Glyn-Jones, S., Land, J., Barbaric, I., Lalanne, Z., Denny, P., Szumska, D., Bhattacharya, S.,

Griffin, J. L., … Dear, T. N. (2010). A mutation in the mitochondrial fission gene Dnm1l leads to cardiomyopathy. *PLoS genetics*, *6*(6), e1001000.
13. Ayala, A., Muñoz, M. F., & Argüelles, S. (2014). Lipid peroxidation: production, metabolism, and signaling mechanisms of malondialdehyde and 4-hydroxy-2-nonenal. *Oxidative medicine and cellular longevity*, *2014*, 360438.
14. Bai, Y., Meng, L., Han, L., Jia, Y., Zhao, Y., Gao, H., Kang, R., Wang, X., Tang, D., & Dai, E. (2019). Lipid storage and lipophagy regulates ferroptosis. *Biochemical and biophysical research communications*, *508*(4), 997–1003.
15. Barreto, R., Waning, D. L., Gao, H., Liu, Y., Zimmers, T. A., & Bonetto, A. (2016). Chemotherapy-related cachexia is associated with mitochondrial depletion and the activation of ERK1/2 and p38 MAPKs. *Oncotarget*, *7*(28), 43442–43460.
16. Bayer, K. U., & Schulman, H. (2019). CaM Kinase: Still Inspiring at 40. *Neuron*, *103*(3), 380–394.
17. Bebber, C. M., Müller, F., Prieto Clemente, L., Weber, J., & von Karstedt, S. (2020). Ferroptosis in Cancer Cell Biology. *Cancers*, *12*(1), 164.
18. Bersuker, K., Hendricks, J. M., Li, Z., Magtanong, L., Ford, B., Tang, P. H., Roberts, M. A., Tong, B., Maimone, T. J., Zoncu, R., Bassik, M. C., Nomura, D. K., Dixon, S. J., & Olzmann, J. A. (2019). The CoQ oxidoreductase FSP1 acts parallel to GPX4 to inhibit ferroptosis. *Nature*, *575*(7784), 688–692.
19. Bo, T., Yamamori, T., Suzuki, M., Sakai, Y., Yamamoto, K., & Inanami, O. (2018). Calmodulin-dependent protein kinase II (CaMKII) mediates radiation-induced mitochondrial fission by regulating the phosphorylation of dynamin-related protein 1 (Drp1) at serine 616. *Biochemical and biophysical research communications*, *495*(2), 1601–1607.
20. Bogeski, I., Kummerow, C., Al-Ansary, D., Schwarz, E. C., Koehler, R., Kozai, D., Takahashi, N., Peinelt, C., Griesemer, D., Bozem, M., Mori, Y., Hoth, M., & Niemeyer, B. A. (2010). Differential redox regulation of ORAI ion channels: a mechanism to tune cellular calcium signaling. *Science signaling*, *3*(115), ra24.
21. Bradshaw, T. Y., Romano, L. E., Duncan, E. J., Nethisinghe, S., Abeti, R., Michael, G. J., Giunti, P., Vermeer, S., & Chapple, J. P. (2016). A reduction in Drp1-mediated fission compromises mitochondrial health in autosomal recessive spastic ataxia of Charlevoix Saguenay. *Human molecular genetics*, *25*(15), 3232–3244.
22. Braschi, E., Zunino, R., & McBride, H. M. (2009). MAPL is a new mitochondrial SUMO E3 ligase that regulates mitochondrial fission. *EMBO reports*, *10*(7), 748–754.
23. Breitzig, M. T., Alleyn, M. D., Lockey, R. F., & Kolliputi, N. (2018). A mitochondrial delicacy: dynamin-related protein 1 and mitochondrial dynamics. *American journal of physiology. Cell physiology*, *315*(1), C80–C90.
24. Briviba, K., Fraser, G., Sies, H., & Ketterer, B. (1993). Distribution of the monochlorobimane-glutathione conjugate between nucleus and cytosol in isolated hepatocytes. *The Biochemical journal*, *294 (Pt 3)*(Pt 3), 631–633.
25. Brown, J. L., Rosa-Caldwell, M. E., Lee, D. E., Blackwell, T. A., Brown, L. A., Perry, R. A., Haynie, W. S., Hardee, J. P., Carson, J. A., Wiggs, M. P., Washington, T. A., & Greene, N. P. (2017). Mitochondrial degeneration precedes the development of muscle atrophy in progression of cancer cachexia in tumour-bearing mice. *Journal of cachexia, sarcopenia and muscle*, *8*(6), 926–938.

26. Bui, H. T., & Shaw, J. M. (2013). Dynamin assembly strategies and adaptor proteins in mitochondrial fission. *Current biology : CB*, *23*(19), R891–R899.
27. Burdo, J., Dargusch, R., & Schubert, D. (2006). Distribution of the cystine/glutamate antiporter system xc- in the brain, kidney, and duodenum. *The journal of histochemistry and cytochemistry: official journal of the Histochemistry Society*, *54*(5), 549–557.
28. Burdo, J., Dargusch, R., & Schubert, D. (2006). Distribution of the cystine/glutamate antiporter system xc- in the brain, kidney, and duodenum. *The journal of histochemistry and cytochemistry : official journal of the Histochemistry Society*, *54*(5), 549–557.
29. Bustillo-Zabalbeitia, I., Montessuit, S., Raemy, E., Basañez, G., Terrones, O., & Martinou, J. C. (2014). Specific interaction with cardiolipin triggers functional activation of Dynamin-Related Protein 1. *PloS one*, *9*(7), e102738.
30. Cao, H., Garcia, F., & McNiven, M. A. (1998). Differential distribution of dynamin isoforms in mammalian cells. *Molecular biology of the cell*, *9*(9), 2595–2609.
31. Cereghetti, G. M., Costa, V., & Scorrano, L. (2010). Inhibition of Drp1-dependent mitochondrial fragmentation and apoptosis by a polypeptide antagonist of calcineurin. *Cell death and differentiation*, *17*(11), 1785–1794.
32. Cereghetti, G. M., Stangherlin, A., Martins de Brito, O., Chang, C. R., Blackstone, C., Bernardi, P., & Scorrano, L. (2008). Dephosphorylation by calcineurin regulates translocation of Drp1 to mitochondria. *Proceedings of the National Academy of Sciences of the United States of America*, *105*(41), 15803–15808.
33. Chang, C. R., & Blackstone, C. (2007). Drp1 phosphorylation and mitochondrial regulation. *EMBO reports*, *8*(12), 1088–1090.
34. Chang, C. R., & Blackstone, C. (2007). Drp1 phosphorylation and mitochondrial regulation. *EMBO reports*, *8*(12), 1088–1090.
35. Chen, H., & Chan, D. C. (2009). Mitochondrial dynamics--fusion, fission, movement, and mitophagy--in neurodegenerative diseases. *Human molecular genetics*, *18*(R2), R169–R176.
36. Chen, L., Chen, X. Y., Wang, Q. L., Yang, S. J., Zhou, H., Ding, L. S., Qing, L. S., & Luo, P. (2020). Astragaloside IV Derivative (LS-102) Alleviated Myocardial Ischemia Reperfusion Injury by Inhibiting Drp1^{Ser616} Phosphorylation-Mediated Mitochondrial Fission. *Frontiers in pharmacology*, *11*, 1083.
37. Chen, L., Hambright, W. S., Na, R., & Ran, Q. (2015). Ablation of the Ferroptosis Inhibitor Glutathione Peroxidase 4 in Neurons Results in Rapid Motor Neuron Degeneration and Paralysis. *The Journal of biological chemistry*, *290*(47), 28097–28106.
38. Chen, P. H., Wu, J., Ding, C. C., Lin, C. C., Pan, S., Bossa, N., Xu, Y., Yang, W. H., Mathey-Prevot, B., & Chi, J. T. (2020). Kinome screen of ferroptosis reveals a novel role of ATM in regulating iron metabolism. *Cell death and differentiation*, *27*(3), 1008–1022.
39. Chen, X., Yu, C., Kang, R., & Tang, D. (2020). Iron Metabolism in Ferroptosis. *Frontiers in cell and developmental biology*, *8*, 590226.
40. Cho, B., Cho, H. M., Jo, Y., Kim, H. D., Song, M., Moon, C., Kim, H., Kim, K., Sesaki, H., Rhyu, I. J., Kim, H., & Sun, W. (2017). Constriction of the mitochondrial inner compartment is a priming event for mitochondrial division. *Nature communications*, *8*, 15754.

41. Cho, D. H., Nakamura, T., Fang, J., Cieplak, P., Godzik, A., Gu, Z., & Lipton, S. A. (2009). S-nitrosylation of Drp1 mediates beta-amyloid-related mitochondrial fission and neuronal injury. *Science (New York, N.Y.)*, *324*(5923), 102–105.
42. Chu, B., Kon, N., Chen, D., Li, T., Liu, T., Jiang, L., Song, S., Tavana, O., & Gu, W. (2019). ALOX12 is required for p53-mediated tumour suppression through a distinct ferroptosis pathway. *Nature cell biology*, *21*(5), 579–591.
43. Cipolat, S., Martins de Brito, O., Dal Zilio, B., & Scorrano, L. (2004). OPA1 requires mitofusin 1 to promote mitochondrial fusion. *Proceedings of the National Academy of Sciences of the United States of America*, *101*(45), 15927–15932.
44. Clemente, L. P., Rabenau, M., Tang, S., Stanka, J., Cors, E., Stroh, J., Culmsee, C., & von Karstedt, S. (2020). Dynasore Blocks Ferroptosis through Combined Modulation of Iron Uptake and Inhibition of Mitochondrial Respiration. *Cells*, *9*(10), 2259.
45. Clemente, L. P., Rabenau, M., Tang, S., Stanka, J., Cors, E., Stroh, J., Culmsee, C., & von Karstedt, S. (2020). Dynasore Blocks Ferroptosis through Combined Modulation of Iron Uptake and Inhibition of Mitochondrial Respiration. *Cells*, *9*(10), 2259.
46. Cocucci, E., Gaudin, R., & Kirchhausen, T. (2014). Dynamin recruitment and membrane scission at the neck of a clathrin-coated pit. *Molecular biology of the cell*, *25*(22), 3595–3609.
47. Conrad, M., & Pratt, D. A. (2019). The chemical basis of ferroptosis. *Nature chemical biology*, *15*(12), 1137–1147.
48. Cook, S. G., Bourke, A. M., O'Leary, H., Zaegel, V., Lasda, E., Mize-Berge, J., Quillinan, N., Tucker, C. L., Coultrap, S. J., Herson, P. S., & Bayer, K. U. (2018). Analysis of the CaMKIIα and β splice-variant distribution among brain regions reveals isoform-specific differences in holoenzyme formation. *Scientific reports*, *8*(1), 5448.
49. Cribbs, J. T., & Strack, S. (2007). Reversible phosphorylation of Drp1 by cyclic AMP-dependent protein kinase and calcineurin regulates mitochondrial fission and cell death. *EMBO reports*, *8*(10), 939–944.
50. Cui, W., Liu, D., Gu, W., & Chu, B. (2021). Peroxisome-driven ether-linked phospholipids biosynthesis is essential for ferroptosis. *Cell death and differentiation*, *28*(8), 2536–2551.
51. Dai, E., Zhang, W., Cong, D., Kang, R., Wang, J., & Tang, D. (2020). AIFM2 blocks ferroptosis independent of ubiquinol metabolism. *Biochemical and biophysical research communications*, *523*(4), 966–971.
52. de Brito, O. M., & Scorrano, L. (2008). Mitofusin 2 tethers endoplasmic reticulum to mitochondria. *Nature*, *456*(7222), 605–610.
53. Delettre, C., Lenaers, G., Griffoin, J. M., Gigarel, N., Lorenzo, C., Belenguer, P., Pelloquin, L., Grosgeorge, J., Turc-Carel, C., Perret, E., Astarie-Dequeker, C., Lasquellec, L., Arnaud, B., Ducommun, B., Kaplan, J., & Hamel, C. P. (2000). Nuclear gene OPA1, encoding a mitochondrial dynamin-related protein, is mutated in dominant optic atrophy. *Nature genetics*, *26*(2), 207–210.
54. Devos, D., Moreau, C., Kyheng, M., Garçon, G., Rolland, A. S., Blasco, H., Gelé, P., Timothée Lenglet, T., Veyrat-Durebex, C., Corcia, P., Dutheil, M., Bede, P., Jeromin, A., Oeckl, P., Otto, M., Meininger, V., Danel-Brunaud, V., Devedjian, J. C., Duce, J. A., & Pradat, P. F. (2019). A ferroptosis-based panel of prognostic biomarkers for Amyotrophic Lateral Sclerosis. *Scientific reports*, *9*(1), 2918.

55. Dixon, S. J., & Stockwell, B. R. (2014). The role of iron and reactive oxygen species in cell death. *Nature chemical biology*, *10*(1), 9–17.
56. Dixon, S. J., Lemberg, K. M., Lamprecht, M. R., Skouta, R., Zaitsev, E. M., Gleason, C. E., Patel, D. N., Bauer, A. J., Cantley, A. M., Yang, W. S., Morrison, B., 3rd, & Stockwell, B. R. (2012). Ferroptosis: an iron-dependent form of nonapoptotic cell death. *Cell*, *149*(5), 1060–1072.
57. Doll, S., Freitas, F. P., Shah, R., Aldrovandi, M., da Silva, M. C., Ingold, I., Goya Grocin, A., Xavier da Silva, T. N., Panzilius, E., Scheel, C. H., Mourão, A., Buday, K., Sato, M., Wanninger, J., Vignane, T., Mohana, V., Rehberg, M., Flatley, A., Schepers, A., Kurz, A., … Conrad, M. (2019). FSP1 is a glutathione-independent ferroptosis suppressor. *Nature*, *575*(7784), 693–698.
58. Doll, S., Proneth, B., Tyurina, Y. Y., Panzilius, E., Kobayashi, S., Ingold, I., Irmler, M., Beckers, J., Aichler, M., Walch, A., Prokisch, H., Trümbach, D., Mao, G., Qu, F., Bayir, H., Füllekrug, J., Scheel, C. H., Wurst, W., Schick, J. A., Kagan, V. E., … Conrad, M. (2017). ACSL4 dictates ferroptosis sensitivity by shaping cellular lipid composition. *Nature chemical biology*, *13*(1), 91–98.
59. Dolma, S., Lessnick, S. L., Hahn, W. C., & Stockwell, B. R. (2003). Identification of genotype-selective antitumor agents using synthetic lethal chemical screening in engineered human tumor cells. *Cancer cell*, *3*(3), 285–296.
60. Drew, R., & Miners, J. O. (1984). The effects of buthionine sulphoximine (BSO) on glutathione depletion and xenobiotic biotransformation. *Biochemical pharmacology*, *33*(19), 2989–2994.
61. Dubois, C., Kondratskyi, A., Bidaux, G., Noyer, L., Vancauwenberghe, E., Farfariello, V., Toillon, R. A., Roudbaraki, M., Tierny, D., Bonnal, J. L., Prevarskaya, N., & Vanden Abeele, F. (2020). Co-targeting Mitochondrial Ca^{2+} Homeostasis and Autophagy Enhances Cancer Cells' Chemosensitivity. *iScience*, *23*(7), 101263.
62. Dutta, D., Williamson, C. D., Cole, N. B., & Donaldson, J. G. (2012). Pitstop 2 is a potent inhibitor of clathrin-independent endocytosis. *PloS one*, *7*(9), e45799.
63. Ellis HM, Horvitz HR. (1968) Genetic control of programmed cell death in the nematode C. elegans. *Cell*. *Mar 28;44*(6):817-29.
64. Ermak, G., & Davies, K. J. (2002). Calcium and oxidative stress: from cell signaling to cell death. *Molecular immunology*, *38*(10), 713–721.
65. Faelber, K., Gao, S., Held, M., Posor, Y., Haucke, V., Noé, F., & Daumke, O. (2013). Oligomerization of dynamin superfamily proteins in health and disease. *Progress in molecular biology and translational science*, *117*, 411–443.
66. Favaro, G., Romanello, V., Varanita, T., Andrea Desbats, M., Morbidoni, V., Tezze, C., Albiero, M., Canato, M., Gherardi, G., De Stefani, D., Mammucari, C., Blaauw, B., Boncompagni, S., Protasi, F., Reggiani, C., Scorrano, L., Salviati, L., & Sandri, M. (2019). DRP1-mediated mitochondrial shape controls calcium homeostasis and muscle mass. *Nature communications*, *10*(1), 2576.
67. Ferreira-da-Silva, A., Valacca, C., Rios, E., Pópulo, H., Soares, P., Sobrinho-Simões, M., Scorrano, L., Máximo, V., & Campello, S. (2015). Mitochondrial dynamics protein Drp1 is overexpressed in oncocytic thyroid tumors and regulates cancer cell migration. *PloS one*, *10*(3), e0122308.
68. Figueroa-Romero, C., Iñiguez-Lluhí, J. A., Stadler, J., Chang, C. R., Arnoult, D., Keller, P. J., Hong, Y., Blackstone, C., & Feldman, E. L. (2009). SUMOylation of the mitochondrial fission protein Drp1 occurs at multiple nonconsensus sites

within the B domain and is linked to its activity cycle. *FASEB journal : official publication of the Federation of American Societies for Experimental Biology*, *23*(11), 3917–3927.
69. Foster, M. W., Hess, D. T., & Stamler, J. S. (2009). Protein S-nitrosylation in health and disease: a current perspective. *Trends in molecular medicine*, *15*(9), 391–404.
70. Francy, C. A., Clinton, R. W., Fröhlich, C., Murphy, C., & Mears, J. A. (2017). Cryo-EM Studies of Drp1 Reveal Cardiolipin Interactions that Activate the Helical Oligomer. *Scientific reports*, *7*(1), 10744.
71. Frank, S., Gaume, B., Bergmann-Leitner, E. S., Leitner, W. W., Robert, E. G., Catez, F., Smith, C. L., & Youle, R. J. (2001). The role of dynamin-related protein 1, a mediator of mitochondrial fission, in apoptosis. *Developmental cell*, *1*(4), 515–525.
72. Friedman, J. R., Lackner, L. L., West, M., DiBenedetto, J. R., Nunnari, J., & Voeltz, G. K. (2011). ER tubules mark sites of mitochondrial division. *Science (New York, N.Y.)*, *334*(6054), 358–362.
73. Friedmann Angeli, J. P., Krysko, D. V., & Conrad, M. (2019). Ferroptosis at the crossroads of cancer-acquired drug resistance and immune evasion. Nature reviews. Cancer, 19(7), 405–414.
74. Friedmann Angeli, J. P., Schneider, M., Proneth, B., Tyurina, Y. Y., Tyurin, V. A., Hammond, V. J., Herbach, N., Aichler, M., Walch, A., Eggenhofer, E., Basavarajappa, D., Rådmark, O., Kobayashi, S., Seibt, T., Beck, H., Neff, F., Esposito, I., Wanke, R., Förster, H., Yefremova, O., … Conrad, M. (2014). Inactivation of the ferroptosis regulator Gpx4 triggers acute renal failure in mice. *Nature cell biology*, *16*(12), 1180–1191.
75. Fuchs, Y., & Steller, H. (2015). Live to die another way: modes of programmed cell death and the signals emanating from dying cells. *Nature reviews. Molecular cell biology, 16*(6), 329–344.
76. Galluzzi, L., Bravo-San Pedro, J. M., Kepp, O., & Kroemer, G. (2016). Regulated cell death and adaptive stress responses. *Cellular and molecular life sciences : CMLS*, *73*(11-12), 2405–2410.
77. Galluzzi, L., Bravo-San Pedro, J. M., Vitale, I., Aaronson, S. A., Abrams, J. M., Adam, D., Alnemri, E. S., Altucci, L., Andrews, D., Annicchiarico-Petruzzelli, M., Baehrecke, E. H., Bazan, N. G., Bertrand, M. J., Bianchi, K., Blagosklonny, M. V., Blomgren, K., Borner, C., Bredesen, D. E., Brenner, C., Campanella, M., … Kroemer, G. (2015). Essential versus accessory aspects of cell death: recommendations of the NCCD 2015. *Cell death and differentiation*, *22*(1), 58–73.
78. Galluzzi, L., Vitale, I., Aaronson, S. et al. Molecular mechanisms of cell death: recommendations of the Nomenclature Committee on Cell Death 2018. (2018) *Cell Death Differ 25*, 486–541.
79. Gammie, A. E., Kurihara, L. J., Vallee, R. B., & Rose, M. D. (1995). DNM1, a dynamin-related gene, participates in endosomal trafficking in yeast. *The Journal of cell biology*, *130*(3), 553–566.
80. Gao, D., Zhang, L., Dhillon, R., Hong, T. T., Shaw, R. M., & Zhu, J. (2013). Dynasore protects mitochondria and improves cardiac lusitropy in Langendorff perfused mouse heart. *PloS one*, *8*(4), e60967.

81. Gao, J., Zhao, N., Knutson, M. D., & Enns, C. A. (2008). The hereditary hemochromatosis protein, HFE, inhibits iron uptake via down-regulation of Zip14 in HepG2 cells. *The Journal of biological chemistry*, *283*(31).
82. Gao, M., Yi, J., Zhu, J., Minikes, A. M., Monian, P., Thompson, C. B., & Jiang, X. (2019). Role of Mitochondria in Ferroptosis. *Molecular cell*, *73*(2), 354–363.e3.
83. Gao, M.; Monian, P.; Quadri, N.; Ramasamy, R.; Jiang, X. (2015). Glutaminolysis and Transferrin Regulate Ferroptosis. *Mol. Cell*, *59*, 298–308.
84. Giacomello, M., Pyakurel, A., Glytsou, C., & Scorrano, L. (2020). The cell biology of mitochondrial membrane dynamics. *Nature reviews. Molecular cell biology*, *21*(4), 204–224.
85. Gong, Y. N., Guy, C., Olauson, H., Becker, J. U., Yang, M., Fitzgerald, P., Linkermann, A., & Green, D. R. (2017). ESCRT-III Acts Downstream of MLKL to Regulate Necroptotic Cell Death and Its Consequences. *Cell*, *169*(2), 286–300.e16.
86. Gordeeva, A. V., Zvyagilskaya, R. A., & Labas, Y. A. (2003). Cross-talk between reactive oxygen species and calcium in living cells. *Biochemistry. Biokhimiia*, *68*(10), 1077–1080.
87. Gray, N. W., Fourgeaud, L., Huang, B., Chen, J., Cao, H., Oswald, B. J., Hémar, A., & McNiven, M. A. (2003). Dynamin 3 is a component of the postsynapse, where it interacts with mGluR5 and Homer. *Current biology : CB*, *13*(6), 510–515.
88. Green, D. R., & Fitzgerald, P. (2016). Just So Stories about the Evolution of Apoptosis. *Current biology: CB, 26*(13), R620–R627.
89. Grohm, J., Kim, S. W., Mamrak, U., Tobaben, S., Cassidy-Stone, A., Nunnari, J., Plesnila, N., & Culmsee, C. (2012). Inhibition of Drp1 provides neuroprotection *in vitro* and *in vivo*. *Cell death and differentiation*, *19*(9), 1446–1458.
90. Grohm, J., Plesnila, N., & Culmsee, C. (2010). Bid mediates fission, membrane permeabilization and peri-nuclear accumulation of mitochondria as a prerequisite for oxidative neuronal cell death. *Brain, behavior, and immunity*, *24*(5), 831–838.
91. Halestrap, A. P., Clarke, S. J., & Javadov, S. A. (2004). Mitochondrial permeability transition pore opening during myocardial reperfusion--a target for cardioprotection. *Cardiovascular research*, *61*(3), 372–385.
92. Han, X. J., Lu, Y. F., Li, S. A., Kaitsuka, T., Sato, Y., Tomizawa, K., Nairn, A. C., Takei, K., Matsui, H., & Matsushita, M. (2008). CaM kinase I alpha-induced phosphorylation of Drp1 regulates mitochondrial morphology. *The Journal of cell biology*, *182*(3), 573–585.
93. Harder, Z., Zunino, R., & McBride, H. (2004). Sumo1 conjugates mitochondrial substrates and participates in mitochondrial fission. *Current biology : CB*, *14*(4), 340–345.
94. Harding, C.; Heuser, J.; Stahl, P. (1983). Receptor-mediated endocytosis of transferrin and recycling of the transferrin receptor in rat reticulocytes.*J. Cell Biol.*, *97*, 329–339.
95. Hidalgo C. (2005). Cross talk between Ca2+ and redox signalling cascades in muscle and neurons through the combined activation of ryanodine receptors/Ca2+ release channels. *Philosophical transactions of the Royal Society of London. Series B, Biological sciences*, *360*(1464), 2237–2246.
96. Hinshaw, J., Schmid, S. (1995). Dynamin self-assembles into rings suggesting a mechanism for coated vesicle budding. *Nature* 374, 190–192.

97. Holmström, K. M., & Finkel, T. (2014). Cellular mechanisms and physiological consequences of redox-dependent signalling. *Nature reviews. Molecular cell biology*, *15*(6), 411–421.
98. Hong, Y. R., Chen, C. H., Cheng, D. S., Howng, S. L., & Chow, C. C. (1998). Human dynamin-like protein interacts with the glycogen synthase kinase 3beta. *Biochemical and biophysical research communications*, *249*(3), 697–703.
99. Honkala, A. T., Tailor, D., & Malhotra, S. V. (2020). Guanylate-Binding Protein 1: An Emerging Target in Inflammation and Cancer. *Frontiers in immunology*, *10*, 3139.
100. Hu, J., Zhang, Y., Jiang, X., Zhang, H., Gao, Z., Li, Y., Fu, R., Li, L., Li, J., Cui, H., & Gao, N. (2019). ROS-mediated activation and mitochondrial translocation of CaMKII contributes to Drp1-dependent mitochondrial fission and apoptosis in triple-negative breast cancer cells by isorhamnetin and chloroquine. *Journal of experimental & clinical cancer research : CR*, *38*(1), 225.
101. Hudasek, K., Brown, S. T., & Fearon, I. M. (2004). H2O2 regulates recombinant Ca2+ channel alpha1C subunits but does not mediate their sensitivity to acute hypoxia. *Biochemical and biophysical research communications*, *318*(1), 135–141.
102. Ikeda, Y., Shirakabe, A., Maejima, Y., Zhai, P., Sciarretta, S., Toli, J., Nomura, M., Mihara, K., Egashira, K., Ohishi, M., Abdellatif, M., & Sadoshima, J. (2015). Endogenous Drp1 mediates mitochondrial autophagy and protects the heart against energy stress. *Circulation research*, *116*(2), 264–278.
103. Ikeda, Y., Shirakabe, A., Maejima, Y., Zhai, P., Sciarretta, S., Toli, J., Nomura, M., Mihara, K., Egashira, K., Ohishi, M., Abdellatif, M., & Sadoshima, J. (2015). Endogenous Drp1 mediates mitochondrial autophagy and protects the heart against energy stress. *Circulation research*, *116*(2), 264–278.
104. Imai, H., Hirao, F., Sakamoto, T., Sekine, K., Mizukura, Y., Saito, M., Kitamoto, T., Hayasaka, M., Hanaoka, K., & Nakagawa, Y. (2003). Early embryonic lethality caused by targeted disruption of the mouse PHGPx gene. *Biochemical and biophysical research communications*, *305*(2), 278–286.
105. Imoto, M., Tachibana, I., & Urrutia, R. (1998). Identification and functional characterization of a novel human protein highly related to the yeast dynamin-like GTPase Vps1p. *Journal of cell science*, *111 (Pt 10)*, 1341–1349.
106. Ingold, I., Berndt, C., Schmitt, S., Doll, S., Poschmann, G., Buday, K., Roveri, A., Peng, X., Porto Freitas, F., Seibt, T., Mehr, L., Aichler, M., Walch, A., Lamp, D., Jastroch, M., Miyamoto, S., Wurst, W., Ursini, F., Arnér, E., Fradejas-Villar, N., … Conrad, M. (2018). Selenium Utilization by GPX4 Is Required to Prevent Hydroperoxide-Induced Ferroptosis. *Cell*, *172*(3), 409–422.e21.
107. Ishihara, N., Nomura, M., Jofuku, A., Kato, H., Suzuki, S. O., Masuda, K., Otera, H., Nakanishi, Y., Nonaka, I., Goto, Y., Taguchi, N., Morinaga, H., Maeda, M., Takayanagi, R., Yokota, S., & Mihara, K. (2009). Mitochondrial fission factor Drp1 is essential for embryonic development and synapse formation in mice. *Nature cell biology*, *11*(8), 958–966.
108. Ishihara, N., Nomura, M., Jofuku, A., Kato, H., Suzuki, S. O., Masuda, K., Otera, H., Nakanishi, Y., Nonaka, I., Goto, Y., Taguchi, N., Morinaga, H., Maeda, M., Takayanagi, R., Yokota, S., & Mihara, K. (2009). Mitochondrial fission factor Drp1 is essential for embryonic development and synapse formation in mice. *Nature cell biology*, *11*(8), 958–966.

109. Itoh K, Nakamura K, Iijima M, and Sesaki H. Mitochondrial Dynamics in Neurodegeneration. (2013) *Trends Cell Biol. Feb; 23*(2): 64–71.
110. James, D. I., Parone, P. A., Mattenberger, Y., & Martinou, J. C. (2003). hFis1, a novel component of the mammalian mitochondrial fission machinery. *The Journal of biological chemistry*, *278*(38), 36373–36379.
111. Jelinek, A., Heyder, L., Daude, M., Plessner, M., Krippner, S., Grosse, R., Diederich, W. E., & Culmsee, C. (2018). Mitochondrial rescue prevents glutathione peroxidase-dependent ferroptosis. *Free radical biology & medicine*, *117*, 45–57.
112. Ji, W. K., Chakrabarti, R., Fan, X., Schoenfeld, L., Strack, S., & Higgs, H. N. (2017). Receptor-mediated Drp1 oligomerization on endoplasmic reticulum. *The Journal of cell biology*, *216*(12), 4123–4139.
113. Jiang, X., & Wang, X. (2004). Cytochrome C-mediated apoptosis. *Annual review of biochemistry*, *73*, 87–106.
114. Jorgensen, I., Rayamajhi, M., & Miao, E. A. (2017). Programmed cell death as a defence against infection. *Nature reviews. Immunology, 17*(3), 151–164.
115. Kagan, V. E., Mao, G., Qu, F., Angeli, J. P., Doll, S., Croix, C. S., Dar, H. H., Liu, B., Tyurin, V. A., Ritov, V. B., Kapralov, A. A., Amoscato, A. A., Jiang, J., Anthonymuthu, T., Mohammadyani, D., Yang, Q., Proneth, B., Klein-Seetharaman, J., Watkins, S., Bahar, I., … Bayır, H. (2017). Oxidized arachidonic and adrenic PEs navigate cells to ferroptosis. *Nature chemical biology*, *13*(1), 81–90.
116. Kajarabille, N., & Latunde-Dada, G. O. (2019). Programmed Cell-Death by Ferroptosis: Antioxidants as Mitigators. *International journal of molecular sciences*, *20*(19), 4968.
117. Kalia, R., Wang, R. Y., Yusuf, A., Thomas, P. V., Agard, D. A., Shaw, J. M., & Frost, A. (2018). Structural basis of mitochondrial receptor binding and constriction by DRP1. *Nature*, *558*(7710), 401–405.
118. Kamimoto, T., Nagai, Y., Onogi, H., Muro, Y., Wakabayashi, T., & Hagiwara, M. (1998). Dymple, a novel dynamin-like high molecular weight GTPase lacking a proline-rich carboxyl-terminal domain in mammalian cells. *The Journal of biological chemistry*, *273*(2), 1044–1051.
119. Karbowski, M., Arnoult, D., Chen, H., Chan, D. C., Smith, C. L., & Youle, R. J. (2004). Quantitation of mitochondrial dynamics by photolabeling of individual organelles shows that mitochondrial fusion is blocked during the Bax activation phase of apoptosis. *The Journal of cell biology*, *164*(4), 493–499.
120. Karbowski, M., Lee, Y. J., Gaume, B., Jeong, S. Y., Frank, S., Nechushtan, A., Santel, A., Fuller, M., Smith, C. L., & Youle, R. J. (2002). Spatial and temporal association of Bax with mitochondrial fission sites, Drp1, and Mfn2 during apoptosis. *The Journal of cell biology*, *159*(6), 931–938.
121. Karbowski, M., Neutzner, A., & Youle, R. J. (2007). The mitochondrial E3 ubiquitin ligase MARCH5 is required for Drp1 dependent mitochondrial division. *The Journal of cell biology*, *178*(1), 71–84.
122. Kareem, H. S., Ariffin, A., Nordin, N., Heidelberg, T., Abdul-Aziz, A., Kong, K. W., & Yehye, W. A. (2015). Correlation of antioxidant activities with theoretical studies for new hydrazone compounds bearing a 3,4,5-trimethoxy benzyl moiety. *European journal of medicinal chemistry*, *103*, 497–505.

123. Katikaneni, A., Jelcic, M., Gerlach, G. F., Ma, Y., Overholtzer, M., & Niethammer, P. (2020). Lipid peroxidation regulates long-range wound detection through 5-lipoxygenase in zebrafish. *Nature cell biology*, *22*(9), 1049–1055.
124. Kerr, J. F., Wyllie, A. H., & Currie, A. R. (1972). Apoptosis: a basic biological phenomenon with wide-ranging implications in tissue kinetics. *British journal of cancer*, *26*(4), 239–257.
125. Knott, A. B., & Bossy-Wetzel, E. (2008). Impairing the mitochondrial fission and fusion balance: a new mechanism of neurodegeneration. *Annals of the New York Academy of Sciences*, *1147*, 283–292.
126. Koch, J., & Brocard, C. (2012). PEX11 proteins attract Mff and human Fis1 to coordinate peroxisomal fission. *Journal of cell science*, *125*(Pt 16), 3813–3826.
127. Korobova, F., Ramabhadran, V., & Higgs, H. N. (2013). An actin-dependent step in mitochondrial fission mediated by the ER-associated formin INF2. *Science (New York, N.Y.)*, *339*(6118), 464–467.
128. Krainz, T., Gaschler, M. M., Lim, C., Sacher, J. R., Stockwell, B. R., & Wipf, P. (2016). A Mitochondrial-Targeted Nitroxide Is a Potent Inhibitor of Ferroptosis. *ACS central science*, *2*(9), 653–659.
129. Krishnan, K. S., Rikhy, R., Rao, S., Shivalkar, M., Mosko, M., Narayanan, R., Etter, P., Estes, P. S., & Ramaswami, M. (2001). Nucleoside diphosphate kinase, a source of GTP, is required for dynamin-dependent synaptic vesicle recycling. *Neuron*, *30*(1), 197–210.
130. Labrousse, A. M., Zappaterra, M. D., Rube, D. A., & van der Bliek, A. M. (1999). C. elegans dynamin-related protein DRP-1 controls severing of the mitochondrial outer membrane. *Molecular cell*, *4*(5), 815–826
131. Lackner, L. L., & Nunnari, J. M. (2009). The molecular mechanism and cellular functions of mitochondrial division. *Biochimica et biophysica acta*, *1792*(12), 1138–1144.
132. Lane, D. J., Merlot, A. M., Huang, M. L., Bae, D. H., Jansson, P. J., Sahni, S., Kalinowski, D. S., & Richardson, D. R. (2015). Cellular iron uptake, trafficking and metabolism: Key molecules and mechanisms and their roles in disease. *Biochimica et biophysica acta*, *1853*(5), 1130–1144.
133. Lavie, J., Serrat, R., Bellance, N., Courtand, G., Dupuy, J. W., Tesson, C., Coupry, I., Brice, A., Lacombe, D., Durr, A., Stevanin, G., Darios, F., Rossignol, R., Goizet, C., & Bénard, G. (2017). Mitochondrial morphology and cellular distribution are altered in SPG31 patients and are linked to DRP1 hyperphosphorylation. *Human molecular genetics*, *26*(4), 674–685.
134. Lee, J. E., Westrate, L. M., Wu, H., Page, C., & Voeltz, G. K. (2016). Multiple dynamin family members collaborate to drive mitochondrial division. *Nature*, *540*(7631), 139–143.
135. Lemmon, M. A., & Ferguson, K. M. (2000). Signal-dependent membrane targeting by pleckstrin homology (PH) domains. *The Biochemical journal*, *350 Pt 1*(Pt 1), 1–18.
136. Lewis, S. C., Uchiyama, L. F., & Nunnari, J. (2016). ER-mitochondria contacts couple mtDNA synthesis with mitochondrial division in human cells. *Science (New York, N.Y.)*, *353*(6296), aaf5549.
137. Li J, Yuan J. Caspases in apoptosis and beyond. Oncogene. 2008 Oct 20;27(48):6194-206.

138. Li, C., Liu, J., Hou, W., Kang, R., & Tang, D. (2021). STING1 Promotes Ferroptosis Through MFN1/2-Dependent Mitochondrial Fusion. *Frontiers in cell and developmental biology*, *9*, 698679.
139. Li, G., Shen, F., Fan, Z., Wang, Y., Kong, X., Yu, D., Zhi, X., Lv, G., & Cao, Y. (2017). Dynasore Improves Motor Function Recovery via Inhibition of Neuronal Apoptosis and Astrocytic Proliferation after Spinal Cord Injury in Rats. *Molecular neurobiology*, *54*(9), 7471–7482.
140. Li, Y., Feng, D., Wang, Z., Zhao, Y., Sun, R., Tian, D., Liu, D., Zhang, F., Ning, S., Yao, J., & Tian, X. (2019). Ischemia-induced ACSL4 activation contributes to ferroptosis-mediated tissue injury in intestinal ischemia/reperfusion. *Cell death and differentiation*, *26*(11), 2284–2299.
141. Liesa, M., Palacín, M., & Zorzano, A. (2009). Mitochondrial dynamics in mammalian health and disease. *Physiological reviews*, *89*(3), 799–845.
142. Linkermann, A., Skouta, R., Himmerkus, N., Mulay, S. R., Dewitz, C., De Zen, F., Prokai, A., Zuchtriegel, G., Krombach, F., Welz, P. S., Weinlich, R., Vanden Berghe, T., Vandenabeele, P., Pasparakis, M., Bleich, M., Weinberg, J. M., Reichel, C. A., Bräsen, J. H., Kunzendorf, U., Anders, H. J., … Krautwald, S. (2014). Synchronized renal tubular cell death involves ferroptosis. *Proceedings of the National Academy of Sciences of the United States of America*, *111*(47), 16836–16841.
143. Lo, S. C., & Hannink, M. (2008). PGAM5 tethers a ternary complex containing Keap1 and Nrf2 to mitochondria. *Experimental cell research*, *314*(8), 1789–1803.
144. Lo, S. C., & Hannink, M. (2008). PGAM5 tethers a ternary complex containing Keap1 and Nrf2 to mitochondria. *Experimental cell research*, *314*(8), 1789–1803.
145. Losón, O. C., Song, Z., Chen, H., & Chan, D. C. (2013). Fis1, Mff, MiD49, and MiD51 mediate Drp1 recruitment in mitochondrial fission. *Molecular biology of the cell*, *24*(5), 659–667.
146. Lu, C. S., Hodge, J. J., Mehren, J., Sun, X. X., & Griffith, L. C. (2003). Regulation of the Ca2+/CaM-responsive pool of CaMKII by scaffold-dependent autophosphorylation. *Neuron*, *40*(6), 1185–1197.
147. Macdonald, P. J., Stepanyants, N., Mehrotra, N., Mears, J. A., Qi, X., Sesaki, H., & Ramachandran, R. (2014). A dimeric equilibrium intermediate nucleates Drp1 reassembly on mitochondrial membranes for fission. *Molecular biology of the cell*, *25*(12), 1905–1915.
148. Macia, E., Ehrlich, M., Massol, R., Boucrot, E., Brunner, C., & Kirchhausen, T. (2006). Dynasore, a cell-permeable inhibitor of dynamin. *Developmental cell*, *10*(6), 839–850.
149. Maes, M. E., Grosser, J. A., Fehrman, R. L., Schlamp, C. L., & Nickells, R. W. (2019). Completion of BAX recruitment correlates with mitochondrial fission during apoptosis. *Scientific reports*, *9*(1), 16565.
150. Maher, P., van Leyen, K., Dey, P. N., Honrath, B., Dolga, A., & Methner, A. (2018). The role of Ca^{2+} in cell death caused by oxidative glutamate toxicity and ferroptosis. *Cell calcium*, *70*, 47–55.
151. Manczak, M., Sesaki, H., Kageyama, Y., & Reddy, P. H. (2012). Dynamin-related protein 1 heterozygote knockout mice do not have synaptic and mitochondrial deficiencies. *Biochimica et biophysica acta*, *1822*(6), 862–874.

152. Martinez, J. H., Alaimo, A., Gorojod, R. M., Porte Alcon, S., Fuentes, F., Coluccio Leskow, F., & Kotler, M. L. (2018). Drp-1 dependent mitochondrial fragmentation and protective autophagy in dopaminergic SH-SY5Y cells overexpressing alpha-synuclein. *Molecular and cellular neurosciences*, *88*, 107–117.
153. Mattson, M. P., Gleichmann, M., & Cheng, A. (2008). Mitochondria in neuroplasticity and neurological disorders. *Neuron*, *60*(5), 748–766.
154. Meister A. (1983). Selective modification of glutathione metabolism. *Science (New York, N.Y.)*, *220*(4596), 472–477.
155. Merkwirth, C., Dargazanli, S., Tatsuta, T., Geimer, S., Löwer, B., Wunderlich, F. T., von Kleist-Retzow, J. C., Waisman, A., Westermann, B., & Langer, T. (2008). Prohibitins control cell proliferation and apoptosis by regulating OPA1-dependent cristae morphogenesis in mitochondria. *Genes & development*, *22*(4), 476–488.
156. Mi, Y., Gao, X., Xu, H., Cui, Y., Zhang, Y., & Gou, X. (2019). The Emerging Roles of Ferroptosis in Huntington's Disease. *Neuromolecular medicine*, *21*(2), 110–119.
157. Mikami, A., Imoto, K., Tanabe, T., Niidome, T., Mori, Y., Takeshima, H., Narumiya, S., & Numa, S. (1989). Primary structure and functional expression of the cardiac dihydropyridine-sensitive calcium channel. *Nature*, *340*(6230), 230–233.
158. Morel, I., Cillard, J., Lescoat, G., Sergent, O., Pasdeloup, N., Ocaktan, A. Z., Abdallah, M. A., Brissot, P., & Cillard, P. (1992). Antioxidant and free radical scavenging activities of the iron chelators pyoverdin and hydroxypyrid-4-ones in iron-loaded hepatocyte cultures: comparison of their mechanism of protection with that of desferrioxamine. *Free radical biology & medicine*, *13*(5), 499–508.
159. Murphy, T. H., Miyamoto, M., Sastre, A., Schnaar, R. L., & Coyle, J. T. (1989). Glutamate toxicity in a neuronal cell line involves inhibition of cystine transport leading to oxidative stress. *Neuron*, *2*(6), 1547–1558.
160. Nagata, S., & Tanaka, M. (2017). Programmed cell death and the immune system. Nature reviews. *Immunology, 17*(5), 333–340.
161. Nakamura, N., Kimura, Y., Tokuda, M., Honda, S., & Hirose, S. (2006). MARCH-V is a novel mitofusin 2- and Drp1-binding protein able to change mitochondrial morphology. *EMBO reports*, *7*(10), 1019–1022.
162. Nakata, T., Takemura, R., & Hirokawa, N. (1993). A novel member of the dynamin family of GTP-binding proteins is expressed specifically in the testis. *Journal of cell science*, *105 (Pt 1)*, 1–5.
163. Neitemeier, S., Jelinek, A., Laino, V., Hoffmann, L., Eisenbach, I., Eying, R., Ganjam, G. K., Dolga, A. M., Oppermann, S., & Culmsee, C. (2017). BID links ferroptosis to mitochondrial cell death pathways. *Redox biology*, *12*, 558–570.
164. Niemann, H. H., Knetsch, M. L., Scherer, A., Manstein, D. J., & Kull, F. J. (2001). Crystal structure of a dynamin GTPase domain in both nucleotide-free and GDP-bound forms. *The EMBO journal*, *20*(21), 5813–5821.
165. Obar, R. A., Collins, C. A., Hammarback, J. A., Shpetner, H. S., & Vallee, R. B. (1990). Molecular cloning of the microtubule-associated mechanochemical enzyme dynamin reveals homology with a new family of GTP-binding proteins. *Nature*, *347*(6290), 256–261.

166. Ong, S. B., Subrayan, S., Lim, S. Y., Yellon, D. M., Davidson, S. M., & Hausenloy, D. J. (2010). Inhibiting mitochondrial fission protects the heart against ischemia/reperfusion injury. *Circulation*, *121*(18), 2012–2022.
167. Osellame, L. D., Singh, A. P., Stroud, D. A., Palmer, C. S., Stojanovski, D., Ramachandran, R., & Ryan, M. T. (2016). Cooperative and independent roles of the Drp1 adaptors Mff, MiD49 and MiD51 in mitochondrial fission. *Journal of cell science*, *129*(11), 2170–2181.
168. Otera, H., & Mihara, K. (2011). Molecular mechanisms and physiologic functions of mitochondrial dynamics. *Journal of biochemistry*, *149*(3), 241–251.
169. Otera, H., Miyata, N., Kuge, O., & Mihara, K. (2016). Drp1-dependent mitochondrial fission via MiD49/51 is essential for apoptotic cristae remodeling. *The Journal of cell biology*, *212*(5), 531–544.
170. Otera, H., Wang, C., Cleland, M. M., Setoguchi, K., Yokota, S., Youle, R. J., & Mihara, K. (2010). Mff is an essential factor for mitochondrial recruitment of Drp1 during mitochondrial fission in mammalian cells. *The Journal of cell biology*, *191*(6), 1141–1158.
171. Pallast, S., Arai, K., Wang, X., Lo, E. H., & van Leyen, K. (2009). 12/15-Lipoxygenase targets neuronal mitochondria under oxidative stress. *Journal of neurochemistry*, *111*(3), 882–889.
172. Palmer, C. S., Osellame, L. D., Laine, D., Koutsopoulos, O. S., Frazier, A. E., & Ryan, M. T. (2011). MiD49 and MiD51, new components of the mitochondrial fission machinery. *EMBO reports*, *12*(6), 565–573.
173. Paul, B. D., Sbodio, J. I., Xu, R., Vandiver, M. S., Cha, J. Y., Snowman, A. M., & Snyder, S. H. (2014). Cystathionine γ-lyase deficiency mediates neurodegeneration in Huntington's disease. *Nature*, *509*(7498), 96–100.
174. Pedrera, L., Espiritu, R. A., Ros, U., Weber, J., Schmitt, A., Stroh, J., Hailfinger, S., von Karstedt, S., & García-Sáez, A. J. (2021). Ferroptotic pores induce Ca^{2+} fluxes and ESCRT-III activation to modulate cell death kinetics. *Cell death and differentiation*, *28*(5), 1644–1657.
175. Pernas, L., & Scorrano, L. (2016). Mito-Morphosis: Mitochondrial Fusion, Fission, and Cristae Remodeling as Key Mediators of Cellular Function. *Annual review of physiology*, *78*, 505–531.
176. Praefcke, G. J., & McMahon, H. T. (2004). The dynamin superfamily: universal membrane tubulation and fission molecules?. *Nature reviews. Molecular cell biology*, *5*(2), 133–147.
177. Proneth, B., & Conrad, M. (2019). Ferroptosis and necroinflammation, a yet poorly explored link. *Cell death and differentiation*, *26*(1), 14–24.
178. Qi, X., Qvit, N., Su, Y. C., & Mochly-Rosen, D. (2013). A novel Drp1 inhibitor diminishes aberrant mitochondrial fission and neurotoxicity. *Journal of cell science*, *126*(Pt 3), 789–802.
179. Ramachandran, R., & Schmid, S. L. (2018). The dynamin superfamily. *Current biology : CB*, *28*(8), R411–R416.
180. Reddy P. H. (2014). Inhibitors of mitochondrial fission as a therapeutic strategy for diseases with oxidative stress and mitochondrial dysfunction. *Journal of Alzheimer's disease : JAD*, *40*(2), 245–256.
181. Reddy P. H. (2014). Inhibitors of mitochondrial fission as a therapeutic strategy for diseases with oxidative stress and mitochondrial dysfunction. *Journal of Alzheimer's disease : JAD*, *40*(2), 245–256.

182. Riegman, M., Sagie, L., Galed, C., Levin, T., Steinberg, N., Dixon, S. J., Wiesner, U., Bradbury, M. S., Niethammer, P., Zaritsky, A., & Overholtzer, M. (2020). Ferroptosis occurs through an osmotic mechanism and propagates independently of cell rupture. *Nature cell biology*, *22*(9), 1042–1048.
183. Robertson, M. J., Deane, F. M., Robinson, P. J., & McCluskey, A. (2014). Synthesis of Dynole 34-2, Dynole 2-24 and Dyngo 4a for investigating dynamin GTPase. *Nature protocols*, *9*(4), 851–870.
184. Romanello, V., & Sandri, M. (2013). Mitochondrial biogenesis and fragmentation as regulators of protein degradation in striated muscles. *Journal of molecular and cellular cardiology*, *55*, 64–72.
185. Romanello, V., & Sandri, M. (2013). Mitochondrial biogenesis and fragmentation as regulators of protein degradation in striated muscles. *Journal of molecular and cellular cardiology*, *55*, 64–72.
186. Romanello, V., & Sandri, M. (2016). Mitochondrial Quality Control and Muscle Mass Maintenance. *Frontiers in physiology*, *6*, 422.
187. Roy, M., Reddy, P. H., Iijima, M., & Sesaki, H. (2015). Mitochondrial division and fusion in metabolism. *Current opinion in cell biology*, *33*, 111–118.
188. Rühl, S., Shkarina, K., Demarco, B., Heilig, R., Santos, J. C., & Broz, P. (2018). ESCRT-dependent membrane repair negatively regulates pyroptosis downstream of GSDMD activation. *Science (New York, N.Y.)*, *362*(6417), 956–960.
189. Santel, A., & Frank, S. (2008). Shaping mitochondria: The complex posttranslational regulation of the mitochondrial fission protein DRP1. *IUBMB life*, *60*(7), 448–455.
190. Santel, A., & Fuller, M. T. (2001). Control of mitochondrial morphology by a human mitofusin. *Journal of cell science*, *114*(Pt 5), 867–874.
191. Saraste, M., Sibbald, P. R., & Wittinghofer, A. (1990). The P-loop--a common motif in ATP- and GTP-binding proteins. *Trends in biochemical sciences*, *15*(11), 430–434.
192. Sato, H., Nomura, S., Maebara, K., Sato, K., Tamba, M., & Bannai, S. (2004). Transcriptional control of cystine/glutamate transporter gene by amino acid deprivation. *Biochemical and biophysical research communications*, *325*(1), 109–116.
193. Sato, H., Shiiya, A., Kimata, M., Maebara, K., Tamba, M., Sakakura, Y., Makino, N., Sugiyama, F., Yagami, K., Moriguchi, T., Takahashi, S., & Bannai, S. (2005). Redox imbalance in cystine/glutamate transporter-deficient mice. *The Journal of biological chemistry*, *280*(45), 37423–37429.
194. Schrader, M., Costello, J. L., Godinho, L. F., Azadi, A. S., & Islinger, M. (2016). Proliferation and fission of peroxisomes - An update. *Biochimica et biophysica acta*, *1863*(5), 971–983.
195. Seiler, A., Schneider, M., Förster, H., Roth, S., Wirth, E. K., Culmsee, C., Plesnila, N., Kremmer, E., Rådmark, O., Wurst, W., Bornkamm, G. W., Schweizer, U., & Conrad, M. (2008). Glutathione peroxidase 4 senses and translates oxidative stress into 12/15-lipoxygenase dependent- and AIF-mediated cell death. *Cell metabolism*, *8*(3), 237–248.
196. She, L., Tu, H., Zhang, Y. Z., Tang, L. J., Li, N. S., Ma, Q. L., Liu, B., Li, Q., Luo, X. J., & Peng, J. (2019). Inhibition of Phosphoglycerate Mutase 5 Reduces Necroptosis in Rat Hearts Following Ischemia/Reperfusion Through

Suppression of Dynamin-Related Protein 1. *Cardiovascular drugs and therapy*, *33*(1), 13–23.

197. Shin, H. W., Shinotsuka, C., Torii, S., Murakami, K., & Nakayama, K. (1997). Identification and subcellular localization of a novel mammalian dynamin-related protein homologous to yeast Vps1p and Dnm1p. *Journal of biochemistry*, *122*(3), 525–530.

198. Shpetner, H. S., & Vallee, R. B. (1989). Identification of dynamin, a novel mechanochemical enzyme that mediates interactions between microtubules. *Cell*, *59*(3), 421–432.

199. Shpetner, H. S., & Vallee, R. B. (1992). Dynamin is a GTPase stimulated to high levels of activity by microtubules. *Nature*, *355*(6362), 733–735.

200. Shrieve, D. C., & Harris, J. W. (1986). Effects of glutathione depletion by buthionine sulfoximine on the sensitivity of EMT6/SF cells to chemotherapy agents or X radiation. *International journal of radiation oncology, biology, physics*, *12*(7), 1171–1174.

201. Smirnova, E., Griparic, L., Shurland, D. L., & van der Bliek, A. M. (2001). Dynamin-related protein Drp1 is required for mitochondrial division in mammalian cells. *Molecular biology of the cell*, *12*(8), 2245–2256.

202. Smirnova, E., Shurland, D. L., Ryazantsev, S. N., & van der Bliek, A. M. (1998). A human dynamin-related protein controls the distribution of mitochondria. *The Journal of cell biology*, *143*(2), 351–358.

203. Sontag, J. M., Fykse, E. M., Ushkaryov, Y., Liu, J. P., Robinson, P. J., & Südhof, T. C. (1994). Differential expression and regulation of multiple dynamins. *The Journal of biological chemistry*, *269*(6), 4547–4554.

204. Staeheli, P., Prochazka, M., Steigmeier, P. A., & Haller, O. (1984). Genetic control of interferon action: mouse strain distribution and inheritance of an induced protein with guanylate-binding property. *Virology*, *137*(1), 135–142.

205. Stepanyants, N., Macdonald, P. J., Francy, C. A., Mears, J. A., Qi, X., & Ramachandran, R. (2015). Cardiolipin's propensity for phase transition and its reorganization by dynamin-related protein 1 form a basis for mitochondrial membrane fission. *Molecular biology of the cell*, *26*(17), 3104–3116.

206. Stockwell, B. R., Friedmann Angeli, J. P., Bayir, H., Bush, A. I., Conrad, M., Dixon, S. J., Fulda, S., Gascón, S., Hatzios, S. K., Kagan, V. E., Noel, K., Jiang, X., Linkermann, A., Murphy, M. E., Overholtzer, M., Oyagi, A., Pagnussat, G. C., Park, J., Ran, Q., Rosenfeld, C. S., … Zhang, D. D. (2017). Ferroptosis: A Regulated Cell Death Nexus Linking Metabolism, Redox Biology, and Disease. *Cell*, *171*(2), 273–285.

207. Sun, X., Ou, Z., Chen, R., Niu, X., Chen, D., Kang, R., & Tang, D. (2016). Activation of the p62-Keap1-NRF2 pathway protects against ferroptosis in hepatocellular carcinoma cells. *Hepatology (Baltimore, Md.)*, *63*(1), 173–184.

208. Tabet, F., Savoia, C., Schiffrin, E. L., & Touyz, R. M. (2004). Differential calcium regulation by hydrogen peroxide and superoxide in vascular smooth muscle cells from spontaneously hypertensive rats. *Journal of cardiovascular pharmacology*, *44*(2), 200–208.

209. Taguchi, N., Ishihara, N., Jofuku, A., Oka, T., & Mihara, K. (2007). Mitotic phosphorylation of dynamin-related GTPase Drp1 participates in mitochondrial fission. *The Journal of biological chemistry*, *282*(15), 11521–11529.

210. Takeda, K., Komuro, Y., Hayakawa, T., Oguchi, H., Ishida, Y., Murakami, S., Noguchi, T., Kinoshita, H., Sekine, Y., Iemura, S., Natsume, T., & Ichijo, H. (2009). Mitochondrial phosphoglycerate mutase 5 uses alternate catalytic activity as a protein serine/threonine phosphatase to activate ASK1. *Proceedings of the National Academy of Sciences of the United States of America*, *106*(30), 12301–12305.
211. Takei, K., McPherson, P. S., Schmid, S. L., & De Camilli, P. (1995). Tubular membrane invaginations coated by dynamin rings are induced by GTP-gamma S in nerve terminals. *Nature*, *374*(6518), 186–190.
212. Takemoto-Kimura, S., Suzuki, K., Horigane, S. I., Kamijo, S., Inoue, M., Sakamoto, M., Fujii, H., & Bito, H. (2017). Calmodulin kinases: essential regulators in health and disease. *Journal of neurochemistry*, *141*(6), 808–818.
213. Tang, D., Chen, X., Kang, R., & Kroemer, G. (2021). Ferroptosis: molecular mechanisms and health implications. *Cell research*, *31*(2), 107–125.
214. Tang, Y., Zhou, J., Hooi, S. C., Jiang, Y. M., & Lu, G. D. (2018). Fatty acid activation in carcinogenesis and cancer development: Essential roles of long-chain acyl-CoA synthetases. *Oncology letters*, *16*(2), 1390–1396.
215. Terentyev, D., Györke, I., Belevych, A. E., Terentyeva, R., Sridhar, A., Nishijima, Y., de Blanco, E. C., Khanna, S., Sen, C. K., Cardounel, A. J., Carnes, C. A., & Györke, S. (2008). Redox modification of ryanodine receptors contributes to sarcoplasmic reticulum Ca2+ leak in chronic heart failure. *Circulation research*, *103*(12), 1466–1472.
216. Tezze, C., Romanello, V., Desbats, M. A., Fadini, G. P., Albiero, M., Favaro, G., Ciciliot, S., Soriano, M. E., Morbidoni, V., Cerqua, C., Loefler, S., Kern, H., Franceschi, C., Salvioli, S., Conte, M., Blaauw, B., Zampieri, S., Salviati, L., Scorrano, L., & Sandri, M. (2017). Age-Associated Loss of OPA1 in Muscle Impacts Muscle Mass, Metabolic Homeostasis, Systemic Inflammation, and Epithelial Senescence. *Cell metabolism*, *25*(6), 1374–1389.e6.
217. Toledo, F. D., Pérez, L. M., Basiglio, C. L., Ochoa, J. E., Sanchez Pozzi, E. J., & Roma, M. G. (2014). The Ca^{2+}-calmodulin-Ca^{2+}/calmodulin-dependent protein kinase II signaling pathway is involved in oxidative stress-induced mitochondrial permeability transition and apoptosis in isolated rat hepatocytes. *Archives of toxicology*, *88*(9), 1695–1709.
218. Touvier, T., De Palma, C., Rigamonti, E., Scagliola, A., Incerti, E., Mazelin, L., Thomas, J. L., D'Antonio, M., Politi, L., Schaeffer, L., Clementi, E., & Brunelli, S. (2015). Muscle-specific Drp1 overexpression impairs skeletal muscle growth via translational attenuation. *Cell death & disease*, *6*(2), e1663.
219. Touvier, T., De Palma, C., Rigamonti, E., Scagliola, A., Incerti, E., Mazelin, L., Thomas, J. L., D'Antonio, M., Politi, L., Schaeffer, L., Clementi, E., & Brunelli, S. (2015). Muscle-specific Drp1 overexpression impairs skeletal muscle growth via translational attenuation. *Cell death & disease*, *6*(2), e1663.
220. Trebak, M., Ginnan, R., Singer, H. A., & Jourd'heuil, D. (2010). Interplay between calcium and reactive oxygen/nitrogen species: an essential paradigm for vascular smooth muscle signaling. *Antioxidants & redox signaling*, *12*(5), 657–674.
221. Vainshtein, A., Grumati, P., Sandri, M., & Bonaldo, P. (2014). Skeletal muscle, autophagy, and physical activity: the ménage à trois of metabolic

regulation in health and disease. *Journal of molecular medicine (Berlin, Germany)*, *92*(2), 127–137.

222. van Dam, E. M., & Stoorvogel, W. (2002). Dynamin-dependent transferrin receptor recycling by endosome-derived clathrin-coated vesicles. *Molecular biology of the cell*, *13*(1), 169–182.

223. van der Ende, M., Grefte, S., Plas, R., Meijerink, J., Witkamp, R. F., Keijer, J., & van Norren, K. (2018). Mitochondrial dynamics in cancer-induced cachexia. *Biochimica et biophysica acta. Reviews on cancer*, *1870*(2), 137–150.

224. Vanden Berghe, T., Linkermann, A., Jouan-Lanhouet, S., Walczak, H., & Vandenabeele, P. (2014). Regulated necrosis: the expanding network of non-apoptotic cell death pathways. *Nature reviews. Molecular cell biology*, *15*(2), 135–147.

225. Varadarajan, S., Butterworth, M., Wei, J., Pellecchia, M., Dinsdale, D., & Cohen, G. M. (2013). Sabutoclax (BI97C1) and BI112D1, putative inhibitors of MCL-1, induce mitochondrial fragmentation either upstream of or independent of apoptosis. *Neoplasia (New York, N.Y.)*, *15*(5), 568–578.

226. Vestal, D. J., & Jeyaratnam, J. A. (2011). The guanylate-binding proteins: emerging insights into the biochemical properties and functions of this family of large interferon-induced guanosine triphosphatase. *Journal of interferon & cytokine research : the official journal of the International Society for Interferon and Cytokine Research*, *31*(1), 89–97.

227. Vila, A., Levchenko, V. V., Korytowski, W., & Girotti, A. W. (2004). Sterol carrier protein-2-facilitated intermembrane transfer of cholesterol- and phospholipid-derived hydroperoxides. *Biochemistry*, *43*(39), 12592–12605.

228. von Karstedt, S., Montinaro, A., & Walczak, H. (2017). Exploring the TRAILs less travelled: TRAIL in cancer biology and therapy. *Nature reviews. Cancer*, *17*(6), 352–366.

229. Wakabayashi, J., Zhang, Z., Wakabayashi, N., Tamura, Y., Fukaya, M., Kensler, T. W., Iijima, M., & Sesaki, H. (2009). The dynamin-related GTPase Drp1 is required for embryonic and brain development in mice. *The Journal of cell biology*, *186*(6), 805–816.

230. Wakabayashi, J., Zhang, Z., Wakabayashi, N., Tamura, Y., Fukaya, M., Kensler, T. W., Iijima, M., & Sesaki, H. (2009). The dynamin-related GTPase Drp1 is required for embryonic and brain development in mice. *The Journal of cell biology*, *186*(6), 805–816.

231. Wang X. (2001). The expanding role of mitochondria in apoptosis. *Genes & development*, *15*(22), 2922–2933.

232. Wang, H., Liu, C., Zhao, Y., & Gao, G. (2020). Mitochondria regulation in ferroptosis. *European journal of cell biology*, *99*(1), 151058.

233. Wang, Z., Jiang, H., Chen, S., Du, F., & Wang, X. (2012). The mitochondrial phosphatase PGAM5 functions at the convergence point of multiple necrotic death pathways. *Cell*, *148*(1-2), 228–243.

234. Wasiak, S., Zunino, R., & McBride, H. M. (2007). Bax/Bak promote sumoylation of DRP1 and its stable association with mitochondria during apoptotic cell death. *The Journal of cell biology*, *177*(3), 439–450.

235. Webster, A., Chintala, S. K., Kim, J., Ngan, M., Itakura, T., Panjwani, N., Argüeso, P., Barr, J. T., Jeong, S., & Fini, M. E. (2018). Dynasore protects the ocular surface against damaging oxidative stress. *PloS one*, *13*(10), e0204288.

236. Wienke, D. C., Knetsch, M. L., Neuhaus, E. M., Reedy, M. C., & Manstein, D. J. (1999). Disruption of a dynamin homologue affects endocytosis, organelle morphology, and cytokinesis in Dictyostelium discoideum. *Molecular biology of the cell*, *10*(1), 225–243.
237. Wong, Y. C., Ysselstein, D., & Krainc, D. (2018). Mitochondria-lysosome contacts regulate mitochondrial fission via RAB7 GTP hydrolysis. *Nature*, *554*(7692), 382–386.
238. Wu, Y., Wang, Q., Feng, N., Granger, J. M., & Anderson, M. E. (2019). Myocardial death and dysfunction after ischemia-reperfusion injury require CaMKIIδ oxidation. *Scientific reports*, *9*(1), 9291.
239. Xie, L. L., Shi, F., Tan, Z., Li, Y., Bode, A. M., & Cao, Y. (2018). Mitochondrial network structure homeostasis and cell death. *Cancer science*, *109*(12), 3686–3694.
240. Xie, Q., Wu, Q., Horbinski, C. M., Flavahan, W. A., Yang, K., Zhou, W., Dombrowski, S. M., Huang, Z., Fang, X., Shi, Y., Ferguson, A. N., Kashatus, D. F., Bao, S., & Rich, J. N. (2015). Mitochondrial control by DRP1 in brain tumor initiating cells. *Nature neuroscience*, *18*(4), 501–510.
241. Xie, Y., Hou, W., Song, X., Yu, Y., Huang, J., Sun, X., Kang, R., & Tang, D. (2016). Ferroptosis: process and function. *Cell death and differentiation*, *23*(3), 369–379.
242. Xie, Y., Zhu, S., Song, X., Sun, X., Fan, Y., Liu, J., Zhong, M., Yuan, H., Zhang, L., Billiar, T. R., Lotze, M. T., Zeh, H. J., 3rd, Kang, R., Kroemer, G., & Tang, D. (2017). The Tumor Suppressor p53 Limits Ferroptosis by Blocking DPP4 Activity. *Cell reports*, *20*(7), 1692–1704.
243. Xu, S., Wang, P., Zhang, H., Gong, G., Gutierrez Cortes, N., Zhu, W., Yoon, Y., Tian, R., & Wang, W. (2016). CaMKII induces permeability transition through Drp1 phosphorylation during chronic β-AR stimulation. *Nature communications*, *7*, 13189.
244. Yagoda, N., von Rechenberg, M., Zaganjor, E., Bauer, A. J., Yang, W. S., Fridman, D. J., Wolpaw, A. J., Smukste, I., Peltier, J. M., Boniface, J. J., Smith, R., Lessnick, S. L., Sahasrabudhe, S., & Stockwell, B. R. (2007). RAS-RAF-MEK-dependent oxidative cell death involving voltage-dependent anion channels. *Nature*, *447*(7146), 864–868.
245. Yan, T., & Zhao, Y. (2020). Acetaldehyde induces phosphorylation of dynamin-related protein 1 and mitochondrial dysfunction via elevating intracellular ROS and Ca^{2+} levels. *Redox biology*, *28*, 101381.
246. Yan, Y., Liu, J., Wei, C., Li, K., Xie, W., Wang, Y., & Cheng, H. (2008). Bidirectional regulation of Ca2+ sparks by mitochondria-derived reactive oxygen species in cardiac myocytes. *Cardiovascular research*, *77*(2), 432–441.
247. Yanatori, I.; Yasui, Y.; Noguchi, Y.; Kishi, F. (2015). Inhibition of iron uptake by ferristatin II is exerted through internalization of DMT1 at the plasma membrane. *Cell Biol. Int.*, *39*, 427–434.
248. Yang, W. S., Kim, K. J., Gaschler, M. M., Patel, M., Shchepinov, M. S., & Stockwell, B. R. (2016). Peroxidation of polyunsaturated fatty acids by lipoxygenases drives ferroptosis. *Proceedings of the National Academy of Sciences of the United States of America*, *113*(34), E4966–E4975.
249. Yang, W. S., SriRamaratnam, R., Welsch, M. E., Shimada, K., Skouta, R., Viswanathan, V. S., Cheah, J. H., Clemons, P. A., Shamji, A. F., Clish, C. B.,

Brown, L. M., Girotti, A. W., Cornish, V. W., Schreiber, S. L., & Stockwell, B. R. (2014). Regulation of ferroptotic cancer cell death by GPX4. *Cell*, *156*(1-2), 317–331.

250. Yang, W.S.; Stockwell, B.R. (2008). Synthetic Lethal Screening Identifies Compounds Activating Iron-Dependent, Nonapoptotic Cell Death in Oncogenic-RAS-Harboring Cancer Cells. *Chem. Biol*. *15*, 234–245.

251. Yant, L. J., Ran, Q., Rao, L., Van Remmen, H., Shibatani, T., Belter, J. G., Motta, L., Richardson, A., & Prolla, T. A. (2003). The selenoprotein GPX4 is essential for mouse development and protects from radiation and oxidative damage insults. *Free radical biology & medicine*, *34*(4), 496–502. Yoo, S. E., Chen, L., Na, R., Liu, Y., Rios, C., Van Remmen, H., Richardson, A., & Ran, Q. (2012). Gpx4 ablation in adult mice results in a lethal phenotype accompanied by neuronal loss in brain. *Free radical biology & medicine*, *52*(9), 1820–1827.

252. Yonashiro, R., Ishido, S., Kyo, S., Fukuda, T., Goto, E., Matsuki, Y., Ohmura-Hoshino, M., Sada, K., Hotta, H., Yamamura, H., Inatome, R., & Yanagi, S. (2006). A novel mitochondrial ubiquitin ligase plays a critical role in mitochondrial dynamics. *The EMBO journal*, *25*(15), 3618–3626.

253. Youle, R. J., & van der Bliek, A. M. (2012). Mitochondrial fission, fusion, and stress. *Science (New York, N.Y.)*, *337*(6098), 1062–1065.

254. Yu, H., Guo, P., Xie, X., Wang, Y., & Chen, G. (2017). Ferroptosis, a new form of cell death, and its relationships with tumourous diseases. *Journal of cellular and molecular medicine*, *21*(4), 648–657.

255. Yu, H., Yang, C., Jian, L., Guo, S., Chen, R., Li, K., Qu, F., Tao, K., Fu, Y., Luo, F., & Liu, S. (2019). Sulfasalazine-induced ferroptosis in breast cancer cells is reduced by the inhibitory effect of estrogen receptor on the transferrin receptor. *Oncology reports*, *42*(2), 826–838.

256. Yu, T., Jhun, B. S., & Yoon, Y. (2011). High-glucose stimulation increases reactive oxygen species production through the calcium and mitogen-activated protein kinase-mediated activation of mitochondrial fission. *Antioxidants & redox signaling*, *14*(3), 425–437.

257. Yuan, H., Li, X., Zhang, X., Kang, R., & Tang, D. (2016). Identification of ACSL4 as a biomarker and contributor of ferroptosis. *Biochemical and biophysical research communications*, *478*(3), 1338–1343.

258. Yuan, J., Amin, P., & Ofengeim, D. (2019). Necroptosis and RIPK1-mediated neuroinflammation in CNS diseases. *Nature reviews. Neuroscience*, *20*(1), 19–33.

259. Zhang, J., Yang, P. L., & Gray, N. S. (2009). Targeting cancer with small molecule kinase inhibitors. *Nature reviews. Cancer*, *9*(1), 28–39.

260. Zhao, J., Liu, T., Jin, S., Wang, X., Qu, M., Uhlén, P., Tomilin, N., Shupliakov, O., Lendahl, U., & Nistér, M. (2011). Human MIEF1 recruits Drp1 to mitochondrial outer membranes and promotes mitochondrial fusion rather than fission. *The EMBO journal*, *30*(14), 2762–2778.

261. Zhou, B., Liu, J., Kang, R., Klionsky, D. J., Kroemer, G., & Tang, D. (2020). Ferroptosis is a type of autophagy-dependent cell death. *Seminars in cancer biology*, *66*, 89–100.

262. Zhou, L., Zhang, Q., Zhang, P., Sun, L., Peng, C., Yuan, Z., & Cheng, J. (2017). c-Abl-mediated Drp1 phosphorylation promotes oxidative stress-induced

mitochondrial fragmentation and neuronal cell death. *Cell death & disease*, *8*(10), e3117.

263. Zilka, O., Shah, R., Li, B., Friedmann Angeli, J. P., Griesser, M., Conrad, M., & Pratt, D. A. (2017). On the Mechanism of Cytoprotection by Ferrostatin-1 and Liproxstatin-1 and the Role of Lipid Peroxidation in Ferroptotic Cell Death. *ACS central science*, *3*(3), 232–243.

264. Zou, Y., Li, H., Graham, E. T., Deik, A. A., Eaton, J. K., Wang, W., Sandoval-Gomez, G., Clish, C. B., Doench, J. G., & Schreiber, S. L. (2020). Cytochrome P450 oxidoreductase contributes to phospholipid peroxidation in ferroptosis. *Nature chemical biology*, *16*(3), 302–309.

265. Züchner, S., Mersiyanova, I. V., Muglia, M., Bissar-Tadmouri, N., Rochelle, J., Dadali, E. L., Zappia, M., Nelis, E., Patitucci, A., Senderek, J., Parman, Y., Evgrafov, O., Jonghe, P. D., Takahashi, Y., Tsuji, S., Pericak-Vance, M. A., Quattrone, A., Battaloglu, E., Polyakov, A. V., Timmerman, V., … Vance, J. M. (2004). Mutations in the mitochondrial GTPase mitofusin 2 cause Charcot-Marie-Tooth neuropathy type 2A. *Nature genetics*, *36*(5), 449–451.

266. Zunino, R., Schauss, A., Rippstein, P., Andrade-Navarro, M., & McBride, H. M. (2007). The SUMO protease SENP5 is required to maintain mitochondrial morphology and function. *Journal of cell science*, *120*(Pt 7), 1178–1188.

PUBLICATIONS

1. Bebber, C. M., Müller, F., **Prieto Clemente, L**., Weber, J., & von Karstedt, S. (2020). Ferroptosis in Cancer Cell Biology. *Cancers*, *12*(1), 164.
2. **Prieto Clemente, L**., Rabenau, M., Tang, S., Stanka, J., Cors, E., Stroh, J., Culmsee, C., & von Karstedt, S. (2020). Dynasore Blocks Ferroptosis through Combined Modulation of Iron Uptake and Inhibition of Mitochondrial Respiration. *Cells*, *9*(10), 2259.
3. **Prieto Clemente, L**., Olmo González, D., Pedrera, L., Stroh, J., García-Sáez, A.J & von Karstedt, S. Cysteine starvation triggers ferroptosis via CamKII-mediated Drp1 activation and mitochondrial depolarization/lipid peroxidation**.** *In preparation*

ACKNOWLEDGEMENTS

First of all, I would like to thank my supervisor Prof. Dr. Silvia von Karstedt, who gave me the opportunity to do my PhD in her lab and for trusting me with this amazing project. She has given me an excellent guidance and motivational support, and taught me how to be a better scientist. I can see how much I have evolved and learn since the first time I started working in the lab, and this is mainly thanks to her.

I thank Prof.Dr Langer and Prof.Dr Riemer who kindly agreed to take part of my dissertation defense. I really appreciate the nice and professional support from CECAD´s facilities, mainly from the Imaging Facility. In addition, I am grateful with the doctoral program where I was enrolled for providing me an exceptional support for attending seminars and conferences.

I am very thankful to all, former and current members, from Silvia von Karstedt´s lab. Especially Isil Yapici, Christina Bebber, Jenny Stroh and my excellent former student Daniel Olmo, for their big support and contribution to this thesis. They started being my colleagues but after 3 years of work and support I have also found really good friends.

Finalmente, pero no menos importante, me gustaría agradecer el apoyo incondicional que he recibido por parte de todos los miembros de mi familia, especialmente a mi madre, Esther, mi padre Ginés, mi hermana Marta, mi abuela Isabel y mis tías Encarni e Irene. Sin ellos no habría logrado llegar tan lejos y no habría conseguido realizar mi tesis doctoral. Me gustaría dedicarle parte de estos agradecimientos a Blanca, la persona que me enseñó a trabajar por primera vez en un laboratorio, ya que, a pesar de la distancia, siempre ha estado presente. Y por supuesto, a todo ese gran equipo de epitelianos que me transmitieron la pasión por la investigación y el buen trabajo en equipo. Especialmente a Victoria, Esteban, Verónica, Jose, Sergio y Nuria.

Por último, quiero dedicar parte de estos agradecimientos a esos amigos, entre los que se encuentran incluidos los anteriores, que siempre me han apoyado y

animado durante esta larga etapa. Especialmente, a mi mejor amiga Elena, que siempre me espera en Madrid. A mi hermana Violeta y a mi gran amiga y Doctora Lohans, no solo por enseñarme ciencia si no también por todas las lecciones de vida aprendidas a su lado. Muchas gracias a todos y todas por apoyarme, escucharme, aconsejarme y cuidarme durante esta dura y larga etapa que ha sido mi doctorado.

EIDESSTATTLICHE ERKLÄRUNG

„Hiermit versichere ich an Eides statt, dass ich die vorliegende Dissertation selbstständig und ohne die Benutzung anderer als der angegebenen Hilfsmittel und Literatur angefertigt habe. Alle Stellen, die wörtlich oder sinngemäß aus veröffentlichten und nicht veröffentlichten Werken dem Wortlaut oder dem Sinn nach entnommen wurden, sind als solche kenntlich gemacht. Ich versichere an Eides statt, dass diese Dissertation noch keiner anderen Fakultät oder Universität zur Prüfung vorgelegen hat; dass sie - abgesehen von unten angegebenen Teilpublikationen und eingebundenen Artikeln und Manuskripten - noch nicht veröffentlicht worden ist sowie, dass ich eine Veröffentlichung der Dissertation vor Abschluss der Promotion nicht ohne Genehmigung des Promotionsausschusses vornehmen werde. Die Bestimmungen dieser Ordnung sind mir bekannt. Darüber hinaus erkläre ich hiermit, dass ich die Ordnung zur Sicherung guter wissenschaftlicher Praxis und zum Umgang mit wissenschaftlichem Fehlverhalten der Universität zu Köln gelesen und sie bei der Durchführung der Dissertation zugrundeliegenden Arbeiten und der schriftlich verfassten Dissertation beachtet habe und verpflichte mich hiermit, die dort genannten Vorgaben bei allen wissenschaftlichen Tätigkeiten zu beachten und umzusetzen. Ich versichere, dass die eingereichte elektronische Fassung der eingereichten Druckfassung vollständig entspricht."

Teilpublikationen:

- **Prieto Clemente, L**., Rabenau, M., Tang, S., Stanka, J., Cors, E., Stroh, J., Culmsee, C., & von Karstedt, S. (2020). Dynasore Blocks Ferroptosis through Combined Modulation of Iron Uptake and Inhibition of Mitochondrial Respiration. *Cells*, *9*(10), 2259.

Laura Prieto Clemente

Köln, 04.10.2021